BIOSYNTHESIS OF OXIDES NANOPARTICLES USING MICROORGANISMS

A THESIS
SUBMITTED TO THE

UNIVERSITY OF PUNE

FOR THE DEGREE OF
DOCTOR OF PHILOSOPHY
IN
BIOTECHNOLOGY

BY
SHADAB ALI KHAN

UNDER THE GUIDANCE OF
DR. ABSAR AHMAD

DIVISION OF BIOCHEMICAL SCIENCES
NATIONAL CHEMICAL LABORATORY
PUNE-411 008
INDIA
OCTOBER, 2011

CONTENT

CERTIFICATE

This is to certify that the work discussed in the thesis entitled **"BIOSYNTHESIS OF OXIDES NANOPARTICLES USING MICROORGANISMS"** by **SHADAB ALI KHAN**, submitted for the degree of *Doctor of Philosophy in Biotechnology* was carried out under my supervision at the Biochemical Sciences Division of the National Chemical Laboratory, Pune, India. Such materials as have been obtained by other sources have been duly acknowledged in this thesis. To the best of my knowledge, the present work or any part thereof has not been submitted to any other University for the award of any other degree or diploma.

Date: **Dr. ABSAR AHMAD**

Place: (Research Guide)

DECLARATION BY THE CANDIDATE

I hereby declare that the thesis entitled **"Biosynthesis of Oxides nanoparticles using microorganisms"**, submitted to Pune University for the degree of ***Doctor of Philosophy in Biotechnology***, was carried out by me under the guidance of **Dr. Absar Ahmad** and has not formed the basis for the award of any degree, diploma, associateship, fellowship, titles in this or any other University or other institute of higher learning**.** I further declare that the material obtained from other sources has been duly acknowledged in the thesis.

Date: Signature of the Candidate

Place: **Shadab Ali Khan**

DEDICATED TO MY
BELOVED
PARENTS AND WIFE...

Acknowledgments

The heart, mind, body and soul are the ingredients to be put together to achieve the greater purpose in life. The completion of this thesis leads me to the last few lines of this beautiful story I have been a part of, and also marks the beginning of a whole new era in my life. I am very grateful to the **'Almighty'** for all that I have received throughout these years, starting right from the day I first entered National Chemical Laboratory, Pune, India to the day of completion of my thesis. My time spent here at N.C.L has overall shaped me as a person and has led me to where I am now.

The materialization of a dream begins with a teacher who believes in you, inspires you and pushes you towards your goals. My first and earnest gratitude goes to my research guide **Dr. Absar Ahmad** who has been a very wonderful teacher to me throughout, has encouraged me intensively and helped me to see life and science in their full depths, beyond the horizons of my own imagination. He has enlightened me through his wide knowledge in science and his deep intuitions have always guided me and kept me going through the darkest of the storms, in the hope of landing shore one day. His qualities of sacrifice, determination, courage, dedication, selflessness and perseverance will always be in my heart and will help me remain humble no matter where I reach tomorrow.

I sincerely thank **Mrs. Sabiha Absar** for considering me a part of their family and her numerous acts of kindness, which I will nurture, lifelong.

I am thankful to. Dr. (Mrs.) Vidya Gupta, Chairman, Division of Biochemical Sciences for her support and help during the research work and allowing me to work in Division of Biochemical Sciences, N.C.L.

I would also like to thank my PhD committee members Dr. C. G. Suresh and Prof. W. N. Gade, BCUD Director, University of Pune, Pune for their help, comments and suggestions.

I would also like to thank Dr. Sanjay Gambhir for radiolabelling and biodistribution studies at Sanjay Gandhi Post Graduate Institute of Medical Sciences (SGPGI).

I am grateful to Dr. Sourav Pal, Present Director and Dr. S. Sivaram, Ex Director, N.C.L. for giving me an opportunity to work in this institute and making the facilities available for carrying out my research work.

I acknowledge the Council of Scientific and Industrial Research (CSIR), New Delhi, Govt. of India for providing me Senior Research Fellowship (SRF) to pursue research at N.C.L.

I am also very thankful to my friends and lab mates for listening to the voice of my heart time and again. They have always been there for me, through thick and thin, connecting the dots of my life in various ways, filling in the void of my parents and family when away from home, and helping me to face each day as it comes, knowing that I have them watching my back if I fall. It was indeed a great pleasure in working with all of them and knowing each one of them more than what meets the eye.

You don't choose your family; it is bestowed upon you as God's wonderful gift. I am deeply thankful to my parents, brothers, sisters, in laws and relatives for being supportive throughout my work. My heart reaches out to them for motivating me at each and every step of my life and providing me with love and affection, a million times more than I could have ever asked for.

Last but not the least, a heartfelt thanks to my wife **Arshi** without whom I would be a very different person today and it would have certainly been much harder to finish my PhD. Learning to love her and receive her love makes me a better person.

ABBREVIATIONS

$GdCl_3$	Gadolinium chloride
$CeN_3O_9.6H_2O$	Cerium (III) nitrate hexahydrate
Gd_2O_3	Gadolinium oxide
CeO_2	Cerium Oxide
TiO2	Titanium dioxide
SiO2	Silica dioxide
2DE	Two dimensional electrophoresis
IEF	Isoelectric focussing
UV-vis	Ultraviolet-visible spectroscopy
PL	Photoluminescence
TEM	Transmission electron microscope
HR-TEM	High resolution transmission microscope
SAED	Selected area electron diffraction
XRD	X-ray diffraction
FTIR	Fourier transform infrared spectroscopy
EDAX	Energy dispersive analysis of x-rays
TGA	Thermogravimetric analysis
DTA	Diffrential thermo analysis
XPS	X-ray photoelectron spectroscopy
NADPH	Nicotinamide adenine dinucleotide phosphate reduced tetra sodium salt
BSA	Bovine serum albumin
EDC	1-Ethyl-3-(3-dimethylaminopropyl)-carbodiimide
HPLC	High performance liquid chromatography
FPLC	Fast protein liquid chromatography
EDTA	Ethylene diamine tetra acetic acid
HEPES	4-(2-hydroxyethyl)-1-piperazineethanesulfonic acid
kDa	Kilo dalton
MES	2 (N-Morpholino) ethanesulfonic acid
NTEE	3-nitro-L-tyrosine ethylester
SDS	Sodium dodecyl sulfate
SDS-PAGE	Sodium dodecyl sulfate polyacrylamide gel electrophoresis

ABSTRACT

Nanotechnology involves the synthesis and/or manipulation of materials at the nanometer scale either by scaling- up from single groups of atoms or by refining or reducing bulk materials. Comprehension of metal nanoparticles exotic physicochemical and optoelectronic properties, and organization of nanoscale structures into predefined superstructures promise to play an increasingly important role in innovative technologies.

Recently, biological methodologies are considered highly promising for nanomaterial synthesis because of eco-friendly approaches alternative to the usual chemical methods. The biomimetic and biomineralization procedures, besides following the green chemical regulations for nanoscale material synthesis are supposed to yield novel and complex structural entities as compared to the conventional methods. Until now, researchers have been successful in obtaining a number of inorganic metal nanoparticles using microorganisms quite efficiently and to some extent started gaining access to design strategies to develop protocols to obtain nanomaterials of desired shape and size. Researchers also started deciphering the mechanistic aspect of formation of inorganic metal nanoparticles which are atleast easy to follow during their course of reaction with microorganisms such as gold nanoparticles. Despite all these efforts in the direction of biological synthesis of nanomaterials, one area which is still least explored or seldom encountered in literature is the green synthesis of oxide nanoparticles. Currently physico-chemical protocols for the synthesis of oxide nanomaterials involve high temperatures, toxic chemicals and harsh environmental condition, thus proving eco-unfriendly, whereas their biological counterparts have shown a great promise to overcome all these deficits.

The present investigation details the study of such biosynthetic routes/protocols for the synthesis of natural protein capped, water dispersible and biomedically important oxide nanoparticles such as Gd_2O_3 and CeO_2 using the fungus *Humicola* sp. Protein capped Gd_2O_3 nanoparticles were then functionalized and conjugated to the anticancer drug taxol and this nano-bioconjugate has shown an enhanced potency in killing cancer cells when incubated with THP-1 cell lines rather than taxol alone, thus creating new avenues in nanosized drug delivery applications. Another mesophilic fungus *Fusarium oxysporum* was then used to obtain silica (SiO_2) nanoparticles through bioleaching of waste material such as fly-ash. *Humicola* sp. once again was

employed to obtain TiO_2 nanoparticles using top-down approach. The fungus *Humicola* sp. not only showed a great potential in biomilling of bulk TiO_2 to nanosize TiO_2 but was also able to biotransform the shape and phase of TiO_2 nanoparticles. Finally, in the last working section of the thesis an attempt has been made for the elucidation of mechanism of formation of gold nanoparticles. Sulphite reductase enzyme and organic capping molecule were purified to homogeneity from an actinomycete *Thermomonospora* sp. and employed for the *in vitro* synthesis of gold nanoparticles. Sulphite reducatse enzyme has been shown to reduce gold metal ions resulting in the subsequent formation of gold nanoparticles whereas the capping molecule has been shown to provide stability to gold nanoparticles without which nanoparticles tend to aggregate.

List of Publications

1. Absar Ahmad, Tushar Jagadale, Vivek Dhas, **Shadab Khan**, Shankar Patil, Renu Pasricha, Venkat Ravi, Satishchandra Ogale, ***Advanced Materials***, 2007, 19, 3295–3299.

2. Baishakhi Mazumder, Imran Uddin, **Shadab Khan,** Venkat Ravi, Kaliaperumal Selvraj, Pankaj Poddar,Absar Ahmad, ***J. Mater. Chem.*,** 2007, 17, 3910–3914.

3. **Shadab khan** and A. Ahmad, Extra cellular biosynthesis of Gd_2O_3 and CeO_2 nanoparticles using the thermophilic fungus *Humicola* sp., conjugation and application in Parkinson's disease. (will be communicated shortly)

4. **Shadab khan**, Absar Ahmad, Phase, Size and Shape Transformation by Fungal Biotransformation: From Micron Size Anatase to Nanosize Brookite TiO_2. (will be communicated shortly)

5. **Shadab khan** and A. Ahmad, Purification of thermostable sulfite reductase and capping protein from *Thermomonospora* sp. and *In vitro* enzyme mediated synthesis of highly monodispersed gold nanoparticles. (will be communicated shortly)

CHAPTER 1

General Introduction

Summary

This chapter deals with the basic introduction of nanotechnology and brief history of nanoscience and nanotechnology. It also discusses the major properties of nanoparticles and various synthesis methods available for nanoparticles production. The chapter then emphasizes on a brief introduction on oxide nanomaterials. This is followed by a review of the literature on biological synthesis of metal and metal oxide nanoparticles. In the penultimate section of the chapter, mechanistic aspects of biological synthesis of nanoparticles have been enlightened. Finally, a chapter - wise outline of the work done in this thesis has been presented.

1.1 History

Human civilizations are often divided into ages according to the materials that dominate the society. In the Stone Age when the tools were largely made of stones, people used those simple stone tools to improve their lifestyle and advanced their civilization. In the Bronze Age, when most tools were made of bronze, a number of technological innovations were fostered that eventually altered the landscape of the civilization, making the Stone Age obsolete. In the Iron Age, when the processing of iron was discovered, society advanced tremendously. Many new tools were built so that rapid transportation became possible. People then explored many lands and seas. We have entered the modern *materials age,* the *plastic age* in the last half of the 20^{th} century and the *silicon age* in the last quarter of the 20^{th} century continuing to this day. These new materials have fundamentally transformed our lifestyle forever and have made a vast world into a global village. It is believed that the "*Designed Materials*" [1] will likely play a role in constructing and processing the future composite and integrated materials. This will be achieved both through discovering nature's designs that have evolved from eons of selection, and through knowledge-based designs. These materials will again undoubtedly transform our civilizations as we know it today. These new materials will be the foundation for future generations of the "Designed Materials Age".

The Designed Materials Age requires new knowledge to build advanced materials. One of the approaches is through molecular self - assembly. Molecular self - assembly is ubiquitous in nature. It has recently emerged as a new approach in chemical synthesis, nanotechnology, polymer science and engineering. Molecular self assembly systems lie at the interface of molecular and structural biology, protein science, chemistry, polymer science and engineering. Molecular self assembly systems represent a significant advancement in the molecular engineering of simple molecular building blocks useful for a wide range of applications. Development of new materials and technologies often broaden the questions we can address, therefore, deepening our understanding of seemingly intractable phenomena. Molecular self - assembly systems will undoubtedly create a new class of nanomaterials at the molecular level, where dimensions are in the range of one billionth of a meter. Nanoscience refers to the study of phenomena which occur at the nanoscale dimensions, on the order of a small molecule, much smaller than the width of a single

strand of hair. When system dimensions approach the nanoscale, some very unique and potentially useful properties emerge. Nanotechnology takes advantage of these fundamental changes of physical properties.

Nanotechnology is being heralded as the next enabling technology that will redesign the future of several technologies, products and markets. It is drawing intense interest and will replace most of the existing technology in use today. It is widely publicized to be an important technology that is going to change every aspect of our lives and lead to generation of new capabilities, new products and new markets. Nanotechnology is a broad and interdisciplinary area of research and has the potential for revolutionizing the ways in which materials and products are created and the range and nature of functionalities that can be accessed. Nanotechnology is concerned with materials and systems whose structures and components exhibit novel and significantly improved physical, chemical and biological properties, phenomena and processes due to their nanoscale size. The goal is to exploit these properties by gaining control of structures and devices at atomic, molecular and supramolecular levels and to learn to efficiently manufacture and use these devices. Maintaining the stability of interfaces and integration of these "nanostructures" at micron-length and macroscopic scales are all keys to success. New behavior at the nanoscale is not necessarily predictable from that observed at large size scales. The most important changes in behavior are caused not by the order of magnitude size reduction but by newly observed phenomena, intrinsic to or becoming predominant at the nanoscale. These phenomena include size confinement, predominance of interfacial phenomena and quantum mechanics.

Nanotechnology and nanoengineering stand to produce significant scientific and technological advances in diverse fields. Nanotechnology typically refers to a technology at or close to the atomic level. At the nanoscale, materials are known to possess special properties, meaning that by controlling the arrangement of molecules at the nanoscale, it may be possible to create new materials with fundamentally new physical properties. Very simply, through nanotechnology, it is possible to manipulate discrete atoms to achieve desired results, for example, to design new materials with desired properties such as drugs, polymers, membranes etc with desired properties. If even a fraction of its promise is realized, nanotechnology could yield new products and processes that may make a profound impact on our daily lives and may lead to a more sustainable technological and social development.

Over the last few years, the scientific and engineering communities have been witnessing an impressive progress in the field of nanoscience and nanotechnology. Nanotechnology deals with small structures and small-sized materials of dimensions in the range of a few nanometers to less than a 100 nanometers. The unit of nanometer derives its prefix *nanos* from a Greek word meaning extremely small. One nanometer (10^{-9} of a meter) is roughly the length occupied by five silicon or ten hydrogen atoms aligned in a line. In comparison, the hydrogen atom is about 0.1nm, a virus may be about 100 nanometers, a red blood corpuscle approximately 7,000 nanometers in diameter and an average human hair is 10,000 nanometers wide.

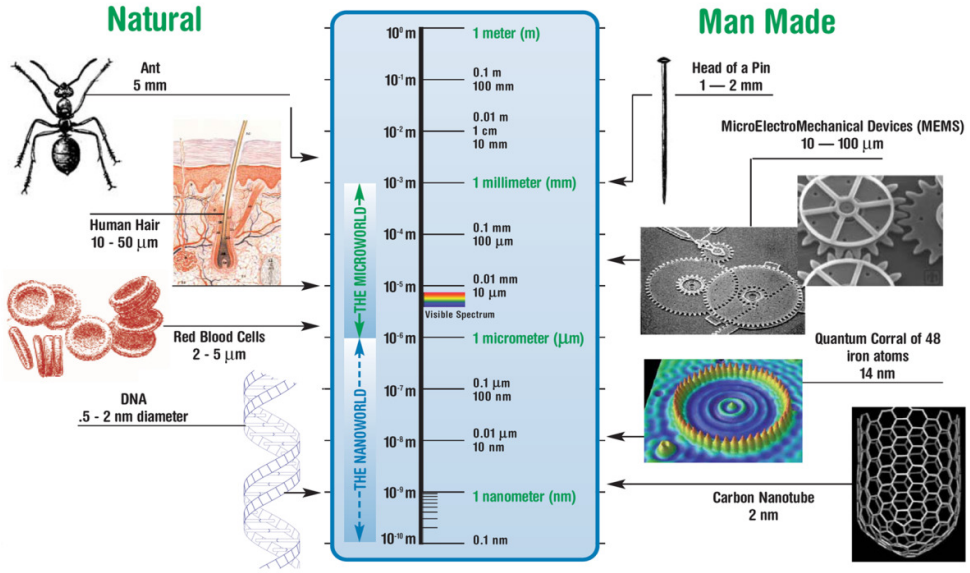

Figure 1: *Representation of the relative sizes of various naturally occurring objects/species and man-made materials. Courtesy: Josh Wolfe's report on Nanotechnology, www.forbeswolfe.com.*

1.2 What is Nanoscience and Nanotechnology?

"Nanoscience" is the study of phenomena exhibited by materials at atomic and molecular level of dimensions ranging from a few nanometers to less than a 100 nanometers. In chemistry, this range of sizes has been associated with colloids, micelles, polymer molecules and similar structures such as very large molecules or aggregates of many molecules. In physics and electrical engineering, nanoscience is most often associated with quantum behavior and the behavior of electrons in nanoscale structures. Biology and biochemistry have also been deeply associated with nanoscience as components of the cell; most interesting structures of biology such as DNA, RNA and subcellular organelles can be considered as nano structures [2].

"Nanotechnology" is the application of science to control matter at the molecular level. At this level, the properties are significantly different from that of bulk materials. It is also referred to as the term for designing, characterization, production and application of structures, devices and systems by controlling shape and size at nanometer scale [3].

In other words, nanoscience and technology is a field that focuses on (i) the development of synthetic methods and surface analytical tools for building structures and materials, (ii) to understand the change in chemical and physical properties due to miniaturization, and (iii) the use of such properties in the development of novel and functional materials and devices. Nanoscience offers an exciting possibility to study a state of matter, which is intermediate between bulk and isolated atoms or molecules, as well as the effect of spatial confinement on electron behavior. It has been well known that living cells are the best examples of machines that operate at the nano level and perform a number of jobs ranging from generation of energy to extraction of targeted materials at very high efficiency [4]. The ribosomes, histones and chromatin, the Golgi apparatus, the interior structure of the mitochondrion, the photosynthetic reaction center and the fabulous ATPases that power the cell are all nanostructures, which work quite efficiently. Ancient Indian medicinal system *Ayurveda* has been using gold in different formulations for curing acute diseases such as rheumatoid Arthritis. With present day understanding of nanoscience, one can unambiguously get enlightened that these formulations contained gold nanoparticles. Thus, the fusion of ancient wisdom and present understanding of nanoscience can impart more light on future development of medical sciences. The area of research in the field of nanotechnology is as diverse as physics, chemistry, material science, microbiology, biochemistry and also molecular biology. The interface of nanotechnology in combination with biotechnology and biomedical engineering is emerging by the use of nanoscale structures in diagnosis, gene sequencing, and drug delivery. Nanotechnology holds promise for enabling us to learn more about the detailed operation of individual cells and neurons, which could help us to re-engineer living systems.

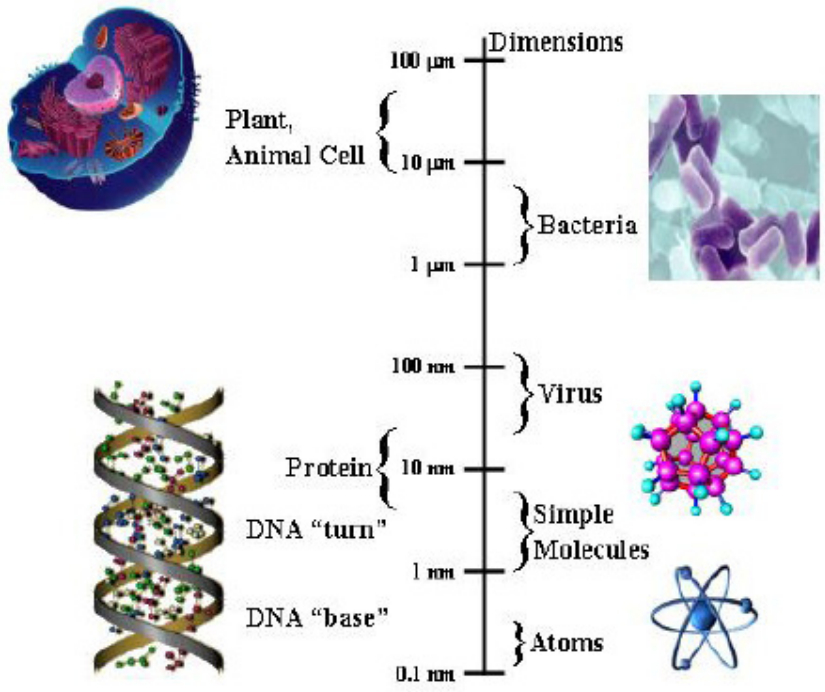

Figure 2: *Representation of the relative sizes of various biomolecules* (source perdue university press release http://www.beyondpesticides.org/dailynewsblog.

The wavelike properties of electrons inside matter are influenced by variations on the nanometer scale. It is possible to vary fundamental properties of materials (e.g. melting temperature, magnetization, and charge capacity) without changing the chemical composition by patterning matter on the nanometer length scale. Life works at the nanometer scale. The systematic organization of matter on the nanometer length scale is a key feature of biological systems. Nanotechnology promises to allow us to place artificial components and assemblies inside cells, and to make new materials using the self-assembly methods of nature. This is a powerful new combination of material science and biotechnology. By virtue of their size, nanoscale components have very high surface areas. Thus, they are ideal for use in composite materials, reacting systems, drug delivery, solar cells and energy storage. The finite size of material entities, as compared to the molecular scale determines an increase of the relative importance of surface tension and local electromagnetic effects, making nanostructured materials harder and less brittle. The interaction wavelength scales of various external wave phenomena become comparable to the material entity size, making materials suitable for various opto-electronic applications. A remarkable aspect of nanomaterials is that a number of factors can influence their physical,

chemical, optical, electronic and magnetic properties. The factors that can strongly modulate their properties include their size, shape, surface composition, dielectric environment and the interparticle interactions. Such remarkable variations in properties of nanomaterials are due to their dimensions being comparable to the de Broglie's wavelength of the charge carriers, which modify their properties significantly. One of the readily perceptible properties in case of metal nanoparticles is their color. The color of metal nanoparticles originates due to their surface plasmons *i.e* the coherent charge density oscillations. Surface plasmon is a special phenomenon, which is observed in metal nanoparticles at nanoscale. It has been found that the size and shape of nanocrystals are key factors for the determination of their unique chemical and physical properties. Bulk materials have their own characteristics and innate properties such as color, phase transition, temperature and band-gap energy. However, nanocrystalline materials no longer retain such bulk properties and exhibit unprecedented novel phenomena associated with nanoscale dimensions. Similarly, when the size of other nanomaterials is below certain size regime (generally few nanometers), size quantization effects become more important, leading to discrete energy levels in the conduction band and can be understood by making analogy with the case of 'particle- in - a box' model. The quantum size effects have been well studied in case of semi conducting nanoparticles and the energy level spacing for a spherical particle of radius 'R' is predicted to be inversely proportional to R^2. Thus, with decreasing size, the effective band gap increases and the relevant absorption and emission spectra - blue shifts. As a consequence, the developments, which were initially concerned with metal nanoparticles led to the realization that essentially all solid materials in nanoscale would be of interest. To explore the novel physical properties and the potential applications of nanostructures and nanomaterials is the first cornerstone in nanotechnology. Nanomaterials are the leading edge to the rapidly developing field of nanotechnology. Their unique size - dependent properties make these materials superior and indispensable in many areas of human activity. Thus, nanoparticles are of scientific interest as they are effectively a bridge between bulk materials and atomic or molecular structures.

1.3 Methods of Nanoparticle fabrication

The nanometer scale is the regime where two complementary approaches to fabricate incredibly small objects meet:

a) Top-down approach

b) Bottom-up approach

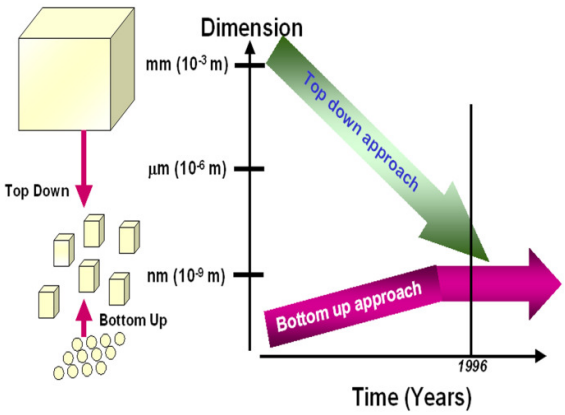

Figure 3: *Methods of Nanoparticle fabrication* [5].

Top-down methods involve starting with a block of material and etching or milling it down to the desired shape and size. The best known example of top-down approach is the photolithography technique used in semiconductor industry to create integrated circuits by etching patterns of silicon wafers. The metal is chiselled out selectively using high energy beam to obtain desired patterns onto silicon substrate. The main challenge for top down manufacture is the creation of increasingly small structure with sufficient accuracy that is the imperfection of surface structure. It can cause significant crystallographic damage to processed pattern and additional defects may be introduced during etching steps. Such imperfections would have a significant impact on the physical properties and surface chemistry of nanostructures and nanomaterials. Regardless of the surface imperfections and other defects, top-down method continues to play an important role in the synthesis and fabrication of nanostructures and nanomaterials.

Bottom-up methods involve the assembly of smaller subunits, atoms or molecules to make a larger structure. It is the atom - by - atom which assembly begins by designing and synthesizing custom- made molecules that have the ability to self - organize into higher order mesoscale and macroscale structure. One example of such an application includes novel drug delivery system using nanoparticles or highly porous self-assembly bilayer tubule system. Another class of application being developed is chemically functionalized dendrimers which are highly branched molecules. The main challenge for bottom-up approach is to make structures large enough and of sufficient

quality to be of use as materials. However, the fascinating consequence of the size and defect dependent applicability of nanomaterials is that the properties of nanocrystals obtained by various routes cannot be generalized, since various synthesis routes may lead to altering defect conditions in these nanocrystals. The display of unique properties by the nanoparticles that can be controlled by many external and internal factors and the scope for diverse applications makes the synthesis of such nanomaterials extremely important and therefore a number of routes for synthesis of nanomaterials are evolving.

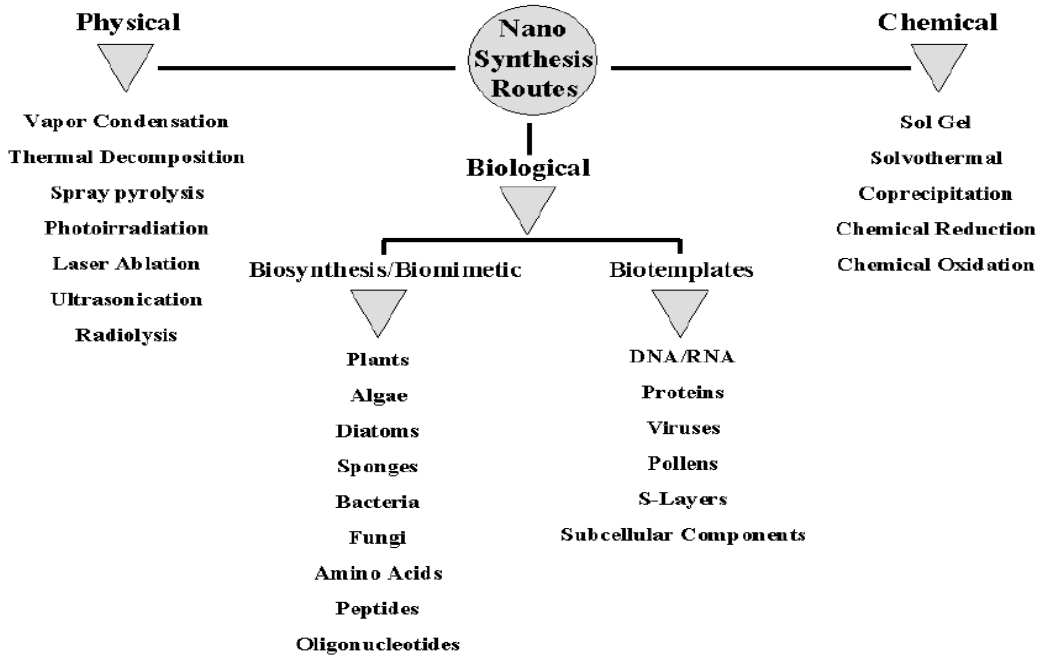

Figure 4: *A schematic outline of nanoparticle synthesis approaches*

1.4 Properties of Nanoparticles

During the course of the miniaturization, it has been observed that materials exhibit some exotic properties in the nanometer regime, which are significantly different from their bulk counterparts. The following are the changes in the properties of the metals of nanometer size.

1.4.1 Size and shape dependent catalytic properties

As the particle size decreases, the fraction of surface atoms significantly increases. For example, a 3 nm particle would have 45% of its atoms on the surface and a 1 nm

particle would have 76% of the atoms on its surface. As any reaction takes place at the surface and the high percentage of surface atoms in metal nanoparticles viable them as good catalysts, the shape of the nanoparticles along with their size influences the surface reactivities. The reactant molecules show differential affinity in absorption towards different faces of the catalyst. Hence metal nanoparticles of different shapes covered by different faces could be used to increase the selectivity of a catalyst. Hence surface reactivity can be a tailored catalyst. The surface reactivity can be tailored in such a way that by varying the shape of the nanoparticles, designing molecular specific catalysis would be possible.

1.4.2 Mechanical properties

Mechanical properties of a material depend strongly on the density of dislocations, grain size and the surface / interface-to-volume ratio. The strength and hardness of the material could be severely affected if there is any decrease in grain size. As compared to the bulk, a nanoparticle has more defects due to the high surface - to - volume ratio. However, the capability of a nanomaterial to undergo extensive tensile deformation without destroying the structure is well reported and is called super plasticity.

1.4.3 Magnetic Properties

The magnetic properties of nanoparticles differ from those of bulk in two ways. The large surface to volume ratio results in a different local environment for the surface atoms in their magnetic coupling or interaction with neighboring atoms, leading to the mixed volume and surface magnetic characteristics. Unlike bulk ferromagnetic materials which usually form multiple magnetic domains, several small ferromagnetic particles could consist of only a single magnetic domain. In case of a single particle being a single domain, super-paramagnetism occurs, in which the magnetizations of the particles are randomly distributed and are aligned only under an applied magnetic field. The alignment disappears once the external field is withdrawn. For example, these could have important implications in ultra-compact information storage where the size of the domain determines the limit of storage density.

1.4.4 Electronic properties

Metal nanoparticles when embedded between metal–insulator, metal junction or between the tip of STM and an electrode show a differential capacitance or charging

at low temperatures even at zero bias. This effect is called "Coulomb blockade" or "Coulomb staircase effect". It was realized that this behavior is caused by the extremely small capacitance of metal nanoparticles. These particles can store charge by addition or removal of electrons. Due to its low capacitance, nanometer sized metallic particles are extremely sensitive to neighbouring charges and therefore, could be useful as sensor materials.

1.4.5 Optical Properties

The optical properties of these nanoparticles are spectacular and therefore have stimulated a great deal of excitement during the last few decades. The color variations arising from changes in the composition, size and shape of nanoparticles, surrounding medium and the very high absorption cross-section have promoted these materials as inorganic chromophores from visible to near infrared region. Due to this reason, they find applications as sensor and imaging agents. These effects are due to the phenomena called "surface plasmon resonance", the frequency at which conduction electrons oscillate in response to the alternating electric field of incident electromagnetic radiation. This phenomenon was explained by Mie, based on the Maxwell equations on scattering. However, only gold, silver and copper nanoparticles possess plasmon resonances in the visible spectrum, which give rise to such intense colors. A nanoparticle is a complicated system of many electrons, where the confinement of electronic motion due to the reduction in size leads to fascinating new effects, potentially tunable with particle size and shape.

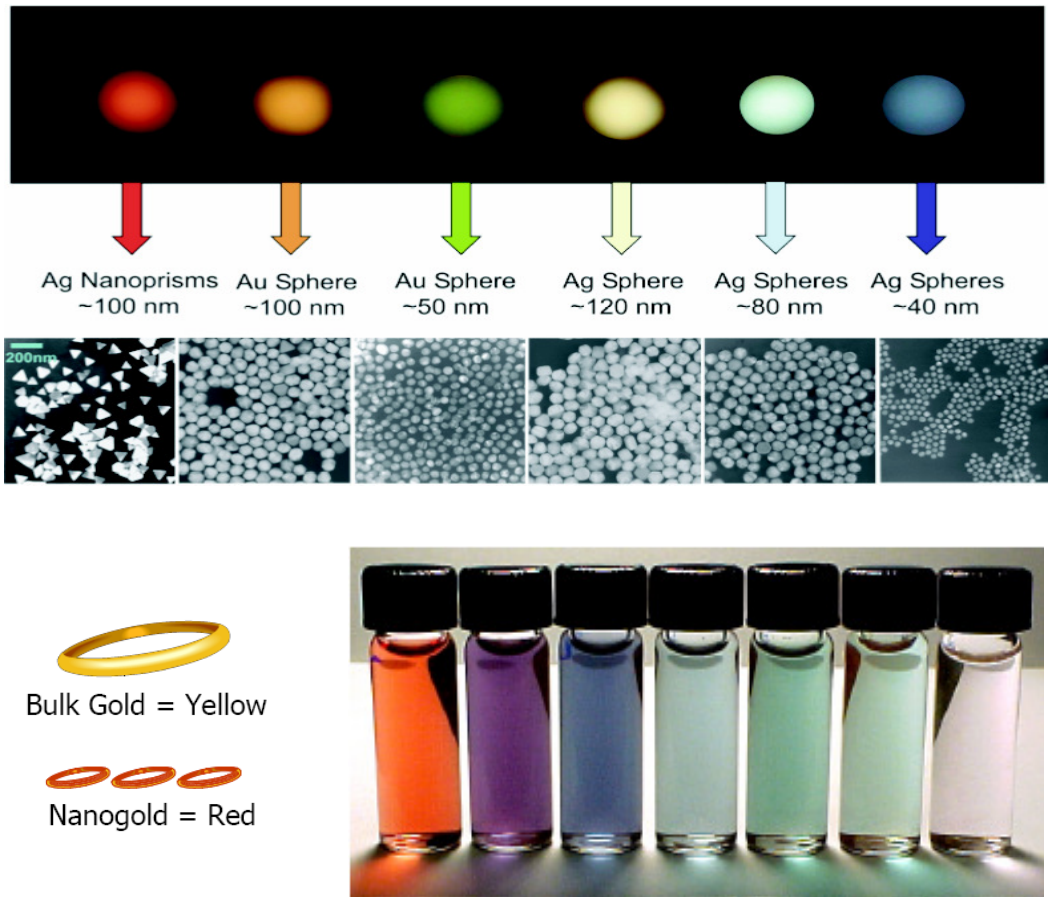

Figure 5: *Different colors of nanogold and nano silver due to difference in size of nanoparticle and the colour of bulk and nanogold. http://planck.cos.ucf.edu/webpage/Page383.htm Picture Courtesy: Northwestern University.*

1.4.6 Surface Plasmon Resonance

Free electrons and the cationic cores in a bulk metal form a plasma state. These free electrons can set into oscillations relative to the cationic lattice when it interacts with light i.e. electromagnetic radiation. Since the order of penetration depth of electromagnetic waves in metals falls in the nanometer range, it polarizes or displaces the surface electrons from its equilibrium position. The Columbic attractions between the cationic lattice and electrons then acts as a restoring force to bring back the electron cloud to the equilibrium position. In this manner, a dipolar oscillation of electrons is created (called plasma oscillation) with a certain frequency called plasmon frequency.

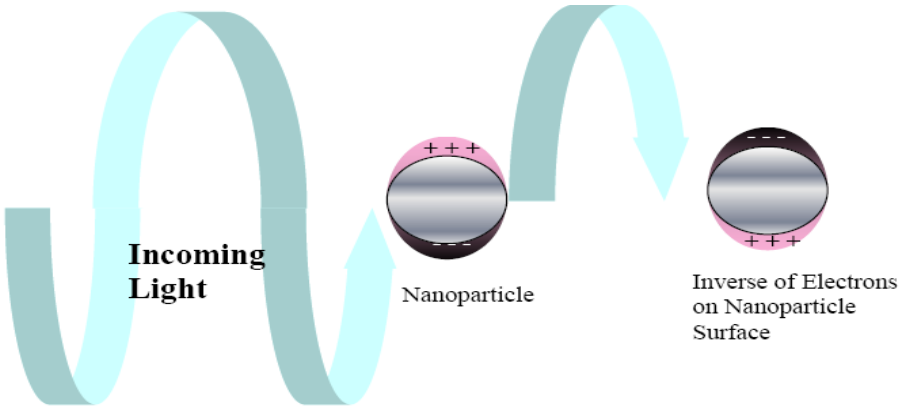

Figure 6: *Origin of Surface Plasmon Resonance (SPR) due to coherent interaction of the electrons in the conduction band with electromagnetic field* [6].

In a bulk metal, the electrons are free and unbound, thus can absorb any amount of energy. When the size of the particle is decreased below the mean free path of the electron, it gives birth to the surface plasmon resonance at visible frequencies in the case of gold, silver and copper nanoparticles. The surface plasmon resonance is a collective excitation mode of the plasma localized near the surface. However, the resonance frequency of the surface plasmon is different from an ordinary plasma frequency. If the frequency of the excitation light field is in resonance with the frequency of this collective oscillation, even a small exciting field leads to a strong oscillation.

1.5 Emergence of Nanotechnology

The first so-called scientific study of nanoparticles took place way back in 1831, when Michael Faraday investigated the ruby red colloids of gold and made public that the color was due to the small size of the metal particles. Gold and silver have found their way into glasses for over 2000 years, usually as nanoparticles. They have most frequently been employed as colorants, particularly for church windows. Until 1959, nobody had thought of using atoms and molecules for fabricating devices. Its first revision was by Nobel Laureate Physicist Richard Feynman in his famous lecture entitled “There is plenty of room at the bottom”. It was much later in 1974 that Norio Taniguchi, a researcher at the University of Tokyo (Japan), used the term “nanotechnology” while engineering the materials precisely at the nanometer level. The primary driving force for miniaturization at that time came from the electronics industry, which aimed to develop tools to create smaller electronic devices on silicon

chips of 40–70 nm dimensions. The use of this term "nanotechnology" has been growing to mean a whole range of tiny technologies, such as material sciences, where designing of new materials for wide-ranging applications are concerned; to electronics, where memories, computers, components and semiconductors are concerned; to biotechnology, where diagnostics and new drug delivery systems are concerned.

1.6 Bio-based approaches for nanomaterial synthesis

Optoelectronic, physicochemical and electronic properties of nanoparticles are determined by their size, shape and crystallinity. Therefore, the synthesis of monodispersed nanoparticles with different size and shape has been a challenge in nanotechnology. Although various physical and chemical methods are extensively used to produce monodispersed nanoparticles, the stability and the use of toxic chemicals is the subject of paramount concern. The use of toxic chemicals on the surface of nanoparticles and non-polar solvents in the synthesis procedure limits their applications in clinical fields. Therefore, development of clean, biocompatible, non-toxic and eco friendly methods for nanoparticles synthesis deserves merit. Although biological methods are regarded as safe, cost-effective, sustainable and environment friendly processes, they also have some drawbacks in culturing of microbes, which is time-consuming and difficult in providing better control over size distribution, shape and crystallinity. The biological nanoparticles are also not monodispersible and the rate of production is slow. These are the problems that have plagued the biological synthesis approaches, but the insights gained from strain selection, optimizing the conditions such as pH, incubation temperature and time, concentration of metal ions and the amount of biological material has come up to give hope in implementation of these approaches in large scale and commercial applications. There are also the possibilities of producing genetically engineered microbes that over - express specific reducing agents and thereby, controlling the size and shape of biological nanoparticles. The combinatorial approach such as photo- biological methods as proved in the case of *Fusarium oxysporum*-mediated silver nanoparticles production [7], will help to increase the rate of production. While exploring the natural secrets for the synthesis of nanoparticles by microbes, which are regarded as potent eco-friendly green nanofactories, scientists have discovered magnetite particles by magnetotactic bacteria [8, 9], siliceous materials by diatoms [10], and gypsum and calcium layers by

S-layer bacteria [11]. Interactions between metals and microbes have been exploited for various biological applications in the fields of bioremediation, biomineralization, bioleaching, and biocorrosion [12] and the microbial synthesis of nanoparticles has emerged as a promising field of research as "nano-biotechnology", thereby interconnecting biotechnology and nanotechnology. Recently a range of inorganic nanomaterials have been synthesized as fast as the chemical methods using plant extracts in order to overcome the above microbial syntheses.

1.6.1 Intracellular synthesis of nanoparticles by bacteria

Microbes produce inorganic materials either intra- or extracellularly, often in nanoscale dimensions with exquisite morphology. Microbial resistance to most toxic heavy metals is due to their chemical detoxification as well as due to energy-dependent ion-efflux from the cell by membrane proteins that function either as ATPase or as chemiosmotic cation or proton anti-transporters. Alterations in solubility also play a role in microbial resistance [13, 14]. Therefore, microbial systems can detoxify the metal ions by either reduction and/or precipitation of soluble toxic inorganic ions to insoluble non-toxic metal nanoclusters.

In order to release the intracellularly synthesized nanoparticles, additional processing steps such as ultrasound treatment or reaction with suitable detergents are required. This can be exploited in the recovery of precious metals from mine wastes and metal leachates. Biomatrixed metal nanoparticles could also be used as catalysts in various chemical reactions [15]. This will help to retain the nanoparticles for continuous usage in bioreactors. For some years now, bacterial activity has been implicated in deposition of mineral ores. Pedomicrobium-like budding bacteria in the Alaskar placer, reported in iron and manganese oxide deposition process has now been found to accumulate gold [16]. *Bacillus subtilis* 168 reduced Au^{+3} ions to Au^{0} intracellularly producing octahedral morphology in the dimensions of 5-25 nm [17, 18]. Interestingly, heterotrophic sulfate-reducing bacterial (SRB) enrichment from a gold mine was used to destabilize gold (I)-thiosulfate complex ($Au(S_2O_3)_{23}^{-}$) to elemental gold (10 nm) in the bacterial envelope, releasing H_2S as end product of metabolism [19]. In Fe (III) reducing bacterium, *Geobacter ferrireducens*, gold was precipitated intracellularly in periplasmic space [20]. Similarly, in anaerobic conditions, in the presence of hydrogen gas, iron (III)-reducing mesophilic bacterial resting cells, *Shewanella* algae reduced Au^{+3} ions at 25°C with 10- 20 nm in periplasmic space

(pH 7.0) and with 15-200 nm on bacterial surfaces (pH 2.8) [21].*Escherichia coli* DH5α mediated bioreduction of chloroauric acid to Au^0 nanoparticles has been reported recently [22]. Similarly, the bioreduction of trivalent aurum was also reported in photosynthetic bacterium *Rhodobacter capsulatus*, which showed biosorption capacity of 92.43 mg $HAuCl_4$/g dry weight in the logarithmic phase of its growth [23]. Silver-based single crystals such as equilaterals, triangles and hexagons with particle sizes upto 200 nm in periplasmic space of the bacterium were produced by *Pseudomonas stutzeri* AG259, a silvermine bacterium. This bacterium also produced a small number of monoclinic crystalline α-form silver sulfide acanthite (Ag_2S) crystallite particles with the composition of silver and sulfur in the ratio of 2:1 [24, 25]. Biosorption and bioreduction of Ag (I) on cell surface was also reported in *Lactobacillus* sp. A09 at 30°C, pH 4.5 in 24 h [26]. Kalathil *et al.* have employed electrochemically active biofilm for the extracellular production of silver nanoparticles in water, using $AgNO_3$ as precursor and sodium acetate as an electron donor. The electrochemically active bacteria present on the anaerobic biofilm act as a catalyst to oxidise the sodium acetate by producing electrons for the reduction of Ag^+ ions [27]. *Streptomyces aureofaciens* has recently been used for the production of silver nanoparticles. Scanning electron microscopy (SEM) analysis confirmed that silver nanoparticles were deposited in the periplasmic space of the bacterial cells [28]. Dried cells of *Corynebacterium* sp. SH09 produced silver nanoparticles at 60°C in 72 h on the cell wall in the size range of 10-15 nm with diamine silver complex $[Ag(NH_3)_2]^+$ [29]. Silver precipitating peptides (AG3 and AG4) were found to have the capacity to precipitate silver from aqueous solution of silver ions and form face-centered cubic (fcc) structured silver crystals [30]. Recently, an airborne *Bacillus* sp. isolated from the atmosphere was also found to reduce Ag^+ ions to Ag^0 [31].Some bacteria have been reported for the production of more than one nanoparticle and bimetallic alloys. Nair and Pradeep [32] found that *Lactobacillus* sp. in buttermilk produced microscopic gold, silver, and gold–silver alloy crystals of well defined morphology within the cell with no disturbance in its viability. Intracellular synthesis of gold and silver nanoparticles by *B. subtilis*, sulfate-reducing bacteria, *Shwenella algae*, *E. coli, R. capsulatus*, *Lactobacillus* sp. and by *P. stutzeri*, *Corynebacterium* sp. , *Bacillus* sp. , and *Lactobacillus* sp. showed different morphologies such as cubic, hexagonal and spherical-hexagonal in the size range of 5-200 nm. *Stenotrophomonas maltophilia* SELTE02, a strain isolated from the rhizospheric soil of *Astragalus*

bisulcatus, which is a selenium hyperaccumulator legume, showed promising transformation of selenite $(SeO_3)^{-2}$ to elemental selenium $(Se)^0$; accumulating selenium granules either in the cell cytoplasm or in the extracellular space [33]. In addition, a facultative anaerobic bacterium *Enterobacter cloacea* SLD1a-1 [34], a purple non-sulfur bacterium *Rhodospirullum rubrum* in oxic and anoxic conditions [35] and *Desulfovibrio desulfuricans* [36] have also been found to bioreduce selenite to selenium , both inside and outside the cell with various morphologies like spherical, fibrillar and granular or with small atomic aggregates. *E. coli* also deposited elemental selenium both in periplasmic space and cytoplasm [37, 38] and *P. stutzeri* also aerobically reduced selenite to elemental selenium [39]. Under aerobic conditions, Hunter and Manter [40] reported a bacterial strain *Tetrathiobacter kashmirensis*, which bioreduced selenite to elemental red selenium. A 90-kDa protein present in the cell-free extract was believed to be responsible for this bioreduction. Recently, Yadav *et al*. [41] showed that *P. aeruginosa* SNT1 isolated from rhizospheric seleniferous soil also biosynthesized nanostructured selenium by biotransforming selenium oxyanions to spherical amorphous allotrophic elemental red selenium, both intracellularly and extracellularly. When growth-decoupled, resting cells of metal ion reducing bacteria *Shwenella* alga were incubated anaerobically in aqueous solution of H_2PtCl_6 at room temperature and neutral pH, they reduced $PtCl_6^{-2}$ ions within 60 min in the presence of lactate as the electron donor to metallic platinum, changing the color from pale yellow to black [42]. Yet another platinum group metal nanoparticle was produced by sulfate-reducing bacterium, *Desulfovibrio desulfuricans* NCIMB 8307. This bacterium anaerobically bioreduced and biocrystallized palladium $(2)^+$ ions to palladium nanoparticles on the surface of cells in the presence of exogenous electron donor as formate within minutes at neutral pH [43]. De Windt *et al*. [44] also showed that another iron-reducing bacterium *S. oneidensis* MR-1 in the presence of formate as the electron donor reduced Pd(II) to Pd(0) nanoparticles on the cell wall and inside the periplasmic space by changing the color of the biomass to black. Metal semiconductor nanocrystals have wide spread applications in various fields of research, particularly in biomedical fields. Cunningham and Lundie [45] demonstrated that within 24-48 h after the addition of $CdCl_2$ and 0.05% cysteine hydrochloride, *Clostridium thermoaceticum* in late-exponential to early-stationary phase, precipitated bright yellow CdS crystals on the surfaces of the cells as well as in the medium. Here, desulfhydration of cysteine was

the source of sulfide for CdS precipitation by cysteine desulfhydrase activity and in a similar process, Smith *et al.* [46] produced "bio-semiconductor" CdS nanoparticles in the size range of 5-200 nm on the cell surface of *Klebsiella pneumoniae*. These "Bio-CdS" possessed the optical and photoactive traits analogous to the chemically synthesized CdS. A few years ago, Sweeney *et al.* [47] showed that *E. coli* can also intracellularly accumulate semiconductor nanocrystals composed of wurtzite crystals in the size range of 2-5 nm with spherical and elliptical shapes when incubated with $CdCl_2$ and sodium sulfide. The production of nanocrystal was 20-fold higher when *E. coli* cells were grown in stationary phase as compared to late logarithmic phase. It was also found that spherical aggregates of 2- 5nm diameter sphalerite (ZnS) particles were formed within the natural biofilms dominated by aerotolerant, sulfate-reducing bacteria of the family *Desulfobacteriaceae* [48]. Among semiconductor nanocrystals, CdS synthesized *by C. thermoaceticum* , *Klebsiella pneumoniae* and *E. coli* showed spherical and elliptical shape in the size of 2-200 nm and ZnS produced by *Desulfobacteriaceae* exhibited spherical morphology with 2-5 nm in size.

1.6.2 Extracellular synthesis of nanoparticles by bacteria

Microbial synthesis of metal nanoparticles depends upon the localization of the reductive components of the cell. When the cell-wall reducing enzymes or soluble secreted enzymes are involved in the reductive process of metal ions, it is obvious to find the metal nanoparticles extracellularly. The extracellular production of nanoparticles has wider applications in optoelectronics, electronics, bioimaging and in sensor technology rather than in intracellular accumulation. *Rhodopseudomonas capsulata*, a prokaryotic bacterium was found to reduce Au^{+3} to Au^{0} at room temperature [49]. Among hyperthermophilic and mesophilic dissimilatory Fe(III) reducing bacteria and archea like *Pyrobalaculum islandicum*, *Thermotoga maritime, S. algae*, *G. sulfurreducens* and *Pyrococcus furiosus,* gold was precipitated by reducing gold(III) to metallic gold in the presence of hydrogen as electron donor. The precipitation occurred extracellularly due to the presence of Au(III) reductases near the outer cell surfaces of Fe(III) reducers. Husseiny *et al.* [50] demonstrated that *P. aeruginosa* (ATCC 90271, strain 1 and strain 2) synthesized gold nanoparticles extracellularly with particle size distribution in the order of 40±10 nm, 25±15 nm and 15±5 nm respectively. As the particle size increased, the color was found to shift from pink to blue due to the SPR of gold nanoparticles. Furthermore, the dried powder of

B. megatherium D01 was also used to reduce gold salts into monodispersed gold nanoparticles and dodecanethiol was used as capping ligand to stabilize the particles at 26°C. Suresh *et al.* have used the bacterium *Shewanella oneidensis* for the biofabrication of extracellularly synthesized spherical gold nanoparticles [51]. In analogous, silver nanoparticles were also found to be produced by dried cells of *Aeromonas* sp. SH10, which reduced $[Ag(NH_3)_2]^+$ to Ag^0 in 4h with an average diameter of ca. 6.4 nm. These particles were monodispersed and uniform in size and remained stable for more than 6 months without aggregation and precipitation [52]. The culture supernatants of *Enterobacteriaceae* (*Klebsiella pneumonia*, *E. coli* and *Enterobacter cloacae*) also rapidly synthesized silver nanoparticles by reducing Ag^+ to Ag^0. These particles ranged in size from 28.2 nm to 122 nm with an average size of 52.5 nm. With the addition of piperitone, silver ion reduction was partially inhibited which showed the involvement of nitroreductase enzymes in the reduction process [53]. Similarly, the culture supernatant of non-pathogenic bacteria, *B. licheniformis* was also used for the extracellular synthesis of silver nanoparticles of 50 nm [54]. Barud *et al.* [55] also demonstrated the formation of homogenous silver containing bacterial cellulose (BC) membranes obtained from BC hydrated membranes of *Acetobacter xylinum* cultures soaked in silver ions and with triethanolamine (Ag^+-TAE) solution . Recently, it has been found that the HIV-1 virus binds exclusively to silver nanoparticles whose size is in the range of 1–10 nm [56].Very recently, Juibari *et al.* used the native extremophilic *Ureibacillus thermosphaericus* strain at 80^0C for the production of silver nanoparticles of size 10-100nm[57]. Similarly Kannan and co-workers extracellularly synthesized antimicrobial silver nanoparticles using *Bacillus subtilis* IA751 [58]. *Rhodobacter sphaeroides* has also been shown to produce silver nanoparticles extracellularly [59]. Sadhasivam and co-workers have employed *Streptomyces hygroscopicus* for the extracellular production of silver nanoparticles and showed their antimicrobial activity against medically important pathogenic microorganisms [60]. Similarly Potara *et al.* reported the synergistic antibacterial activity of chitosan–silver nanocomposites on *Staphylococcus aureus* [61]. Parikh *et al.* very recently reported that extracellular biosynthesis of crystalline silver nanoparticles is a unique biochemical character of all the members of genus *Morganella*, which was found independent of environmental changes. Significantly, the inability of other closely related members of the family *Enterobacteriaceae* towards AgNPs synthesis strongly suggests that AgNPs synthesis in the presence of

Ag^+ ions is a phenotypic character that is uniquely associated with genus *Morganella* [62]. Another metalloid semiconductor tellurium, belonging to *chalcogen* family has been reduced from tellurite to elemental tellurium by two anaerobic bacteria, *B. selenireducens* and *Sulfurospirillum barnesii*. In case of *B. selenireducens*, initially formed nanorods of 10 nm diameter and 200 nm length were clustered together to form larger rosettes of 1000 nm but with *S. barnesii,* small and irregularly shaped extracellular nanospheres of diameter 50 nm were formed [63]. Marshall *et al.* [64] found that c-type cytochrome (MtrC) on the outer membrane and extracellular side of dissimilatory metal-reducing bacterium *S. oneidensis* MR-1 was involved in the reduction of U(VI) predominantly with extracellular polymeric substance as UO2-EPS in cell suspension and intracellularly in periplasm. *Klebsiella aerogenes* synthesized CdS crystallites of spherical shape as bound to the cell wall and as detached electron-dense particles in the dimension of 20 to 200 nm when exposed to Cd^{2+} in the growth medium [65]. Bai *et al*. [66] showed that *Rhodopseudomonas palustris*, a purple, non-sulfur, photosynthetic bacterium extracellularly synthesized CdS nanocrystals at room temperature. TEM and electron diffraction analyses confirmed the spherical distribution of fcc structured nanoparticles of size in the range of 8.01±0.25 nm. The cysteine desulfhydrase (C-S lyase) activity was found to be responsible for the formation of CdS nanocrystals and also found that bacterial cellulose (BC) isolated from the strain *Gluconoacetobacter xylinus* was also used in the synthesis of CdS nanoparticle of 30 nm deposited on BC nanofibres [67]. Immobilized *Rhodobacter sphaeroides* extracellularly produced spherical shaped zinc sulfide (ZnS) semiconductor nanoparticles of 8 nm in size [68]. In analogous, immobilized purple, nonsulfur photosynthetic bacterium, *R. sphaeroides* produced extracellularly fcc structured lead sulfide (PbS) nanoparticles of size 10.5±0.15 nm with monodispersed spherical morphology [69]. All these bacteria, *G. xylinus* and *R. sphaeroides* produced only spherical shaped semiconductor nanocrystals in the size range of 8-200 nm in size.

1.6.3 Biosynthesis of nanoparticles by fungi

In recent years, fungi such as *Fusarium oxysporum* [70-79], *Colletotrichum* sp. [80], *Trichothecium* sp., *Trichoderma asperellum*, *T. viride* [81-83], *Phaenerochaete chrysosporium* [84], *F. solani* USM 3799 [85], *F. semitectum* [86], *A. fumigatus* [87], *Coriolus versicolor* [88], *Aspergillus niger* [89], *Phoma glomerata* [90], *Penicillium*

brevicompactum [91], *Cladosporium cladosporioides* [92], *Penicillium fellutanum* [93] and *Volvariella volvaceae* [94] have been explored for nanoparticles synthesis. Fungi are more advantageous as compared to other microorganisms in many ways. Fungal mycelial mesh can withstand flow pressure and agitation and other conditions in bioreactors or other chambers more efficiently as compared to plant materials and bacteria. These are fastidious to grow, easy to handle and easy for fabrication. The extracellular secretions of reductive proteins are more and can be easily handled in downstream processing. Also, since the nanoparticles precipitated outside the cell are devoid of unnecessary cellular components, they can be directly used in various applications.

1.6.4 Intracellular synthesis of nanoparticles by fungi

The nanoparticles formed inside the organism could be smaller as compared to the size of extracellularly reduced nanoparticles. The size limit could have been related to the particles nucleating inside the organisms. Mukherjee *et al*. [95] demonstrated the intracellular synthesis of gold nanoparticles using eukaryotic microorganisms such as *Verticillium* sp. (AAT-TS-4) and *Trichothecium* sp. and they were found to accumulate gold nanoparticles intracellularly [81]. In addition, *Verticillium luteoalbum* produced spherical gold nanoparticles <10 nm in diameter at pH 3.0 but with pH 5.0 spheres and rods were also observed along with triangular and hexagonal morphologies [96, 97]. *Phoma* PT35 was able to selectively accumulate silver [98] and *Phoma* sp. 3.2883 was in-fact a biosorbent suited for preparing silver nanoparticles [99]. *Verticillium* sp. has been shown to produce silver nanoparticles when exposed to aqueous silver nitrate solution [71, 100]. Recently, Vigneshwaran *et al*. [101] also showed that the use of *Aspergillus flavus* results in the accumulation of silver nanoparticles on the surface of its cell wall when incubated with silver nitrate solution for 72h. Ali *et al.* have reported extracellular synthesis of silver nanoparticles in the range of 100-200 nm [102]. Very recently, the filamentous fungus *Neurospora crassa* has been found to produce mono and bimetallic Au/Ag nanoparticles intracellularly [103].

1.6.5 Extracellular synthesis of nanoparticles by fungi

Synthesis of nanoparticles outside the cell, extracellularly, has many applications as it is void of unnecessary adjoining cellular components from the cell. Mostly, fungi are

regarded as the organisms that produce nanoparticles extracellularly because of their enormous secretary components which are involved in the reduction and capping of nanoparticles. Shankar *et al*. [104] found an endophytic fungus, *Colletotrichum* sp. isolated from the leaves of geranium plant (*Pelargonium graveolens*), which rapidly reduced gold ions to zero-valent gold nanoparticles. Similarly, when the fungus *Trichothecium* sp. was cultured in static condition, it reduced Au^{+3} to form gold nanoparticles [81]. Bhainsa and D'Souza [87] reported the use of *Aspergillus fumigatus* in the production of monodispersed silver nanoparticles of size 5-25 nm within 10 min of addition of silver nitrate. *P. chrysosporium* when challenged with silver nitrate solution, extracellular synthesis of silver nanoparticles in the size range of 50-200 nm was achieved [84]. Also, Basavaraja *et al.* [86] demonstrated that when culture filtrate of *F. semitectum* was treated with silver ions, it reduced to silver nanoparticles with size range of 10-60 nm and spherical morphology indicating polydispersity. Similarly, *Aspergillus niger* isolated from soil, produced spherical silver nanoparticles of size 20 nm in diameter [89]. In addition, *F. solani* (USM-3799), a phytopathogenic fungus of onion produced polydispersed spherical silver nanoparticles in the range of 16-23 nm [85]. Extracellular mycosynthesis of silver nanoparticles by *F. acuminatum* EII. and Ev. (USM-3793) isolated from infected ginger was studied by Ingle *et al*. [105]. The non-pathogenic and bio controlling agent *Trichoderma asperellum* also produced silver nanoparticles in the size range of 13-18 nm with well-defined morphology and stability over several months [82]. Vahabi and co-workers very recently have shown the usage of *Trichoderma reesei* for the synthesis of AgNPs with the diameters in the range of 5-50 nm. *Trichoderma reesei* is an environment friendly fungus and is well known for its formation of extracellular enzymes and metabolites in very large amounts, much higher than other fungi. This process is an excellent candidate for industrial scale production of silver nanoparticles [106]. The fungal filtrate of *P. glomerata* showed the synthesis of spherical silver nanoparticles in the range of 60-80 nm when challenged with silver nitrate. These nanoparticles also exhibited antibacterial activity against *E. coli*, *P. aeruginosa* and *Staphylococcus aureus* [90]. Fungal proteins by white - rot fungus, *C. versicolor*, have been used as bioreducing and biocapping agents to produce extra- and intracellular silver nanoparticles in alkaline conditions [88]. Rhizospheric fungus, [93] *P. fellutanum*, from mangrove root-soil of *Rhizophora annamalayana* Kathir, was found to produce silver nanoparticles in 24h. Intriguingly, *F. oxysporum f.* sp.

lycopersici was found to produce platinum nanoparticles intercellularly, on cell wall or membrane and extracellularly in the medium in the size range between 10 and 100 nm and with varying shapes of triangles, hexagons, squares and rectangles [77]. Senapati *et al*. [71, 72] showed the formation of extracellular silver nanoparticles and bimetallic gold-silver (Au-Ag) alloy nanoparticles by *F. oxysporum*. Strontianite ($SrCO_3$) crystals of needle like morphology with higher order quasi-linear superstructures with aqueous Sr^{+3} ions were reported [76]. Similarly, *F. oxysporum* upon incubation with $CdCl_2$ and $SeCl_4$ produced highly luminescent water-soluble quantum dots (CdSe) with SPR band at 370 nm at room temperature [78]. Chen and co-workers have used the white - rot fungus *Coriolus versicolor* for the coarsening of extracellularly biosynthesized cadmium nanocrystals [107]. *Candida glabrata* and *Fusarium oxysporum* have been found to produce silver nanoparticles extracellulary and give very good antibacterial activity against *Staphylococcus aureus* (ATCC 29213), *Escherichia coli* (ATCC 25922), *Klebsiella pneumonia* (ATCC 15240), *Bacillus subtilis*, *Enterococcus faecalis* (ATCC 29212) and *Pseudomonas aeruginosa* [108].

1.6.6 Actinomycete mediated synthesis of nanoparticles

Actinomycetes, though classified as prokaryotes, share important characteristics of fungi. They are popularly known as “ray fungi”. A novel extremophilic actinomycete, *Thermomonospora* sp. was found to synthesize extracellularly monodispersed spherical gold nanoparticles of an average size of 8 nm [109]. Electrophoretic analysis showed that the proteins of molecular weight ranging from 80 kDa to 10 kDa were involved in stabilization of nanoparticles. In contrast, an alkalotolerant actinomycete, *Rhodococcus* sp. intracellularly accumulated gold nanoparticles with a dimension of 5-15 nm [110]. Till date, actinomycetes are regarded as the primary source for synthesizing secondary metabolites like antibiotics in general. These new discoveries would take a lead in screening of further actinomycetes in the synthesis of nanomaterials.

1.6.7 Yeast mediated synthesis of nanoparticles

Among the eukaryotic microorganisms, yeast has been exploited mainly for the synthesis of semiconductors. *Candida glubrata* produced intracellularly, monodispersed, spherically shaped, peptide bound CdS quantum crystallites of 20 Å

by neutralizing the toxicity of metal ions and forming metal–thiolate complex with phytochelatins [111]. *Schizosaccharomyces pombe* also produced wurtzite-type hexagonal lattice structured CdS nanoparticles in mid-log phase in the range of 1–1.5 nm [112]. Kowshik *et al.* [113] first reported the synthesis of fcc structured PbS nanocrystallites exhibiting quantum semiconductor properties from yeast *Torulopsis* sp. which was intracellularly produced in the vacuoles with a dimension of 2-5 nm in spherical morphology when incubated with Pb^{2+} exhibiting λ max of 330 nm in UV-vis spectrophotometer. Marine yeast *Rhodosporidium diobovatum* has been shown to produce lead sulphide nanoparticles intracellularly with crystallite size of 2-5nm [114]. In addition, Baker's yeast *S. cerevisiae* was also reported to absorb and reduce Au^{+3} to elemental gold in the peptidoglycan layer of the cell wall *in situ* by the aldehyde group present in reducing sugars [115]. Similarly, another yeast *Pichia jadinii* (*Candida utilis*), intracellularly formed gold nanoparticles of spherical, triangular and hexagonal morphologies throughout the cell mainly in the cytoplasm of size <100 nm in 24h [96, 97]. This tropical marine yeast, *Yarrowia lipolytica* NCIM 3589, also synthesized gold nanoparticles associated with cell wall. The reduction of gold ions occurred in pH dependent manner. When cells were incubated at pH 2.0, it produced hexagonal and triangular gold crystals due to the nucleation on the cell surfaces giving rise to golden color in the visible region at 540 nm at pH 7.0 and pH 9.0 with pink and purple colors respectively and with an average size of 15 nm [116]. Extracellular production of silver nanoparticles was reported only in yeast MKY3, a silver tolerant strain, which synthesized hexagonal silver nanoparticles (2-5 nm) in log phase of growth [117]. Very recently *Candida guilliermondii* has also been used for the extra cellular synthesis of gold and silver nanoparticles. TEM analysis confirmed the formation of near spherical, well dispersed gold and silver nanoparticles in the size range of 50-70 nm and 10-20 nm respectively [118].

1.6.8 Virus mediated biosynthesis of nanoparticles

Some biological molecules like fatty acids, amino acids and polyphates are used as templates in the growth of semiconductor nanocrystals. In particular, by changing the ratio of different fatty acids (chain lengths), shapes of CdSe, CdS and CdTe nanocrystals can be achieved [119]. Some other biological methodologies are also available for eco-friendly synthesis of inorganic materials. Biological materials like DNA [120-122], protein cages [123], biolipid cylinders [124-125], viroid capsules

[126], bacterial rapidosomes [127], S-layers [128] and multicellular superstructures [129] have been used in template-mediated synthesis of inorganic nanoparticles and microstructures. Interestingly, tobacco mosaic virus (TMV) was used as template for the synthesis of iron oxides by oxidative hydrolysis, co-crystallization of CdS and PbS, and the synthesis of SiO_2 by sol–gel condensation. It happened with the help of external groups of glutamate and aspartate on the external surface of the virus [130]. Self-assembled viral capsids of genetically engineered viruses were exploited as biological templates for the assembly of quantum dot nanowires. The peptides like A7 and J140, which have the ability to nucleate ZnS and CdS nanocrystals were expressed as pVIII fusion proteins into the crystalline capsid of the virus, M13 bacteriophages. These organized template peptides (A7/J140-pVIIIM13) were selected by using a pIII phage display and exposed to semiconductor precursor solutions. ZnS nanocrystals assembled on the viral capsid were found to be of hexagonal wurtzite of 5 nm, or CdS assembled as nanowires of 3–5 nm. Hybrid nanowires (ZnS–CdS) were achieved with a dual-peptide virus, engineered to express A7 and J140 within the same viral capsid [131, 132].

1.7 Oxide nanomaterials

Metal oxides play a very important role in many areas of chemistry, physics and materials science [133-138]. The metal elements are able to form a large diversity of oxide compounds [139]. These can adopt a vast number of structural geometries with an electronic structure that can exhibit metallic, semiconducting or insulating characters. In technological applications, oxides are used in the fabrication of microelectronic circuits, sensors, piezoelectric devices, fuel cells, coatings for the passivation of surfaces against corrosion and as catalysts. In the emerging field of nanotechnology, the goal is to make nanostructures or nanoarrays with special properties with respect to those of bulk or single particle species [140-144]. Oxide nanoparticles can exhibit unique physical and chemical properties due to their limited size and high density of corner or edge surface sites. Particle size is expected to influence three important groups of basic properties in any material. The first one comprises the structural characteristics, namely the lattice symmetry and cell parameters [145]. Bulk oxides are usually robust and stable systems with well-defined crystallographic structures. However, the growing importance of surface free energy and stress with decreasing particle size must be considered. Changes in

thermodynamic stability associated with size can induce modification of cell parameters and/or structural transformations [146-148] and in extreme cases the nanoparticle can disappear due to interactions with its surrounding environment and a high surface free energy [149]. In order to display mechanical or structural stability, a nanoparticle must have a low surface free energy. As a consequence of this requirement, phases that have a low stability in bulk materials can become very stable in nanostructures. This structural phenomenon has been detected in TiO_2, VOx, Al_2O_3 or MoOx oxides [148,149,150]. Size induced structural distortions associated with changes in cell parameters have been observed, for example, in nanoparticles of Al_2O_3 [149], NiO [151], Fe_2O_3 [152], ZrO_2 [153], MoO_3 [155], CeO_2 [154] and Y_2O_3 [155]. As the particle size decreases, the increasing number of surface and interface atoms generates stress/strain and concomitant structural perturbations [156]. Beyond this "intrinsic" strain, there may also be "extrinsic" strain associated with a particular synthesis method which may be partially relieved by annealing or calcinations [157]. Also, non-stoichiometry is a common phenomenon [157]. On the other hand, interactions with the substrate on which the nanoparticles are supported can complicate the situation and induce structural perturbations or phases not seen for the bulk state of the oxide [150, 158]. The second important effect of size is related to the electronic properties of the oxide. In any material, the nanostruture produces the so-called "quantum size" or "confinement effects" which essentially arise from the presence of discrete, atom-like electronic states. From a solid-state point of view, these states can be considered as being a superposition of bulk-like states with a concomitant increase in oscillator strength [159]. Additional general electronic effects of quantum confinement experimentally probed on oxides are related to the energy shift of exciton levels and optical bandgap [160, 161]. An important factor to consider while dealing with the electronic properties of a bulk oxide surface are the long-range effects of the Madelung field, which are not present or limited in a nanostructured oxide [162-164]. Theoretical studies for oxides show a redistribution of charge when going from large periodic structures to small clusters or aggregates which must be roughly considered to be relatively small for ionic solids, while significantly larger for covalent ones [165-170]. The degree of ionicity or covalency in a metal oxygen bond can however strongly depend on size in systems with partial ionic or covalent character; an increase in the ionic component to the metal-oxygen bond in parallel to the decreasing size has been proposed [147]. Structural and electronic properties

obviously drive the physical and chemical properties of the solid, the third group of properties influenced by size in a simple classification. In their bulk state, many oxides have wide band gaps and a low reactivity [171]. A decrease in the average size of an oxide particle does in fact change the magnitude of the band gap, [164, 172] with strong influence in the conductivity and chemical reactivity [173, 174]. Surface properties are a somewhat particular group included in this subject due to its importance in chemistry. Solid-gas or solid-liquid chemical reactions can be mostly confined to the surface and/or sub-surface regions of the solid. As mentioned above, the two - dimensional (2D) nature of surfaces have a notable structure, typically a rearrangement or reconstruction of bulk geometries [135, 143, 175] and electronics; e.g. presence of mid-gap states and its consequences [174, 176]. In the case of nanostructured oxides, surface properties are strongly modified with respect to the 2D-infinite surfaces, producing solids with unprecedented absorption or acid/base characteristics [177]. Furthermore, the presence of under-coordinated atoms (like corners or edges) or 0 vacancies in an oxide nanoparticle should produce specific geometrical arrangements as well as occupy electronic states located above the valence band of the corresponding bulk material, [178, 179, 180] enhancing in this way the chemical activity of the system [175, 177, 181, 182].

1.8 Biological synthesis of oxide nanoparticles

Oxide nanoparticle is an important type of compound nanoparticle synthesized by microbes. This section deals with the biosynthesis of oxide nanoparticles from two aspects: magnetic oxide nanoparticles and nonmagnetic oxide nanoparticles.

1.8.1 Magnetic nanoparticles

Magnetic nanoparticles are recently developed new materials and owing to their unique microconfiguration and properties like super paramagnetism and high coercive forces, they have broad applications in biological separation and biomedicine fields. Magnetic nanoparticles like Fe_3O_4 (magnetite) and Fe_2O_3 (maghemite) are known to be biocompatible. They have been actively investigated for targeted cancer treatment (magnetic hyperthermia), stem cell sorting and manipulation, guided drug delivery, gene therapy, DNA analysis and magnetic resonance imaging (MRI) [183]. Magnetotactic bacteria synthesize intracellular magnetic particles comprising iron oxide, iron sulfides or both [184, 185]. In order to distinguish these particles from

artificially synthesized magnetic particles (AMPs), they are referred to as bacterial magnetite particles (BacMPs) [186]. BacMPs which are aligned in chains within the bacterium are postulated to function as biological compass needles that enable the bacterium to migrate along the oxygen gradients in aquatic environments under the influence of the Earths geomagnetic field [187]. BacMPs can easily disperse in aqueous solutions because they are enveloped by organic membranes that mainly consist of phospholipids and proteins. Furthermore, an individual BacMP contains a single magnetic domain or magnetite that yields superior magnetic properties [188]. Since the first report of magnetotactic bacteria in 1975 [187], various morphological types including *Cocci*, *Spirilla*, *Vibrios*, ovoid bacteria, rod-shaped bacteria and multicellular bacteria possessing unique characteristics have been identified and observed to inhabit various aquatic environments [188, 189]. *Magnetotactic cocci*, for example, have shown high diversity and distribution and have been frequently identified at the surface of aquatic sediments. The discovery of this bacterial type, including the only cultured *Magnetotactic coccus* strain MC-1, suggested that they are microaerophilic. In the case of the *Vibrio* bacterium, three facultative anaerobic marine *Vibrios*-strains MV-1, MV-2 and MV-4 have been isolated from estuarine salt marshes. These bacteria have been classified as members of 9 α-Proteobacteria, possibly belonging to the *Rhodospirillaceae* family, observed to synthesize BacMPs of a truncated hexa octahedron shape and grow chemoorganoheterotrophically as well as chemolitho autotrophically. The members of the family *Magnetospirillaceae*, on the other hand can be found in fresh water sediments. With the use of growth medium and magnetic isolation techniques established, a considerable number of the magnetotactic bacteria isolated to date have been found to be members of this family. The *Magnetospirillum magnetotacticum* strain MS-1 was the first member of the family to be isolated [189], while the *Magnetospirillum gryphiswaldense* strain MSR-1 is also well studied with regard to both its physiological and genetic characteristics. *Magnetospirillum magneticum* AMB-1 isolated by Arakaki *et al.* in 1991 was facultative anaerobic *Magnetotactic spirilla* [186]. A number of new magnetotactic bacteria have been found in various aquatic environments since the year 2000. Uncultured magnetotactic bacteria have been observed in numerous habitats [190]. Most known cultured magnetotactic bacteria are mesophilic and tend to not grow much above 30°C. Uncultured magnetotactic bacteria were mostly at 30°C and below. There are only a few reports describing thermophilic magnetotactic bacteria. Lefèvre

et al. reported one of the magnetotactic bacteria called HSMV-1 which was found in samples from springs whose temperatures ranged from 32 to 63°C [191]. TEM images of unstained cell of HSMV-1 showed a single polar flagellum and a single chain of bullet-shaped magnetosomes. The average number of magnetosome crystals per cell is 12 ± 6 with an average size of 113 ± 34 by 40 ± 5 nm. The results from the paper clearly showed that some magnetotactic bacteria can be considered at least moderately thermophilic. They extended the upper temperature limit for environments where magnetotactic bacteria exist and likely grow (~63°C) and where magnetosome magnetite is deposited [191]. Zhou *et al.* reported magnetic Fe_3O_4 materials with mesoporous structure which were synthesized by co-precipitation method using yeast cells as a template [192,193]. Atul *et al*. reported extracellular synthesis of magnetite using fungi [209].

1.8.2 Nonmagnetic oxide nanoparticles

Besides magnetic oxide nanoparticles, other oxide nanoparticles have also been studied including Sb_2O_3, TiO_2, SiO_2, $BaTiO_3$ and ZrO_2 nanoparticles [73, 74, 75, 194-196]. Prasad and co-workers found a green, low-cost and reproducible *Saccharomyces cerevisiae* mediated biosynthesis of Sb_2O_3 nanoparticles [194]. The synthesis was performed akin to room temperature. Analysis indicates that Sb_2O_3 nanoparticles unit was a spherical aggregate having a size of 2–10 nm [73]. Bansal *et al*. used *F. oxysporum* to produce SiO_2 and TiO_2 nanoparticles from aqueous anionic complexes $SiF6^{2-}$ and $TiF6^{2-}$ respectively [74]. They also prepared tetragonal $BaTiO_3$ and quasi-spherical ZrO_2 nanoparticles from *F. oxysporum* with a size range of 4-5 nm and 3-11 nm respectively [75, 73]. With an immense capability, a metal-tolerant marine bacterium, *Brevibacterium casei* also extracellularly synthesized cubic spinel-structured single-crystalline ferromagnetic Co_3O_4 nanoparticles functionalized with proteins in the size range of 5–7 nm using aqueous cobalt acetate as precursor at room temperature [197]. Very recently, it was also shown that *F. oxysporum* produced optoelectronic material Bi_2O_3 nanocrystals in the size between 5-8 nm extracellularly with quasi spherical morphology and good tunable properties. When bismuth nitrate was added as precursor, the as-synthesized nanocrystals were in monoclinic and tetragonal phases [79]. Ahmad and co-workers have demonstrated the usage of fungus *Humicola* sp. for the synthesis of chemically difficult to synthesize multifunctional copper aluminium oxide ($CuAlO_2$) nanoparticles [198]. The fungus successfully

controls the valence state of copper to +1 which is a prerequisite for the synthesis. TEM analysis showed that the particles were almost monodispersed and were having mean size of 5nm.

1.9 Probable mechanisms of nanoparticles formation by microorganisms

Different mechanisms have been reported for different microorganisms for forming nanoparticles. However, almost all reports agree with one common way, wherein metal ions are first trapped on the surface or inside of the microbial cells. The trapped metal ions are then reduced to nanoparticles in the presence of enzymes. In general, microorganisms impact nanoparticle formation by secreting their products in response to the stress conditions developed during the course of reaction with the precursor metal ions and ultimately results in the production of desired products i.e. nanomaterials. In this section the possible formation mechanisms for metals and oxide nanoparticles will be discussed.

1.9.1 Mechanisms of formation of metal nanoparticles

While a large number of microbial species are capable of producing metal NPs, the mechanism of nanoparticle biosynthesis had not been established yet. The metabolic complexity of viable microorganisms complicates the analysis and identification of active species in the nucleation and growth of metal NPs. Recent works by Ahmad *et al.* [199] and He *et al.* [200] have postulated that microorganisms secrete enzymes, which may be responsible for the reduction of metal ions, which result in the nucleation and growth of NPs. The exact mechanism for the intracellular formation of gold and silver nanoparticles by microorganisms is not fully understood. But the fact that nanoparticles were formed on the surface of the mycelia and not in the solution supports the following hypothesis: the gold or silver ions are first trapped on the surface of the fungal cells via electrostatic interactions between the ions and negatively charged cell wall from the carboxylate groups in the enzymes. Next, the enzyme reduces the metal ions to form gold or silver nuclei, which subsequently grow through further reduction and accumulation [201]. Kalishwaralal and co-workers speculated that the nitrate reductase enzyme is involved in the synthesis of silver nanoparticles in *B. licheniformis* [54]. This enzyme is induced by nitrate ions and reduces silver ions to metallic silver. The possible mechanism that may involve the reduction of silver ions is the electron shuttle enzymatic metal reduction process.

NADH and NADH-dependent nitrate reductase enzymes are important factors in the biosynthesis of metal nanoparticles. *B. licheniformis* is known to secrete the cofactor NADH and NADH-dependent enzymes, especially nitrate reductase, that might be responsible for the bioreduction of Ag^{+} to Ag^{0} and the subsequent formation of silver nanoparticles. Microbes have evolved various measures to respond to heavy metal stress via processes such as transport across cell membrane, entrapment in extracellular capsules, precipitation, complexation and oxidation-reduction reactions [202]. In microbial bioreduction processes, myriads of proteins, carbohydrates and biomembranes are involved. The enzymatic route of *in vitro* synthesis of silver hydrosol of 10–25 nm using α-NADPH-dependent nitrate reductase (44 kDa) from *F. oxysporum* with capping peptide, phytochelatin was demonstrated recently [203]. The mechanistic aspect was explained by Duran *et al.* [204] that apart from enzymes, quinine derivates of napthoquinones and anthraquinones also act as redox centres in the reduction of silver nanoparticles. Extracellular biosynthesis of silver nanoparticles using *Aspergillus flavus* NJP08 has also been achieved very recently. SDS-PAGE profiles of the extracellular proteins showed the presence of two intense bands of 32 and 35 kDa, responsible for the synthesis and stability of silver nanoparticles, respectively [205]. A similar finding was also reported in the reduction of gold (III) chloride to metallic gold by α-NADPH-dependent sulfite reductase of molecular mass of 35.6 kDa and phytochelatin [206]. A dimeric hydrogenase enzyme (44.5 and 39.4 kDa) of *F. oxysporum* that showed optimum activity at pH 7.5 and 38°C passively reduced H_2PtCl_6 to platinum nanoparticles was also reported [207]. To date, only very few reports have been documented on optimization in biological process. A 29-kDa "gold shape-directing protein (GSP)" present in the extract of green algae *Chlorella vulgaris* was used in the bioreduction and in the synthesis of shape-and size-controlled distinctive triangular and hexagonal gold nanoparticles. An increase in the concentration of GSP led to the production of gold plates with lateral sizes upto micrometers [208]. Such mechanistic components should be unraveled for efficient biological processes. In a nut shell, it can be described that the formation of metal nanoparticles (either intra or extracellularly) occur mainly through the actions of NADPH dependent enzymes and biomolecules (secreted by microorganisms) which reduces the metal ions resulting in the synthesis of corresponding nanoparticles.

1.9.2 Mechanisms of formation of oxide nanoparticles

Very little is known about the mechanism as far as biosynthesis of oxide nanoparticles is concerned. Since biosynthesis of oxide nanomaterial is still a new field, few mechanistic aspects of their synthesis started coming into picture. Bansal and co-workers have shown the involvement of cationic proteins of molecular weight around 24 to 28kDa from *Fusarium oxysporum* in the biosynthesis of zirconia nanoparticles [73]. Similarly, the same group has demonstrated the biosynthesis of silica and titania nanoparticles using cationic proteins of molecular weight 21 and 24 kDa respectively, from the same fungus [74]. Since the molecular weights of these proteins are quite close to those observed in the earlier study on zirconia formation with the same fungus, the authors concluded that they are the same proteins or their post-translationally modified variants. Certain cationic proteins of *Fusarium oxysporum* and *Verticillium* sp. have been shown to hydrolyze anionic iron complexes resulting in the production of magnetite nanoparticles extracellularly [209]. Although researchers started looking into the insights of mechanisms of formation of oxide nanoparticles, issues such as *in vitro* and tailor made synthesis of oxide nanomaterials need to be properly addressed.

1.10 Potential Biomedical Applications of Nanomaterials

Nanomaterials, due to their unique physical, mechanical, and chemical properties are used in electronics and numerous consumer products. A diverse array of engineered nanomaterials is being produced in hundreds of tons a year. The commercial value of the nanotechnology industry, by some estimates, is anticipated to exceed several hundreds of billions of dollars annually. Over the past few years, it has become increasingly clear that nano-sized materials offer immense potential for various biomedical applications. Nanomaterials are comprised of chemically diverse and heterogeneous compounds. They may be engineered from pure carbon, inorganic or polymeric compounds. Although a wide spectrum of applications of nanomaterials have been proposed, significant clinical applications have been accomplished with inorganic metal nanoparticles including gold, iron oxide, etc. Polymeric nanomaterials that include biodegradable polymeric materials and liposomal preparations. Biomedical applications of engineered carbon particles and inorganic materials are being actively pursued and require further validation before they can be used in pre-clinical settings. Thus, nanomedicine, as a field, may be considered as an emerging

area. The properties and reactivity of nanomaterials significantly differ from their macromolecular counterparts. This distinctive property of nanoparticles is a consequence of the display of more atoms on their surfaces as the particle size decreases, which is due to increased surface area. The molecules displayed on the surfaces exponentially increase as the particle size decreases to <100 nm [210]. Consequently, nanomaterials are likely to be more reactive, exhibit higher surface charge and agglomerate into larger clusters or react with other materials. The size of the nanoparticles is also an important determinant of their physico-chemical properties such as solubility, optical and catalytic behavior. The surface reactivity of nanoparticles is often modified by coating with various materials for stability and biocompatibility, and hence surface modifications are among the critical determinants of the usage of nanomaterials. Although 'pristine' (unmodified) nanomaterials (such as carbon nanotubes and fullerenes) have been synthesized and their properties have been investigated in depth, advances in chemistry of nanomaterials have enabled researchers to attach a large array of diverse molecules including proteins, peptides, DNA, drugs, and carbohydrates. The ability to conjugate such functionalities has heralded the area of nanomedicine and is likely to result in creating multifunctional nanoparticles. Here, we will try to throw some light on emerging biomedical applications of nanomaterials.

1.10.1 Cancer Therapy

In most cases, cancer-related deaths occur due to the failure of chemotherapy and/or radiation therapy of the metastatic disease. Therefore, for a successful cancer treatment, it is critical to detect tumors early - on during the disease progression and ablate tumor metastasis. Nanotechnology has several applications in improving cancer therapy and some nanosized drugs are currently in clinical trials [211]. Prominent among those are liposomal doxorubicin and albumin conjugated Paclitaxel, which have been shown to reduce toxicity due to the adverse side effects of respective drugs. Liposomal doxorubicin (Doxil) has been shown to be an effective anti-neoplastic agent with improved biodistribution (longer plasma circulation times) which reduces severe dose-limiting cardiotoxicity associated with the drug treatment [212]. Like many drugs, Paclitaxel is poorly soluble in water and is administered as a formulation with Cremophor EL (polyethoxylated castor oil) and causes side effects such as hypersensitivity, nephrotoxicity and neurotoxicity. While several different

formulations have been made to minimize the toxic effects of this drug, albumin-conjugated nano-sized paclitaxel (Abraxane), a Cremophor - free formulation, has been shown to be well-tolerated and yet more effective than the conventional drug [213]. Additionally, a number of nanosized formulations of other chemotherapeutic drugs such as 5-fluorouracil and camptothecin are being tested. Further, new formulations of aqueous compatible nanosized drugs (such as paclitaxel) are being developed through supercritical fluid technologies [214]. In other applications, the unique properties of nanoparticles are being exploited for the treatment of cancer. In this strategy, nanoparticles serve as multifunctional therapeutic agents, instead of being utilized as simple passive carriers of cargo. These multifunctional nanoparticles can potentially carry drugs to the target tissue, image the target tissues and release the cargo in response to a signal or upon reaching appropriate cellular compartment. Further, the targeted nanoparticles may be used as therapeutic agents. Targeting the nanotherapeutic agents may be achieved by coupling a specific antibody or a small molecular weight ligand (e.g. folic acid) that recognizes a protein selectively expressed on tumor cells [211]. Magnetic iron oxide particles [215], nanotubes [216], or other particles may be used as core nanoparticles and the imaging can be accomplished through MRI (with iron oxide nanoparticles) or fluorescence methods if quantum dots [217] are incorporated into the multifunctional nanoparticles. For example, optical stimulation with an NIR laser of folic acid receptor targeted SWNTs has been shown to act as a trigger for the release of the internalized nanotube attached cargo (in this case oligodeoxy nucleotides) [218]. Further, NIR was also used to generate local heating and then caused photothermal ablation of the targeted cell populations. In another example, tumor-targeting antibody Herceptin, which is prepared against HER2 receptor (amplified in breast tumors), was coupled to gold nanoshells. This enabled the gold nanoshells to be targeted to HER2 over - expressing tumor cells and when irradiated with NIR, tumor cells were specifically killed [229]. Further, the ability of fullerenes to generate highly reactive singlet oxygen has also been tested as a potential photodynamic therapy of tumor cells [220]. Thus, the concepts of multifunctional nanoparticles for cancer therapy have been validated in experimental systems.

1.10.2 Diabetes

Diabetes mellitus is a serious metabolic disease in which patients are unable to regulate blood glucose levels. Management of both Type I (insulin-dependent) and Type II (insulin-independent) diseases requires a careful maintenance of blood glucose levels. Type I patients require insulin administration whereas the Type II disease is managed by drugs which reduce glucose and insulin. Nanotechnology-based solutions are also being explored in the management of diabetes. Nanoparticle-based biomolecular sensors have been developed to measure glucose levels accurately in blood. For example, glucose oxidase coupled to nanotubes has been shown to serve as catalytic biomolecular sensors [221]. Several types of biodegradable nanoparticles have been developed as drug carriers for oral [222] and transmucosal delivery [223] of insulin, as an alternative to insulin injections. Biocompatible and biodegradable pH-sensitive alginate nanospheres which release insulin for extended periods in less acidic intestinal environments, but not in acidic gastric environments, are being developed [222].

1.10.3 HIV/AIDS treatment and prevention

Currently there is no cure and nor preventive vaccine for HIV/AIDS. Combination antiretroviral therapy has dramatically improved treatment, but it has to be taken for a lifetime, has major side effects and is ineffective in patients in whom the virus develops resistance**.** Nanomaterials have been shown to have therapeutic effects of their own. Studies have shown that the capsid of HIV could be a target for structure-based drug design for inhibiting viral replication [224, 225]. As a result, both computational and experimental studies have identified compounds that could inhibit the assembly of the HIV capsid. Various nanomaterials have been found to inhibit viral replication *in vitro* and it is suggested that these effects are based on structural interference with viral assembly. Various fullerene (C-60)-based structures and dendrimers have been shown to have anti- HIV activity *in vitro* [226-228]. Inorganic nanoparticles, such as gold and silver, are also being used for the prevention of this fatal disease. Silver nanoparticles showed size-dependent interaction with HIV; inhibiting the virus from binding to $CD4^+$ T cells while gold nanoparticles conjugated to the molecule SDC 1721 (a segment of the CCR5 inhibitor TAK-779) showed strong anti-HIV activity compared with free SDC 1721 [229-231]. While these efforts have not yet progressed beyond *in vitro* studies, they illustrate the potential of

therapeutic nanomaterials to inhibit HIV replication. Various nanotechnology-based drug delivery systems have been successfully used to deliver various antiretroviral drugs *in vitro* and *in vivo*. Nanosuspensions that were used to deliver the drug rilpivirine (TMC278) resulted in sustained release over 3 months in dogs and 3 weeks in mice [232]. Other therapeutic drugs such as Indinavir [233], Stavudine [234], Zidovudine [235], Efavirenz [236] and Lamivudine [237] are also being delivered to the target tissues using nano-based delivery systems. These results are a major indication of how nanotechnology-based drug delivery could improve antiviral treatment. Gene therapy based on siRNA has shown promise for HIV/AIDS treatment. Nanotechnology platforms for delivery of siRNA for HIV/AIDS treatment are in their early stages but recent work has been met with optimism. Single-walled nanotubes [238], dendrimers [239], fusion proteins [240], peptide-antibody conjugates [241] have all been used for delivery of siRNA to HIV-specific cells. Intravaginal microbicides are preventive agents that are topically applied to the vagina to prevent the transmission of HIV/AIDS or other sexually transmitted diseases. Nanotechnology-based approaches are being developed to use dendrimers [242], siRNA [243] and nanoparticles [244] for microbicidal functions. Polymeric nanoparticles have been used to deliver the CCR5 inhibitor PSC-RANTES and HIV-specific siRNA as microbicides [245].

1.10.4 As Biosensors

Gold nanoparticles have been studied and exploited in the development of an assortment of biosensors to detect specific biomolecules significant in disease etiology. Determination of choline in various human samples is clinically important and is usually assayed through the estimation of the enzyme choline esterase. A biosensor developed by combining choline oxidase (ChOx), multi-wall carbon nanotubes (MWCNTs), gold nanoparticles and poly-diallyl dimethyl ammonium chloride (PDDA) for the specific detection of choline provided an alternative, significantly sensitive, rapid and efficient approach of detection [246]. Similarly, uric acid (UA) detection was facilitated using gold nanoparticles. UA is an important end product of purine metabolism and abnormal levels of uric acid are associated with various metabolic diseases such as gout, hyperuricaemia, pneumonia, kidney damage, cardiovascular diseases and Lesch-Nyhan syndrome. Several methods including colorimetric, enzymatic and electrochemical methods are available for the

determination of UA concentration in human fluids. However, UA can be detected using gold nanoparticles by an amperometric method, in blood serum and urine with detection limit as low as 50 nM [247]. Correspondingly, a gold-platinum alloy nanoparticle based nanosensor with high selectivity, fast response time, sensitivity and good reproducibility was used to immobilize cholesterol oxidase on the basis of amperometric changes [248]. The principle used for the detection was based on hydrogen peroxide activity. In yet another study, a simple but significant colorimetric biosensor was developed using gelatin-coated gold nanoparticles with 6-mercaptohexan-1-ol (MCH) for proteinase activity assay where gelatin serves as a proteinase substrate [249]. Proteinase digestion separates gelatin and brings the nanoparticles closer due to the presence of MCH, thereby causing the gold nanoparticles to aggregate and hence changing their surface plasmon resonance. The final resultant of the proteinase activity is a shift in the SPR, changing the color of the solution which can be easily determined through the change in the absorbance ratio. Such method holds significant promise in the detection of proteinase activity in various biological samples.

1.10.5 Detection

Gold nanoparticles are also being used for the detection of various biological molecules including proteins, enzymes, DNA, antigens, antibodies, etc.

1.10.5.1 Detection of Biological Molecules

Gold nanoparticles have been used for the detection of proteins, based on their characteristic surface plasmons [250]. For this, gold nanoparticles have been functionalized using bifunctional molecules which were conjugated on one side to the gold nanoparticles through their thiol group and on the other side to the electron-rich aromatic side chains of proteins through a diazonium moiety. The model was tested using thrombin as the protein. The vibrations of the diazo-bond formed between the bifunctional molecule and the target protein tends to enhance due to the conjugation of gold nanoparticles constituting the Raman marker. After the functionalized gold nanoparticles interact with antithrombin as a sensitive recognition element, immobilized on a substrate, thrombin can be detected through surface enhanced Raman Spectroscopy. Selectively immobilized oligonucleotide modified gold nanoparticles have been used to develop a chip-based array through electro-deposition

on screen printed gold nanoparticles [251]. The method allows a multimodular detection based on the use of multiple oligonucleotides and also excludes the non-specific interactions. Similarly, a simple optical detection system was developed using DNA functionalized gold nanoparticles [252]. The method uses fluorescence quenching by gold nanoparticles for fluorophores attached to the detection sequences. The method is simple as it does not require the stem loop structure, characteristic of traditional molecular beacons and gives lesser background due to the electrostatic attraction between fluorescent dye and the gold nanoparticles and repulsion between gold nanoparticles and DNA. It also provides real-time monitoring, possible automation and lesser risk of contamination due to no washing steps. The reduction in fluorescence is used as a measure of binding of detection sequence with target DNA sequence.

1.10.5.2 Detection of Microorganisms

Detection of microorganisms can be achieved by several biochemical, microbiological and molecular methods. Recent advances in the field of nanotechnology have made it possible to detect microorganisms by using nanoparticles functionalized with oligonucleotides complementary to the gene tags of the microorganisms. In one such study, oligonucleotides complementary to the unique sequences of the heat-shock protein 70 (HSP 70) of *Cryptosporidium parvum* was used to functionalize gold nanoparticles, which could be used to detect the oocytes of *Cryptosporidium* in a colorimetric assay, offering a simple and robust method of molecular detection [253]. Gold nanoparticles were used to detect *Salmonella enteritidis* and *Listeria monocytogenes*, where gold nanoparticles were deposited within the flagella and in the biofilm network [254]. Similarly, GNP-Poly (para-phenylene ethynylene) could efficiently identify both Gram positive and gram negative bacteria based on the differential response by each bacteria [255]. In another study, gold nanoparticles funtionalized with hairpin DNA was used to image live HEp-2 cells infected with Respiratory syncytial virus [256].

1.11 Outline of the thesis

The work presented in this thesis describes the biosynthesis of oxide nanoparticles using thermophilic fungus such as *Humicola* sp. and mesophilic fungus *Fusarium oxysporum*, in an attempt to address an issue of developing biosynthetic protocols for

oxide nanomaterials and their scale-up. The main outcome of this research is the green synthesis routes of bio medically important oxide nanoparticles. Probably for the first time, biosynthesized oxide nanoparticles have been used to conjugate with anticancer drug, which could open up the doors for new nanosized drug delivery system to treat cancer. An attempt has been made to extract technologically important silica nanoparticles from waste material such as fly-ash. A very novel approach for biotransformation of size, shape and phase using fungus has been described in detail. Finally, elucidation of mechanism of formation of gold nanoparticles using alkalothermophilic (extremophilic) actinomycete *Thermomonspora* sp. has been carried out by purification of sulfite reductase enzyme and capping protein. The chapter-wise discussion of these studies is as follows:

Chapter 1 deals with the basic introduction and brief history of nanoscience and nanotechnology. Properties and synthesis methods of nanoparticles have been discussed. Review of literature on biological synthesis and mechanisms of formation of gold, silver and oxide nanoparticles and potential biomedical applications of nanomaterials have also been discussed.

Chapter 2 describes the biological synthesis of gadolinium and cerium oxide nanoparticles using the thermophilic fungus *Humicola* sp. Following their synthesis, the gadolinium oxide nanoparticles were functionalized and conjugated to anticancer drug (premodified) Taxol. The cytotoxicity of this nanodrug conjugate was then checked on THP-1 Cell lines to access its efficiency and biocompability for its applications in drug delivery systems.

Chapter 3 deals with the fungal bioleaching of waste product such as fly-ash in order to get technologically important crystalline silica nanoparticles. When the mesophilic fungus *Fusarium oxysporum* reacted with fly-ash, it could successfully leach out protein capped silica nanoparticles extracellularly within 24h of reaction.

Chapter 4 demonstrates the use of the thermophilic fungus *Humicola* sp. for the biotransformation of size, shape and phase of bulk TiO_2 particles at 50^oC. When bulk, disc-shaped anatase type TiO_2 particles were reacted with *Humicola* sp., it biotranformed into brookite type TiO_2 circular nanoparticles.

Chapters 5 gives insights into the elucidation of mechanism of formation of gold nanoparticles. The chapter deals with the purification of sulfite reductase enzyme and capping protein from the alkalothermophilic actinomycete *Thermomonospora* sp. followed by the *in vitro* synthesis of gold nanoparticles using purified enzyme and capping protein.

Chapter 6 includes a brief summary of the work presented in this thesis and the scope for possible further research in these areas.

1.12 References

[1] S. Zhang, *Biotechnology Advances* **2002**, 20, 321.

[2] A. Dowling, *Nanoscience and Nanotechnology: Opportunities and Uncertainties*, A Report by The Royal Society & The Royal Academy of Engineering, London, July **2004**.

[3] D. H. Bamford, G. Cao, *Nanostructures and Nanomaterials Synthesis, Properties and Applications*, Imperial College Press, London, **2004** *Curr.Biol* **2000**, 10, R558.

[4] D. S. Goodsell, *Bionanotechnology: Lessons from Nature*, Wiley-Liss, Hoboken, New York, **2004.**

[5] C.M. Niemeyer, *Angew. Chem. Int. Ed.* **2001**, 40, 4128.

[6] A. Henglein, *J. Phys. Chem.* **1993**, 97, 5457.

[7] A .Mohammadian, S. A. Shojaosadati, M.H. Rezaee, *Sci Iran* **2007**, 14, 323.

[8] D.R. Lovley, J.F. Stolz, G.L. Nord, E.J.P. Phillips, *Nature* **1987**, 330, 252.

[9] D.P.E. Dickson, *J Magn Magn Mater.* **1999**, 203, 46.

[10] D. Pum, U.B. Sleytr, *Trends Biotechnol.* **1999**, 17, 8.

[11] A. J. Milligan, F. M. M. Morel, *Science* **2002**, 297, 1848.

[12] T. Klaus-Joerger, R. Joerger, E. Olsson, C.G. Granqvist, *Trends Biotechnol.* **2001**, 19, 15.

[13] R. M Bruins, S. Kapil, S. W. Oehme, *Ecotoxicol Environ Saf.* **2000**, 45, 198.

[14] T. J. Beveridge, M. N. Hughes, H. Lee, K. T. Leung, R. K. Poole, I. Savvaidis, S. Silver, J. T. Trevors, *Adv Microb Physiol* . **1997**, 38, 177.

[15] N. C. Sharma, S. V. Sahi, S. Nath, J. G. Parsons, J. L. Gardea-Torresdey, T. Pal, *Environ Sci Technol.* **2007**, 41, 5137.

[16] S. Mann, *Nature* **1992**, 357, 358.

[17] T. J. Beveridge, R. G. E. Murray, *J Bacteriol.* **1980**, 141, 876.

[18] G. Southam, T. J. Beveridge, *Geochim Cosmochim Acta* **1994**, 58, 4527.

[19] M. Lengke, G. Southam. *Geochim Cosmochim Acta* **2006**, 70, 3646.

[20] K. Kashefi, J. M. Tor, K. P. Nevin, D. R. Lovley, *Appl Environ Microbiol*. **2001**, 67, 3275.

[21] Y. Konishi, T. Tsukiyama, T. Tachimi, N. Saitoh, T. Nomura, S. Nagamine. *Electrochim Acta* **2007**, 53, 186.

[22] L. Du, H. Jiang, H. Xiaohua, Wang E. *Electrochem Commun*. **2007**, 9, 1165.

[23] Y. Feng, Y. Yu, Y. Wang, X. Lin, *Curr Microbiol.* **2007**, 55, 402.

[24] R. Joerger, T. Klaus, C. G Granqvist, *Adv Mater.* **2000**, 12, 407.

[25] T. Klaus, R. Joerger, E. Olsson, C. G. Granqvist, *Proc Natl Acad Sci*. **1999**, 96, 13611.

[26] Jin-Zhou. Fu, Yue-Ying. Liu, Ping-Ying. Gu, Ding-Liang. Shang, Zhong-Yu. Lin, Bing-Xin. Yao, Sheng-Zhou. Weng, *Acta Phys Chim Sin*. **2000**, 16, 779.

[27] S. Kalathil, J. Lee, M. H. Cho, *Green Chem.* **2011**, 13, 1482.

[28] K.V. Prabhu, C. Sundaramoorthi, S. Devarasu, *Journal of Pharmacy Research* **2011**, 4, 820.

[29] H. Zhang, Q. Li, Y. Lu, D. Sun, X. Lin, X. Deng, N. He, S. Zheng, *J Chem Technol Biotechnol*. **2005**, 80, 285.

[30] R. R. Naik, S. J. Stringer, G. Agarwal, S. E. Jones, M. O. Stone, *Nat Mater*. **2002**, 1, 169.

[31] N. Pugazhenthiran, S. Anandan, G. Kathiravan, N. K. U. Prakash, S. Crawford, M. Ashokkumar, *J Nanopart Res*. **2009**, 11, 1811.

[32] B. Nair, T. Pradeep, *Cryst Growth Des*. **2002**, 2, 293.

[33] S. D. Gregorio, S. Lampis, G. Vallini. *Environ Int*. **2005**, 31, 233.

[34] M. E. Losi, W. T. Frankenberger Jr, *Appl Environ Microbiol*. **1997**, 63, 3079.

[35] J. Kessi, M. Ramuz, E. Wehrli, M. Spycher, R. Bachofen, *Appl Environ Microbiol.* **1999**, 65, 4734.

[36] F. A. Tomei, L. L. Barton, C. L. Lemanski, T. G. Zocco, N. H. Fink, O. Sillerud, *J Ind Microbiol.* **1995**, 14, 329.

[37] T. L. Gerrard, J. N. Telford, H. H. Williams, *J Bacteriol*. **1974**, 119, 1057.

[38] R. A. Silverberg, P. T. S. Wong, Y. K. Chau, *Arch Microbiol*. **1976**, 147, 1.

[39] L. Lortie, W. D. Gould, S. Rajan, R. G. L. McCready, K. J. Cheng, *Appl Environ Microbiol*. **1992**, 58, 4042.

[40] W. Hunter, D. Manter, *Curr Microbiol*. **2008,** 57, 83.

[41] V. Yadav, N. Sharma, R. Prakash, K. K. Raina, L. M. Bharadwaj, N. T. Prakash, *Biotechnology* **2008**, 7, 299.

[42] Y. Konishi, K. Ohno, N. Saitoh, T. Nomura, S. Nagamine, H. Hishida, Y. Takahashi, T. Uruga, *J Biotechnol*. **2007**, 128, 648.

[43] P. Yong, N. A. Rowsen, J. P. G. Farr, I. R. Harris, L. E. Macaskie, *Biotechnol Bioeng*. **2002**, 80, 369.

[44] D. De Windt, P. Aelterman, W. Verstraete, *Environ Microbiol*. **2005**, 7, 314.

[45] D. P. Cunningham, L. L. Lundie, *Appl Environ Microbiol*. **1993**, 59, 7.

[46] P. R. Smith, J. D. Holmes, D. J. Richardson, D. A. Russell, J. R. Sodeau, *J Chem Soc Faraday Trans*. **1998**, 94, 1235.

[47] R. Y. Sweeney, C. Mao, X. Gao, J. L. Burt, A. M. Belcher, G. Georgiou, B. L. Iverson, *Chem Biol*. **2004**, 11, 1553.

[48] M. Labrenz, G.K. Druschel, T. Thomsen-Ebert, B. Gilbert, S.A. Welch, K.M. Kemner, *Science* **2000**, 290, 1744.

[49] S. He, Z. Guo, Y. Zhang, S. Zhang, J. Wang, N. Gu, *Mater Lett*. **2007**, 61, 3984.

[50] M. I. Husseiny, M. Abd El-Aziz, Y. Badr, M. A. Mahmoud, *Spectrochim Acta A* **2007**, 67, 1003.

[51] A. K. Suresh, D. A. Pelletier, W. Wang, M. L. Broich, Ji-Won Moon, B. Gu, D. P. Allison, D. C. Joy, T. J. Phelps, M. J. Doktycz, *Acta Biomaterialia* **2011**, 7, 2148.

[52] F. U. Mouxing, L. I. Qingbiao, S. U. N. Daohua, L. U. Yinghua, H. E. Ning, D. Xu, W. Huixuam, H. Jiale, *Chinese J Chem Eng*. **2006**, 14, 114.

[53] A. R. Shahverdi, S. Minaeian, H. R. Shahverdi, H. Jamalifar, A. A. Nohi, *Proc Biochem.* **2007**, 42, 919.

[54] K. Kalishwaralal, V. Deepak, S. Ramakumarpandian, H. Nellaiah, G. Sangiliyandi. *Mat Lett.* **2008**, 62, 4411.

[55] H. S. Barud, C. Barrios, T. Regiani, R. F. C. Marques, M. Verelst, J. Dexpert-Ghys, Y. Messaddeq, S. J. L. Ribeiro, *Mat Sci Eng C* **2008**, 28, 515.

[56] J. L. Elechiguerra, J. L. Burt, J. R. Morones, A. C. Bragad, X. Gao, H. H. Lara, *J Nanobiotechnol.* **2005**, 3, 6.

[57] M. M. Juibari, S. Abbasalizadeh, G. S. Jouzani , M. Noruzi, *Materials Letters* **2011,** 65,1014.

[58] N. Kannan, S. Subbalaxmi, *Research Journal of Nanoscience and Nanotechnology* **2011**, 1, 87.

[59] Hong-Juan Bai, Bin-Sheng Yang, Chun-Jing Chai, Guan-E Yang, Wan-Li Jia, Zhi-Ben Yi, *World J Microbiol Biotechnol.***2011**, 27, 2723.

[60] S. Sadhasivam, P. Shanmugam, K. Yun, *Colloids and Surfaces B: Biointerfaces* **2010,** 81, 358.

[61] M. Potara, E. Jakab, A. Damert, O. Popescu, V. Canpean, S. Astilean, *Nanotechnology* **2011**, 22, 135101.

[62] R. Y. Parikh, R. Ramanathan, P. J. Coloe, S. K. Bhargava, M. S. Patole, Y. S. Shouche, V. Bansal, *PLoS ONE* **2011** , 6, e21401.

[63] S. M. Baesman, T. D. Bullen, J. Dewald, D. Zhang, S. Curran, F. S. Islam, T. J. Beveridge, R. S. Oremland, *Appl Environ Microbiol.* **2007**, 73, 2135.

[64] M. J. Marshall, A. S. Beliaev, A. C. Dohnalkova, D. W. Kennedy, L. Shi, Z. Wang, M. I. Boyanov, B. Lai, K. M. Kemner, J. S. Mclean, S. B. Reed, G. E. Culley, V. L. Bailey, C. J. Simonson, D. A. Saffarini, M. F. Romine, Y. Gorbi, J. M. Zachara, J. K. Fredrickson, *PLoS Biol.* **2006**, 4, 1324.

[65] J. D. Holmes, P. R. Smith, R. Evans-Gowing, D. J. Richardson, D. A. Russell, J. R. Sodeau, *Arch Microbiol.* **1995**, 163, 143.

[66] H. J. Bai, Z. M. Zhang, Y. Guo, G. E. Yang, *Coll Surf B: Biointerf.* **2009**, 70, 142.

[67] X. Li, S. Chen, W. Hu, S. Shi, W. Shen, X. Zhang, H. Wang, *Carbohyd Poly*. **2009**, 76, 509.

[68] H. J. Bai, Z. M. Zhang, J. Gong, *Biotechnol Lett*. **2006**, 28, 1135.

[69] H. J. Bai, Z. M. Zhang, *Mater Lett*. **2009**, 63, 764.

[70] P. Mukherjee, S. Senapati, D. Mandal, A. Ahmad, M. I. Khan, R. Kumar, M.Sastry, *ChemBioChem*. **2002**, 3, 461.

[71] S. Senapati, D. Mandal, A. Ahmad, M. I. Khan, M. Sastry, R. Kumar, *Ind J Phys.***2004**, 78, 101.

[72] S. Senapati, A. Ahmad, M. I. Khan, M. Sastry, R. Kumar, *Small* **2005**, 1, 517.

[73] V. Bansal, D. Rautaray, A. Ahmad, M. Sastry, *J Mater Chem*. **2004**, 14, 3303.

[74] V. Bansal, D. Rautaray, A. Bharde, K. Ahire, A. Sanyal, A. Ahmad, M. Sastry, *J Mater Chem*. **2005**, 15, 2583.

[75] V. Bansal, P. Poddar, A. Ahmad, M. Sastry, *J Am Chem Soc*. **2006**, 128, 11958.

[76] D. Rautaray, A. Sanyal, S. D. Adyanthaya, A. Ahmad, M. Sastry, *Langmuir* **2004**, 20, 6827.

[77] T. L. Riddin, M. Gericke, C. G. Whiteley, *Nanotechnol*. **2006**, 17, 3482.

[78] S. A. Kumar, A. Ayoobul, A. Absar, M. I. Khan, *J Biomed Nanotechnol*. **2007**, 3, 190.

[79] I. Uddin, S. Adyanthaya, A. Syed, K. Selvaraj, A. Ahmad, P. Poddar, *J Nanosci Nanotechnol*. **2008**, 8, 3909.

[80] S. S. Shankar, A. Ahmad, R. Pasricha, M. Sastry, *J Mat Chem*. **2003**, 13, 1822.

[81] A. Ahmad, S. Senapati, M. I. Khan, R. Kumar, M. Sastry, *J Biomed Nanotechnol*. **2005**, 1, 47.

[82] P. Mukherjee, M. Roy, B. P. Mandal, G. K. Dey, P. K. Mukherjee, J. Ghatak, A. K. Tyagi, S. P. Kale, *Nanotechnology* **2008**, 19, 075103.

[83] M. Fayaz, K. Balaji, M. Girila, R. Yadav, P. T. Kalaichelvan, R. Venketesan, *Nanomedicine* **2010**, 6, 103.

[84] N. Vigneshwaran, A. A. Kathe, P. V. Varadarajan, R. P. Nachane, R. H. Balasubramanya, *Coll Surf B: Interf*. **2006**, 53, 55.

[85] A. Ingle, M. Rai, A. Gade, M. Bawaskar, *J Nanopart Res*. **2009**, 11, 2079.

[86] S. Basavaraja, S. D. Balaji, A. Lagashetty, A. H. Rajasab, A. Venkataraman, *Mat Res Bull.* **2008**, 43, 1164.

[87] K. C. Bhainsa, S. F. D'Souza, *Coll Surf B: Interf*. **2006**, 47, 160.

[88] R. Sanghi, P. Verma, *Bioresour Technol.* **2009**, 100, 501.

[89] A. K. Gade, P. P. Bonde, A. P. Ingle, P. Marcato, N. Duran, M. K. Rai, *J Biobased Mater Bioenergy* **2008**, 2, 1.

[90] S. S. Birla, V. V. Tiwari, A. K. Gade, A. P. Ingle, A. P. Yadav, M. K. Rai, *Lett Appl Microbiol*. **2009**, 48, 173.

[91] N. S. Shaligram, M. Bule, R. Bhambure, R. S. Singhal, S. K. Singh, G. Szakacs, A. Pandey, *Proc Biochem.* **2009**, 44, 939.

[92] D. S. Balaji, S. Basavaraja, R. Deshpande, B. D. Mahesh, B. K. Prabhakar, A. Venkataraman, *Coll Surf B: Biointerf.* **2009**, 68, 88.

[93] K. Kathiresan,S. Manivanan,M.A. Nabeel, B. Dhivya, *Coll Surf B: Biointerf.* **2009**, 71, 133.

[94] D. Philip, *Spectrochim Acta Part A* **2009**, 73, 374.

[95] Mukherjee, A. Ahmad, D. Mandal, S. Senapati, S. R. Sainkar, M. I. Khan, R. Ramani, R. Parischa, P. V. Ajaykumar, M. Alam, M. Sastry, R. Kumar, *Angew Chem Int Ed*. **2001**, 40, 3585.

[96] M. Gericke, A. Pinches, *Hydrometallurgy* **2006**, 83, 132.

[97] M. Gericke, A. Pinches, *Gold Bull.* **2006**, 39, 22.

[98] L. Pighi, T. Pumpel, F. Schinner, *Biotechnol Lett.* **1989**, 11, 275.

[99] J. C. Chen, Z. H. Lin, X. X. Ma, *Lett Appl Microbiol*. **2003**, 37, 105.

[100] P. Mukherjee, A. Ahmad, D. Mandal, S. Senapati, S. R. Sainkar, M. I. Khan, R. Parischa, P. V. Ajaykumar, M. Alam, R. Kumar, M. Sastry, *Nano lett*. **2001**, 1, 515.

[101] N. Vigneshwaran, N. M. Ashtaputre, P. V. Varadarajan, R. P. Nachane, K. M. Paralikar, R. H. Balasubramanya, *Mat Lett.* **2007**, 61, 1413.

[102] D. M. Ali, M. Sasikala, M. Gunasekaran, N. Thajuddin, *Digest Journal of Nanomaterials and Biostructures* **2011**, 6, 385.

[103] E. Castro-Longoria, A. R. Vilchis-Nestor, M. Avalos-Borja, *Colloids and Surfaces B: Biointerfaces* **2011**, 83, 42.

[104] S. S. Shankar, A. Ahmad, R. Pasricha, M. Sastry, *J Mat Chem.* **2003**, 13, 1822.

[105] A. Ingle, A. Gade, S. Pierrat, C. Sonnichsen, M. Rai, *Curr Nanosci*. **2008**, 4, 141.

[106] K. Vahabi, G. A. Mansoori, S. Karimi, *Insciences J.* **2011**, 1, 65.

[107] Gui-Qiu Chen, Zheng-Jun Zou, Guang-Ming Zeng, M. Yan, Jia-Qi Fan, An-Wei Chen, F. Yang, Wen-Juan Zhang, L. Wang, *Chemosphere* **2011,** 83, 1201.

[108] S. K. Raja Namasivayam, S. Ganesh, Avimanyu, *Int J Med Res.* **2011**, 1, 131.

[109] A. Ahmad, S. Senapati, M. I. Khan, R. Kumar, M. Sastry, *Langmuir* **2003**, 19, 3550.

[110] A. Ahmad, S. Senapati, M. I. Khan, R. Kumar, R. Ramani, V. Srinivas, M. Sastry, *Nanotechnol*. **2003**, 14, 824.

[111] C. T. Dameron, R. N. Reese, R. K. Mehra, A. R. Kortan, P. J. Carroll, M. L. Steigerwald, L. E. Brus, D. R. Winge, *Nature* **1989**, 338, 596.

[112] M. Kowshik, W. Vogel, J. Urban, S. K. Kulkarni, K. M. Paknikar, *Adv Mater*. **2002**, 14, 815.

[113] M. Kowshik, N. Deshmukh, W. Vogel, J. Urban, S. K. Kulkarni, K. M. Paknikar, *Biotechnol Bioeng*. **2002**, 78, 583.

[114] S. Seshadri, K.Saranya, M. Kowshik, *Formulation and Engineering of Biomaterials Biotechnology Progress* **2011**, 27, 1464.

[115] Z. Lin, J. Wu, R. Xue, Y. Yang, *Spectrochimica Acta Part A* **2005**, 61, 761.

[116] M. Agnihotri, S. Joshi, A.R. Kumar, S. Zinjarde, S. Kulkarni, *Mat Lett*. **2009**, 63, 1231.

[117] M. Kowshik, S. Ashtaputre, S. Kharrazi, W. Vogel, J. Urban, S. K. Kulkarni, K. M. Paknikar, *Nanotechnol*. **2003**, 14, 95.

[118] A. Mishra1, S. K. Tripathy, Soon-Yun, *Journal of Nanoscience and Nanotechnology* **2011**, 11, 243.

[119] A. Henglein, *Chem Rev*. **1989**, 89, 1861.

[120] A. P. Alivisatos, K. P. Johnsson, X. Peng, T. E. Wilson, C. J. Loweth, M. P. Bruchez, P. G. Shultz, *Nature* **1996**, 382, 609.

[121] C. A. Mirkin, R. L. Letsinger, R. C. Mucic, J. J. Storhoff , *Nature* **1996**, 382, 607.

[122] E. Braun, Y. Eichen, U. Sivan, G. Ben-Yoseph, *Nature* **1998**, 391, 775.

[123] K. K. W. Wong, T. Douglas, S. A. Glider, D. D. Awschalom, S. Mann, *Chem Mater*. **1998**, 10, 279.

[124] D. D. Archibald, S. Mann, *Nature* **1993**, 364, 430.

[125] S. Baral, P. Schoen, *Chem Mater* **1993**, 5, 145.

[126] T. Douglas, M. Young, *Nature* **1998**, 393, 152.

[127] M. Pazirandeh, S. Baral, J. R. Campbell, *Biomimetics* **1992**, 1, 41.

[128] W. Shenton, D. Pum, U. Sleytr, S. Mann, *Nature* **1997**, 389, 585.

[129] S. A. Davis, S. L. Burkett, N. H. Mendelson, S. Mann, *Nature* **1997**, 385, 420.

[130] W. Shenton, T. Douglas, M. Young, G. Stubbs, S. Mann, *Adv Mater*. **1999**, 11, 253.

[131] S. W. Lee, C. Mao, C. E. Flynn, A. M. Belcher, *Science* **2002**, 296, 892.

[132] C. Mao, C. E. Flynn, A. Hayhurst, R. Sweeney, J. Qi, G. Georgiou, B. Iverson, A. M. Belcher, *Proc Natl Aca Sci USA* **2003**, 100, 6946.

[133] C. Noguera, *Physics and Chemistry at Oxide Surfaces*; Cambridge University Press:Cambridge, UK, **1996**.

[134] H.H. Kung, *Transition Metal Oxides: Surface Chemistry and Catalysis*; *Elsevier*, Amsterdam, **1989**.

[135] V.E. Henrich, P.A. Cox, *The Surface Chemistry of Metal Oxides*; Cambridge University Press: Cambridge, UK, **1994**.

[136] A.F. Wells, *Structural Inorganic Chemistry, 6th Ed*; Oxford University Press: New York, **1987**.

[137] J.A. Rodríguez, M. Fernández-García, (Eds.) *Synthesis, Properties and Applications of Oxide Nanoparticles.* Whiley: New Jersey, **2007**.

[138] M. Fernández-García, A. Martínez-Arias, J.C. Hanson, J.A. Rodríguez, *Chem. Rev.* **2004**, 104, 4063.

[139] R.W.G. Wyckoff, *Crystal Structures, 2nd ed*; Wiley: New York, **1964**.

[140] H. Gleiter, *Nanostruct. Mater.* **1995**, 6, 3.

[141] M. Valden, X. Lai, D. W. Goodman, *Science* **1998**, 281, 1647.

[142] J. A. Rodriguez, G. Liu, T. Jirsak, Hrbek, Z. Chang, J. Dvorak, A. Maiti, *J. Am. Chem. Soc.* **2002**, 124, 5247.

[143] M. Baumer, H. Freund, J. *Progress in Surf. Sci.* **1999**, 61,127.

[144] M. L. Trudeau, J. Y. Ying, *Nanostruct Mater.* **1996**, 7, 245.

[145] P. Ayyub, V. R. Palkar, S. Chattopadhyay, M. Multani, *Phys. Rev. B* **1995**, 51, 6135.

[146] (a) N. Millot, D. Aymes, F. Bernard, J. C. Niepce, A. Traverse, F. Bouree, B. L. Cheng, P. Perriat, *J. Phys. Chem. B* **2003**, 107, 5740. (b) J. Schoiswohl, G. Kresse, S. Surnev, M. Sock, M. G. Ramsey, F. P. Netzer, *Phys. Rev. Lett.* **2004**, 92, 206103.

[147] J. M. McHale, A. Auroux, A. J. Perrota, A. Navrotsky, *Science* **1997**, 277, 788.

[148] H. Zhang, J. F. Bandfield, *J. Mater. Chem.* **1998**, 8, 2073.

[149] V. M. Samsonov, N. Yu. Sdobnyakov, A. N. Bazulev, *Surf. Sci.* **2003**, 532-535, 526-530.

[150] Z. Song, T. Cai, Z. Chang, G. Liu, J. A. Rodriguez, J. J. Hrbek, *J. Am. Chem. Soc.* **2003**, 125, 8060.

[151] S. Thota, J. Kumar, *Journal of Physics and Chemistry of Solids* **2007**, 68, 1951.

[152] P. Ayyub, M. Multani, M. Barma, V. R. Palkar, R. Vijayaraghavan, *J. Phys. C: Solid State Phys.* **1988**, 21, 229.

[153] R. C. Garvie, M. F. Goss, *J. Mater. Sci.* **1986,** 21, 1253.

[154] M. D. Hernández-Alonso, A. B. Hungría, J. M. Coronado, A. Martínez-Arias, J. C. Conesa, J. Soria, M. Fernández-García, *Phys. Chem. Chem. Phys.* **2004**, 6, 3524.

[155] G. Skandan, C. M. Foster, H. Frase, M. N. Ali, J. C. Parker, H. Hahn, *Nanostruct. Mater.* **1992**, 1, 313.

[156] R. C. Cammarata, K. Sieradki, *Phys. Rev. Lett.* **1989**, 62, 2005.

[157] (a) M. Fernandez-Garcia, X. Wang, C. Belver, A. Hanson, J. C. Iglesias-Juez, J. A. Rodriguez, *Chem. Mater.* **2005**, 17, 4181; (b) K. A. Alim, V. A. Fonobevor, A. A. Balandin, *Appl. Phys. Lett.* **2005**, 86, 053103.

[158] S. Surnev, G. Kresse, M. G. Ramsey, F. P. Netzer, *Phys. Rev. Lett.* **2001**, 87, 86102.

[159] P. Moriarty, *Rep. Prog. Phys.* **2001**, 64, 297.

[160] A. D. Yoffre, *Advances in Physics* **1993**, 42, 173.

[161] L. Brus, *J. Phys. Chem.* **1986**, 90, 2555.

[162] G. Pacchioni, A. M. Ferrari, P. S. Bagus, *Surf. Sci.* **1996**, 350, 159.

[163] J. A. Mejias, A. M. Marquez, J. Fernandez-Sanz, M. Fernandez-Garcia, J. M. Ricart, C. Sousa, F. Illas, *Surf. Sci.* **1995**, 327, 59.

[164] M. Fernández-García, J. C. Conesa, F. Illas, *Surf. Sci.* **1996**, 349, 207.

[165] T. Albaret, F. Finocchi, C. Noguera, *Faraday Discuss.* **2000**, 114, 285.

[166] J. A. Rodriguez, A. Maiti, *J. Phys. Chem. B* **2000**, 104, 3630.

[167] J. A. Rodriguez, T. Jirsak, S. Chaturvedi, *J. Chem. Phys.* **1999**, 111, 8077.

[168] T. Bredow, E. Apra, M. Catti, G. Pacchioni, *Surf. Sci.* **1998**, 418, 150.

[169] M. Casarin, C. Maccato, A. Vittadini, *Surf. Sci.Lett.* **1997**, 377, L1079.

[170] C.A. Scamehorn, N. M. Harrison, M. I. McCarthy, *J. Chem. Phys.* **1994**, 101, 1547.

[171] J. A. Rodriguez, *Theor. Chem. Acc.* **2002**, 107, 117.

[172] J. A. Rodriguez, S. Chaturvedi, M. Kuhn, J. Hrbek, *J. Phys. Chem. B* **1998**, 102, 5511.

[173] R. Hoffmann, *Solids and Surfaces: A Chemist's View of Bonding in Extended Structures*; VCH: New York, **1988**.

[174] T. A. Albright, J. K. Burdett, M. H. Whangbo, *Orbital Interactions in Chemistry*; Wiley-Interscience: New York, **1985**.

[175] H. Luth, *Surface and interface of solid materials*; Springer, Berlin, **1997**.

[176] J. Bardeen, *Phys. Rev.* **1947**, 71, 717.

[177] J. Jeevanadam, K. J. Klabunde, *Adsorbents* in "Synthesis, Properties and Applications of Oxide Nanoparticles" (J. A. Rodríguez, Fernández-García, M; Eds.). Whiley: N. J., **2007**. Ch. 14.

[178] J. L. Anchell, A. C. Hess, *J. Phys. Chem.* **1996**, 100, 18317.

[179] J. A. Rodriguez, J. Hrbek, J. Dvorak, T. Jirsak, A. Maiti, *Chem. Phys. Lett.* **2001**, 336, 377.

[180] A. M. Ferrari, G. Pacchioni, *J. Phys. Chem.* **1995**, 99, 17010.

[181] R. Richards, W. Li, S. Decker, C. Davidson, O. Koper, V. Zaikovski, A. Volodin, T. Rieker, *J. Am. Chem. Soc.* **2000**, 122, 4921.

[182] J. A. Rodriguez, X. Wang, G. Liu, J. C. Hanson, J. Hrbek, C. H. F. Peden, A. Iglesias- Juez, M. Fernández-García, *J. Molec. Catal. A: Chemical* **2005**, 228, 11.

[183] T. X. Fan, S. K. Chow, D. Zhang, *Progress in Materials. Science* **2009**, 54, 542.

[184] D. A. Bazylinski, A. J. G. Reed, R. B. Frankel, *Microscopy Research and Technique* **1994**, 27, 389.

[185] D. A. Bazylinski, R. B. Frankel, B. R. Heywood, S. Mann, J. W. King, P. L. Donaghey, A. K. Hanson, *Applied and Environmental Microbiology* **1995**, 61, 3232.

[186] A. Arakaki, H. Nakazawa, M. Nemoto, T. Matsunaga, *Journal of the Royal Society Interface* **2008**, 5, 977.

[187] R. P. Blakemore, *Science* **1975**, 190, 377.

[188] R. H. Thornhill, J. G. Burgess, T. Matsunaga, *Applied and Environmental Microbiology* **1995**, 61, 495.

[189] S. Spring, K. H. Schleifer, *Syst. Applied Microbiology* **1995**, 18, 147.

[190] C. T. Lefèvre, F. Abreu, U. Lins, D. A. Bazylinski, *Applied and Environment Microbiology* **2010**, 76, 3220.

[191] C. T. Lefèvre, F. Abreu, M. L. Schmidt, U. Lins, R. B. Frankel, B. P. Hedlund, D. A. Bazylinski, *Applied and Environment Microbiology* **2010**, 76, 3740.

[192] W. Zhou, W. He, S. Zhong, Y. Wang, H. Zhao, Z. Li, S. Yan, *Journal of Magnetism and Magnetic Materials* **2009**, 321, 1025.

[193] W. Zhou, W. He, X. Zhang, S. Yan, X. Sun, X. Tian, X. Han, *Powder Technology* **2009**, 106.

[194] A. K. Jha, K. Prasad, K. Prasad, *Biochemical Engineering Journal* **2009**, 43, 303.

[195] A. K. Jha, K. Prasad, *Colloids and Surfaces B: Biointerfaces* **2010**, 75, 330.

[196] A. K. Jha, K. Prasad, A. R. Kulkarni, *Colloids and Surfaces B: Biointerfaces* **2009**, 71, 226.

[197] U. Kumar, A. Shete, A. S. Harle, O. Kasyutich, W. Schwarzacher, A. Pundle, P. Poddar, *Chem Mater*. **2008**, 20, 1484.

[198] A. Ahmad, T. Jagadale, V. Dhas, S. Khan, S. Patil, R. Pasricha, V. Ravi, S. Ogale, *Advanced Materials* **2007**, 19, 3295.

[199] A. Ahmad, P. Mukherjee, S. Senapati, D. Mandal, M. I. Khan, R. Kumar, M. Sastry, *Colloids Surf B Biointerfaces* **2003**, 28, 313.

[200] S. He, Z. Guo, Y. Zhang, S. Zhang, J. Wang, N. Gu *Mater Lett*. **2007**, 61, 3984.

[201] K. Sneha, M. Sathishkumar, J. Mao, I. S. Kwak, Y. Yun, *Chemical Engineering Journal* **2010**, 162, 989.

[202] A. Malik, *Environ Inter*. **2004**, 30, 261

[203] A. S. Kumar, M. K. Abyaneh, S. W. Gosavi, S. K. Kulkarni, R. Pasricha, A. Ahmad, M. I. Khan, *Biotechnol Lett*. **2007**, 29, 439.

[204] N. Duran, P. D. Marcato, O. L. Alves, G. I. H. De Souza, E. Esposito, *J Nanobiotechnol.* **2005**, 3, 8.

[205] N. Jain, A. Bhargava, S. Majumdar, J. C. Tarafdar, J. Panwar, *Nanoscale* **2011**, 3, 635.

[206] S. A. Kumar, M. K. Abyaneh, S. W. Gosavi, S. K. Kulkarni, A. Ahmad, M. I. Khan, *Biotechnol Appl Biochem.* **2007**, 47, 191.

[207] Y. Govender, T. L. Riddin, M. Gericke, C. G. Whiteley, *J Nanopart Res*. **2010**, 12, 261.

[208] J, Xie, J. Y. Lee, D. I. C. Wang, Y. P. Ting, *Small* **2007**, 3, 672.

[209] A. Bharde, D. Rautaray, V. Bansal, A. Ahmad, I. Sarkar, S. M. Yusuf, M. Sanyal, M. Sastry, *Small* **2006**, 2, 135.

[210] G.Oberdorster , E. Oberdorster, J. Oberdorster, *Environ Health Persp*. **2005**, 113, 823.

[211] L. Brannon-Peppas, J. O. Blanchette, *Adv Drug Deliv Rev*. **2004**, 56, 1649.

[212] M. E. R. O'Brien, N. Wigler, M. Inbar, R. Rosso, E. Grischke, A. Santoro, R. Catane, D. G. Kieback, P. Tomczak, S. P. Ackland, F. Orlandi, L. Mellars, L. Alland, C. Tendler, *Ann Oncol*. **2004**, 15, 440.

[213] A. Moreno-Aspitia, E. A. Perez, *Future Oncol*. **2005**, 1,755.

[214] P. Pathak, G. L. Prasad, M. J. Meziani, A. A. Joudeh, Y. P. Sun, *Langmuir* **2007**, 23, 2674.

[215] A. K. Gupta, M. Gupta, *Biomaterials* **2005**, 26, 3995.

[216] C. Klumpp, K. Kostarelos, M. Prato, A. Bianco, *Biochim Biophys Acta*. **2006**, 1758, 404.

[217] M. V. Yezhelyev, X. Gao, Y. Xing, A. Al-Hajj, S. Nie, R. M. O'Regan, *The Lancet Oncol*. **2006**, 7, 657.

[218] N. W. Shi Kam, M. O'Connell, J. A. Wisdom, H. Dai, *PNAS* **2005**, 102, 11600.

[219] C. Loo, A. Lin, L. Hirsch, M. H. Lee, J. Barton, N. Halas, J. West, R. Drezek, *Technol Cancer Res Treat*. **2004**, 3, 33.

[220] Y. Tabata, Y. Murakami, Y. Ikada, *Fullerene Sci Technol*. **1997**, 5, 989.

[221] P. W. Barone, S. Baik, D. A. Heller, M. S. Strano, *Nat Mater* **2005**, 4, 86.

[222] N. K. K. Raj, C. P. Sharma, *J Biomater Appl*. **2003**, 17, 183.

[223] H. M. Joshi, D. R. Bhumkar, K. Joshi, V. Pokharkar, M. Sastry, *Langmuir* **2006**, 22, 300.

[224] B. K. Ganser-Pornillos, M. Yeager, W. I. Sundquist, *Curr. Opin. Struct. Biol.* **2008**, 18, 203.

[225] O. Pornillos, B. K. Ganser Pornillos, B. N. Kelly, Y. Hua, F. G. Whitby, C. D. Stout, W. I. Sundquist, C. P. Hill, M. Yeager, *Cell* **2009**, 137, 1282.

[226] S. H. Friedman, D. L. Decamp, R. P. Sijbesma, G. Srdanov, F. Wudl, G. L. Kenyon, *J. Am. Chem. Soc.* **1993**, 115, 6506.

[227] S. Bosi, T. Da Ros, G. Spalluto, J. Balzarini, M. Prato, *Bioorg. Med. Chem. Lett.* **2003**, 13, 4437.

[228] R. A. Kotelnikova, G.N. Bogdanov, E.C. Frog, A. I. Kotelnikov, V. N. Shtolko, V. S. Romanova, S. M. Andreev, A. A. Kushch, N. E. Fedorova, A. A. Medzhidova, G. G. Miller, *J. Nanopart. Res.***2003**, 5, 561.

[229] J. L. Elechiguerra, J. L. Burt, J. R. Morones, A. Camacho-Bragado, X. Gao, H.H. Lara, M. J. Yacaman, *J. Nanobiotechnology* **2005**, 3, 6.

[230] R. W. Sun, R. Chen, N. P. Chung, C. M. Ho, C. L. Lin, C. M. Che, *Chem. Commun.* **2005**, 40, 5059.

[231] M. C. Bowman, T. E. Ballard, C. J. Ackerson, D. L. Feldheim, D. M. Margolis, C. Melander, *J. Am. Chem. Soc.* **2008**, 130, 6896.

[232] L. Baert , G. van't Klooster, W. Dries, M. François, A. Wouters , E. Basstanie, K. Iterbeke, F. Stappers, P. Stevens, L. Schueller, P. Van Remoortere, G. Kraus , P. Wigerinck, J. Rosier, *Eur. J. Pharm. Biopharm.* **2009**, 72, 502.

[233] H. Dou , C. J. Destache, J. R. Morehead, R. L. Mosley, M. D. Boska, J. Kingsley, S. Gorantla, L. Poluektova, J. A. Nelson, M. Chaubal, J. Werling, J. Kipp, B. E. Rabinow, H. E. Gendelman, *Blood* **2006**, 108, 2827.

[234] M. Garg, A. Asthana, H. B. Agashe, G. P. Agrawal, N. K. Jain, *J. Pharm. Pharmacol.* **2006**, 58, 605.

[235] C. D. Kaur, M. Nahar, N. K. Jain, *J. Drug Target* **2008**, 16, 798.

[236] T. Dutta, H. B. Agashe, M. Garg, P. Balakrishnan, M. Kabra , N. K. Jain, *J. Drug Target* **2007**, 15, 89.

[237] L. Wan, X. Zhang, S. Pooyan, M. S. Palombo, M. J. Leibowitz, S. Stein, P. J. Sinko, *Bioconjug. Chem.* **2008**, 19, 28.

[238] Z. Liu, M. Winters, M. Holodniy, H. Dai, *Angew. Chem. Int. Ed.* **2007**, 46, 2023.

[239] N. Weber, P. Ortega, M. I. Clemente, D. Shcharbin, M. Bryszewska, F. J. de la Mata, R. Gómez, M. A. Muñoz-Fernández, *J. Control Release* **2008**, 132, 55.

[240] A. Eguchi, B. R. Meade, Y. C. Chang, C. T. Fredrickson, K. Willert, N. Puri, S. F. Dowdy, *Nat. Biotechnol.* **2009**, 27, 567.

[241] E. Song, P. Zhu, S. K. Lee, D. Chowdhury, S. Kussman, D. M. Dykxhoorn, Y. Feng, D. Palliser, D. B. Weiner, P. Shankar, W. A. Marasco, J. Lieberman, *Nat. Biotechnol.* **2005**, 23, 709.

[242] R. Rupp, S. L. Rosenthal, L. R. Stanberry, *Int. J. Nanomedicine* **2007**, 2, 561.

[243] D. Palliser, D. Chowdhury, Q. Y. Wang, S. J. Lee, R. T. Bronson, D. M. Knipe, J. Lieberman, *Nature* **2006**, 439, 89.

[244] K. A. Woodrow, Y. Cu ,C. J. Booth, J. K. Saucier-Sawyer, M. J. Wood, W. M. Saltzman, *Nat. Mater.* **2009**, 8, 526.

[245] A. S. Ham, M. R. Cost, A. B. Sassi, C. S. Dezzutti, L. C. Rohan, *Pharm. Res.* **2009**, 26, 502.

[246] X. Qin, H. Wang, X. Wang, Z. Miao, L. Chen, W. Zhao, M. Shan, Q. Chen, *Sens. Actuators* **2010**, 147, 593.

[247] P. Kannan, A. S. John, *Anal. Biochem*. **2009**, 386, 65.

[248] A. Safavi, F. Farjami, *Biosens. Bioelectron*. **2010**, 26, 2547.

[249] Y. C. Chuang, J. C. Li, S. H. Chen, T. Y. Liu, C. H. Kuo, W. T. Huang, C. S. Lin, *Biomaterials* **2010**, 31, 6087.

[250] A. R. Bizzarri, S. Cannistraro, *Nanomed. Nanotech. Biol. Med*. **2007**, 3, 306.

[251] M. Moreno, E. Rincon, J. M. Pérez, V. M. González, A. Domingo, E. Dominguez, *Biosens. Bioelectron.* **2009**, 25, 778.

[252] Z. S. Wu, J. H. Jiang, L. Fu, G. L. Shen, R. Q. Yu, *Anal. Biochem.* **2006**, 353, 22.

[253] D. J. Javier, A. Castellanos-Gonzalez, S. E. Weigum, A. C. White, R. Richards-Kortum, *J. Clin. Microbiol.* **2009**, 47, 4060.

[254] E. Sawosz, A. Chwalibog, J. Szeliga, M. Grodzik, M. Rupiewicz, T. Niemiec, K. Kacprzyk, *Int. J. Nanomed.* **2010**, 5, 631.

[255] R. L. Phillips, O. R. Miranda, C. C. You, V. M. Rotello, U. H. Bunz, *Angew. Chem. Int. Ed. Engl.* **2008**, 47, 2590.

[256] A. Jayagopal, K. C. Halfpenny, J. W. Perez, D. W. Wright, *J. Am. Chem. Soc.* **2010**, 132, 9789.

CHAPTER 2

Fungus mediated synthesis of oxides nanoparticles and its application.

Summary

This chapter discusses the use of thermophilic fungus *Humicola* sp. in the biosynthesis of oxide nanoparticles of medical importance. The fungus *Humicola* sp. when exposed to aqueous solutions of oxide precursors such as Gadolinium chloride ($GdCl_3$) and Cerium (III) nitrate hexahydrate ($CeN_3O_9.6H_2O$) results in the extracellular formation of oxide nanoparticles of Gd_2O_3 and CeO_2 respectively. The biosynthesized nanoparticles were then characterized by UV-vis spectroscopy, X-Ray Diffraction (XRD), Transmission Electron Microscopy (TEM), X-ray Photoemission Spectroscopy (XPS), Energy Dispersive Analysis of X-rays (EDAX), Fourier Transform Infrared spectroscopy (FTIR), Thermo gravimetric -Differential Thermal Analysis (TGA-DTA), etc. The highly fluorescent protein capped Gd_2O_3 nanoparticles were radiolabelled with technicium-99 m and injected into rats in order to see biodistribution. The biosynthesized Gd_2O_3 nanoparticles were conjugated with an anticancerous drug Taxol. This conjugate was then characterized by UV-vis spectroscopy and Fluorescence microscopy and purified by High Performance Liquid Chromatography (HPLC). This purified conjugate was tested on Human acute monocytic leukemia cell line (THP-1) to access the efficiency of Gd_2O_3-taxol conjugate in drug delivery applications.

2.1 Introduction

Among the primary goals of nanotechnology is the improvement of production methods, especially those that are simpler and cleaner. The objectives are the production of size-controlled clusters, increasing the yield of desirable nanoparticles, reduction of the subsequent pollutant contribution, etc. Biosynthetic methods have particularly been used to produce different types of particles [1-10] and even nanorods [11-13]. However, they have been focused mainly on metallic [1-6], [11-13], bimetallic nanomaterials [7-10] and sulphide (quantum dots) nanomaterials [4]. Just a few reports have evaluated the use of biosynthesis [14, 15] to make metal oxides. Oxide nanoparticles are important in applications such as catalysis, electronics, hyperthermia, drug delivery, antimicrobial coatings, separation processes, etc. and are conventionally synthesized under harsh environments like the extremes of temperature, pressure and pH. In contrast, biological processes occur under ambient conditions, viz. room temperature, atmospheric pressure and physiological pH. While purely biological and bioinspired methods for the synthesis of oxides provide environmentally benign and energy conserving processes, they have not been extended to the formation of technologically important oxide nanoparticles from microorganisms. Although there have been reports on the biosynthesis of oxide nanoparticles, no attempts have been made to employ microorganisms for the synthesis of nanoparticles of rare earth metals. Nanoparticles of rare earth metals or Lanthanides can serve as excellent fluorescent probes in various biomedical research programmes, due to their sharp fluorescence emission peaks, high quantum efficiency, bright and monochromatic emissions, large Stokes shift and extraordinarily long fluorescence lifetime [16-22]. In this work, we have employed the thermophilic fungus *Humicola* sp. for the biosynthesis of oxide nanoparticles of two very important rare earth metals viz. Gadolinium and Cerium.

Gadolinium oxide nanoparticles are very important by virtue of their applications as nuclear, electronic, laser, optical, catalyst and phosphor materials [23-27]. Many organic compounds use Gd_2O_3 for their dimerization [24], in imaging plate neutron detectors, as neutron convertor [24, 25], as additives in UO_2 fuel rods for nuclear reactors [26], as additive in ZrO_2 to enhance toughness [27], etc.

Gd_2O_3 has several potential applications in biomedicine too. For example, it is being used in magnetic resonance imaging since it has superparamagnetism and involves

T1 relaxation, and can be useful as multimodal contrast agent for *in vivo* imaging [28]. It can also be doped easily by other lanthanides, hence can be exploited as fluorescent tags thus replacing other fluorescent organic molecules. Gadolinium oxide nanoparticles also find their application in site-specific drug delivery systems for cancer therapy. A potential cancer therapy whose therapeutic success can be greatly enhanced using tumor-specific delivery systems is neutron capture therapy (NCT). NCT utilizes a stable (non radioactive) nuclide delivered to tumor cells which upon irradiation by thermal or epithermal neutrons, produces localized cytotoxic radiations [29]. Although most of the initial clinical trials were carried out using Boron-10 as the NCT agent, gadolinium (Gd) has been proposed as an alternative [29]. The tumor-killing effect of Gd-NCT is attributed to the emission of high-energy prompt gamma rays followed by a series of low-energy Auger and internal conversion electrons [30]. Apart from the fact that Gd compounds are used as contrast agents in magnetic resonance imaging (MRI), the suitability of Gadolinium-157 in NCT has been attributed to: (i) the large neutron capture cross section area that is 66-fold larger than Boron-10; thus gadolinium requires shorter neutron irradiation time; and (ii) Gd-neutron-capture reaction leads to emission of photons with tumor killing energy deposition at longer ranges in tissues. As far as synthesis methods for Gd_2O_3 nanoparticles are concerned, even the chemical and physical protocols are limited and its synthesis is seldom encountered in literature. The most common methods are thermal decomposition of precursor salts, mechanochemical processing, milling and calcinations [31-35]. Unfortunately, these methods give agglomerated particles and most importantly occur at high temperatures and employ harsh environments making it very difficult to find any usage of Gd_2O_3 nanoparticles atleast in biomedical applications. Hence, to overcome all these barriers, we for the first time have employed fungus based approach for the synthesis of this very important material. In this chapter, we have shown that the thermophilic fungus *Humicola* sp. can be used for the synthesis of Gd_2O_3 nanoparticles at ambient temperature. Since Gd_2O_3 nanoparticles have proved their worth in site-specific drug delivery systems for cancer therapy, we extended the work of biosynthesis of Gd_2O_3 nanoparticles to bioconjugation with anticancerous drug Taxol. Taxol is one of the most popular chemotherapeutic agents used now-a-days for the treatment of breast, ovarian and lung cancers [36, 37]. Being able to promote tubulin assembly into microtubules [37, 38], taxol brings significant impact mainly because of its mechanism of action [39].

On the other hand, its drawbacks come from the lack of tumor specificity and low solubility in water. To overcome these barriers, we planned to attach taxol onto the biocompatible Gd_2O_3 nanoparticles. There have been several reports showing the bioconjugation of Taxol with gold and iron oxide nanoparticles [40, 41]. In this work, we have conjugated this drug of immense importance with gadolinium oxide nanoparticles and checked the efficiency of this Gd_2O_3-taxol conjugate on THP-1 cell lines to assure its use in drug delivery applications.

Cerium oxide (ceria) is a wide band gap semiconductor that has long been known for its catalytic capabilities [42] and has been synthesized and studied in both thin-film [43, 44] and nanoparticle form [45, 46]. As a thin-film, cerium oxide has unique properties such as a high refractive index, a high dielectric constant and a lattice constant similar to Si, making it suitable as an insulating material in Si device technology [46-48]. These properties make cerium oxide useful for applications in microelectronics and optics. Recently, ceria nanoparticles have attracted attention within the research community as a potential agent to inhibit cellular ageing [49, 50]. Mixed brain cell cultures have been shown to have an increased lifespan when a solution containing ceria nanoparticles is introduced into their environment. The likely mechanism for the longevity increase is the scavenging of free radical species in the cells that would normally damage the cell, causing the cell to age [51]. The scavenging effect is attributed to the presence of Ce (III) ions that reduce the free radical species as the Ce (III) ions are oxidized to Ce (IV). Cerium oxide nanoparticles (nanoceria) have properties that can be used in nano therapeutics to decrease mediators of chronic inflammation. So far, their unique properties have been utilized in ultraviolet absorbance [52], oxygen sensing [53] and automotive catalytic converters [54]. Biologically, it has recently been reported that cerium oxide can act as a catalyst that mimics the antioxidant enzyme superoxide dismutase [55]. Additionally, the ability of engineered cerium oxide nanoparticles to confer neuronal [53], ocular [56, 57] and radio protection [58] has been demonstrated, while the protective mechanism has not been thoroughly investigated. This versatile biomaterial has a unique electronic structure mainly due to its large surface-area-to-volume ratio that creates oxygen defects [59, 60]. It is these defects, or “reactive sites” on the nanoceria surface that can act as sites for free radical scavenging and are currently being investigated as therapeutic interventions in biological systems [60-62]. While

previous studies report the scavenging action of nanoceria, clinically relevant parameters such as the biological mechanism, toxicological limits of dosage and histopathology of nanoceria uptake have not been reported yet. Free radical scavenging with nanoparticles functions by inhibiting reactive oxygen species (ROS) [61, 62]. Free radicals are molecules that contain an unpaired electron in their outermost shell. ROS are unstable and highly reactive compounds that can strip electrons from cellular macromolecules and render them dysfunctional [61]. Chain reactions of self-propagating free radicals mediate lipid peroxidation and cause cell membrane structure damage, thereby inducing cell death. Free radicals are generated in low levels during normal metabolism, but production increases during diseased states, increased metabolism, and cell turnover. Free radical species produced within the cell include superoxide (O_2^-), the hydroxyl radical (OH^-), NO, peroxynitrite ($ONOO^-$), lipid hydroperoxides and others [61] Due to the inherent structure of cerium oxide (CeO_2) nanoparticles, data suggests that nanoceria may reduce cellular structural damage by scavenging and inhibiting ROS as well as other inflammatory mediators in biological systems [54]. This antioxidant property of cerium oxide nanoparticles has shown a possibility in the treatment of neurodegenerative diseases such as Alzheimer's and Parkinson's disease [53, 61]. In an attempt to explore more potential applications of cerium oxide nanoparticles which could be restricted owing to their synthesis methods involving toxic chemicals and hydrophobic solvent systems, we for the first time made an attempt to use thermophilic fungus *Humicola* sp. for the biosynthesis of cerium oxide nanoparticles.

This chapter deals with 1) Extracellular biosynthesis of Gd_2O_3 nanoparticles using thermophilic fungus *Humicola* sp. and its conjugation with taxol and 2) Extracellular biosynthesis of CeO_2 nanoparticles using thermophilic *Humicola* sp.

2.2 Extracellular biosynthesis of gadolinium oxide (Gd_2O_3) nanoparticles using *Humicola* sp.

2.2.1 Materials and Methods

Gadolinium chloride ($GdCl_3$) and Sodium carbonate were obtained from Sigma Aldrich. Malt extract, yeast extract, glucose and peptone were obtained from HiMedia and used as-received.

2.2.2 Biosynthesis of gadolinium oxide nanoparticles

The thermophilic fungus *Humicola* sp. was isolated, purified and identified from self heating compost obtained from Pune and maintained on MGYP (malt extract, glucose, yeast extract and peptone) agar slants. Stock cultures were maintained by subculturing at monthly intervals. After growing the fungus at pH 9 and 50°C for 96h, the slants were preserved at 15°C. From an actively growing stock culture, subcultures were made on fresh slants and after 96h incubation at pH 9 and 50°C, were used as the starting material for fermentation experiments. For the synthesis of gadolinium oxide nanoparticles, the fungus was grown in 250 ml Erlenmeyer flasks containing 100 ml of MGYP medium which is composed of malt extract (0.3%), glucose (1%), yeast extract (0.3%) and peptone (0.5%). Sterile 10% sodium carbonate was used to adjust the pH of the medium to 9. After the pH of the medium was adjusted, the culture was grown with continuous shaking on a rotary shaker (200 rpm) at 50°C for 96h. After 96h of fermentation, mycelial mass were separated from the culture broth by centrifugation (5000 rpm) at 20°C for 20 min and then were washed thrice with sterile distilled water under sterile conditions. The harvested mycelial mass (20 g of wet mycelia) was then resuspended in 100 ml of 10^{-3} M aqueous gadolinium chloride solution in 250 ml Erlenmeyer flask at pH 9. The whole mixture was put onto a shaker at 50°C (200 rpm) and maintained in the dark.

2.2.3 Characterization of gadolinium oxide nanoparticles

UV-vis spectroscopy

The synthesis of gadolinium oxide nanoparticles in solution was monitored by periodic sampling of aliquots (2ml) of the aqueous component. The measurement was carried out on a Shimadzu dual-beam spectrophotometer (model UV-1601 PC) operated at a resolution of 1 nm.

Transmission Electron Microscopy (TEM)

The shape and size analysis of gadolinium oxide nanoparticles was carried out on a JEOL model 1200 EX TEM operated at 80 KV. For this purpose, carbon coated copper grids were prepared by drop-casting the particles suspended in aqueous medium. HR-TEM measurements were carried out on a TECHNAI G2 F30 S-TWIN instrument (Operated at an acceleration voltage of 300 kV with a lattice resolution of

0.14 nm and a point image resolution of 0.20 nm). The Selected Area Electron Diffraction (SAED) pattern analysis was carried out on the same grid.

Fourier Transform Infrared (FTIR) spectroscopy

The FTIR spectroscopy measurement of as-synthesized gadolinium oxide nanoparticles powder after (96h reaction with fungus) taken in KBr pellet was carried out using a Perkin-Elmer Spectrum One instrument. Spectrometer was operated in the diffuse reflectance mode at a resolution of 2 cm^{-1}. To obtain good signal to noise ratio, 128 scans of the film were taken in the range of 450-4000 cm^{-1}.

X-Ray Diffraction (XRD) Measurements

To analyze the structure of the gadolinium oxide nanoparticles, X-Ray Diffraction (XRD) studies of the biosynthesized Gd_2O_3 powder casted on glass substrates were carried out on a Philips X'PERT PRO instrument equipped X'celerator. The sample was scanned using X'celerator with a total number of active channels of 121. Iron-filtered Cu Kα radiation (λ=1.5406 Å) was used. XRPD patterns were recorded in the 2 θ range of 20°- 80° with a step size of 0.02° and a time of 5 seconds per step at 40 kV voltage and a current of 30 mA.

X-ray Photoemission Spectroscopy (XPS)

XPS of the biogenic Gd_2O_3 nanoparticles was carried out on a VG MicroTech ESCA 3000 instrument after depositing Gd_2O_3 nanoparticles on the Si substrate.

Energy Dispersive Analysis of X-rays (EDAX)

Energy Dispersive Analysis of X-rays (EDAX) measurements of the Gd_2O_3 nanoparticles were carried out on a Leica Stereoscan-440 SEM equipped with a Phoenix EDAX attachment. EDAX spectra were recorded in the spot-profile mode by focusing the electron beam onto a region on the surface coated with Gd_2O_3 nanoparticles.

2.2.4 Radiolabelling of Gadolinium oxide (Gd_2O_3) nanoparticles with Tc-99m:

99mTc-Gd nanoparticles were prepared by dissolving 10 mg of Gd_2O_3 nanoparticles in 1ml of distilled water followed by the addition of 100 μg of $SnCl_2.2H_2O$ and the

pH was adjusted to 6.5. The content was filtered through a 0.22 µm membrane filter into a sterile vial. Approximately 2mci Tc-99m was added to the content, mixed and incubated for 10-15min. The percent radiolabel was determined by using instant thin layer chromatography (ITLC) method.

Radiochemical purity (RCP):

The radiochemical purity of Tc-99m with Gd_2O_3 nanoparticles was estimated by instant thin layer chromatography (ITLC) using silica gel coated fiber sheets. ITLC was performed using 100% acetone and 0.9% saline as the mobile phase. A measured amount of 2-3 µl of the radiolabeled complex was applied at a point 1 cm from one end of an ITLC-SG strip and allowed to run for approximately 10 cm. Amount of reduced/hydrolyzed Tc-99m was determined using pyridine: acetic acid: water (3:5:1.5 v/v) as mobile phase and ITLC as the stationary phase and the radioactivity distribution over the strip was determined with a radioactivity well counter (ECIL). Radiochemical purity (RCP) was calculated as the fraction of radioactivity that remained at the origin and was designated as % RCP.

2.2.5 Biodistribution of radiolabelled nanoparticles:

Male Sprauge Dawley rat weighing (180-220 gm) was selected for evaluating the localization of the labelled complex. 99mTc- Gd_2O_3 nanoparticles 14.8 MBq were administered through the penile vein of rat. The biodistribution studies of labelled Gd_2O_3 nanoparticles were evaluated after 45 min post injection.

2.2.6 Results and Discussions

UV-vis spectroscopy

Figure 2.1 shows the UV-visible spectroscopy of precursor salt $GdCl_3$ (Curve 1) and biosynthesized Gd_2O_3 nanoparticles after 96h of reaction with the fungus *Humicola* sp. (Curve 2). From the figure it is very clear that $GdCl_3$ does not absorb any energy during the entire spectrum and does not show any vibrations at all, whereas UV-vis spectrum of biosynthesized Gd_2O_3 nanoparticles indicates two regions of absorption at 270 nm and 330 nm. It is very well established that the absorption edge at *ca* 270 nm arises due to electronic transitions in the delocalized π electrons present in indole ring of aromatic amino acids such as Tryptophan, Tyrosine and to some extent Phenylalanine residues present in the proteins moiety [63]. These residues of proteins may be secreted in the solution by the fungus *Humicola* sp. in response to the stress conditions encountered by the fungus in presence of $GdCl_3$. Some of these amino acid residues constitute the protein layer which can cap the nanoparticles. As soon as $GdCl_3$ gets dissolved in water along with fungal biomass, it ionizes to Gd^{3+} and $3Cl^-$. These Gd^{3+} ions are then attracted towards anionic proteins (secreted by fungus in solution). Certain reductase enzymes present in the anionic protein fraction act on Gd^{3+} converting it to Gd^{2+}. These Gd^{2+} ions are then acted upon by oxidase enzymes again secreted by the fungus in the solution mixture, resulting in the formation of Gd_2O_3 nanoparticles. Hence, complementary action of oxidases and reducatses which are secreted by the fungus *Humicola* sp. play a very vital role in the formation of Gd_2O_3 nanoparticles. Biosynthesized Gd_2O_3 nanoparticles (curve 2, figure 2.1) show an absorption edge at *ca* 330 nm. This edge may be attributed to d—d and f—f transitions occurring in mixed valence transition metal compounds [64].

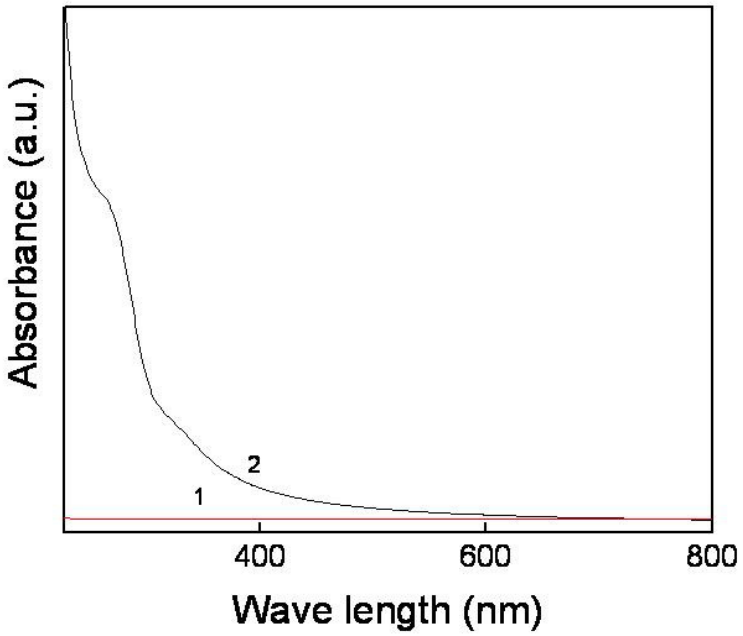

Figure 2.1: Curve (1) UV-vis spectrum of gadolinium chloride and Curve (2) UV-vis spectrum of biosynthesized gadolinium oxide nanoparticles solution after 96h of reaction with the fungal biomass.

Transmission Electron Microscopy (TEM)

Figure 2.2 (A) represents the transmission electron microscopic (TEM) image of fungus – $GdCl_3$ reaction mixture after 96h of reaction. The particles are irregular in shape, presenting an overall quasi-spherical morphology. Particle size distribution analysis of Gd_2O_3 nanoparticles confirmed that the nanoparticles are in the range of 3-8 nm with an average size of 6nm (figure 2.2B). Inter planar distance of Gd_2O_3 nanoparticles was estimated to be 2.75 Å and corresponds to plane {400} of Gd_2O_3 nanoparticles (figure 2.2C). Selected area electron diffraction (SAED) analysis (figure 2.2D) of biosynthesized Gd_2O_3 nanoparticles shows that the nanoparticles are crystalline in nature. Diffraction spots could be well indexed with cubic structure of Gd_2O_3 nanoparticles and the obtained three rings correspond to the {400}, {321} and {222} plane of Gd_2O_3 and are in good agreement with the reported values [65].

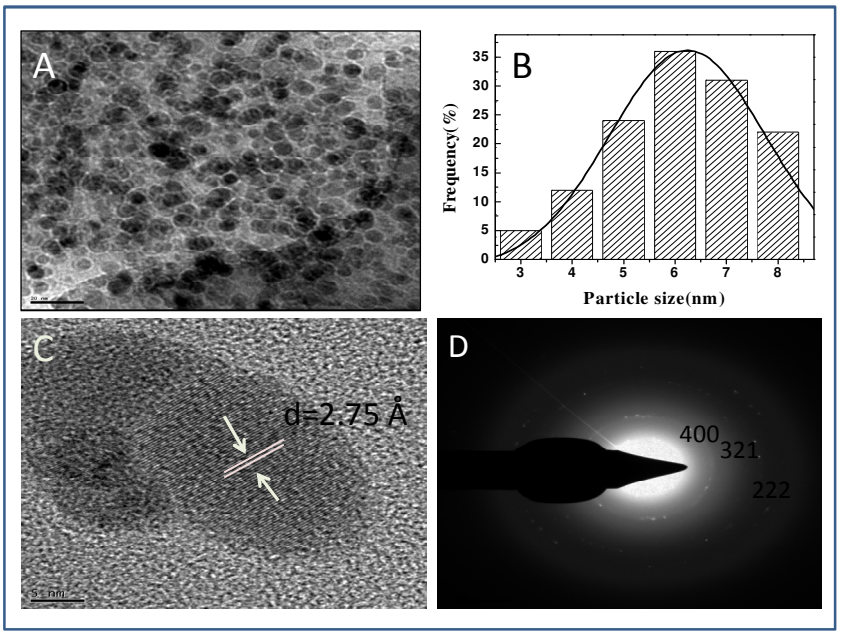

Figure 2.2: (A) TEM micrograph recorded from drop-cast films of Gd_2O_3 nanoparticle solution formed by the reaction of $GdCl_3$ with the fungal biomass of Humicola sp. *for 96h. (B)Particle size distribution determined from TEM micrograph. (C)HR-TEM image of Gd_2O_3 nanoparticles showing inter planar distance. (D) Selected Area Electron Diffraction (SAED) pattern recorded from the Gd_2O_3 nanoparticles.*

X-Ray Diffraction (XRD) Measurements

Figure 2.3 shows the X-Ray Diffraction (XRD) analysis of the biosynthesized gadolinium oxide nanoparticles carried out by depositing Gd_2O_3 powder on Si substrate showing intense peaks corresponding to plane {211}, {222}, {400}, {411}, {332}, {431}, {440}, {611}, {622}, {444} and {662}. The peak position and 2θ values agree with those reported for gadolinium oxide nanoparticles [65].

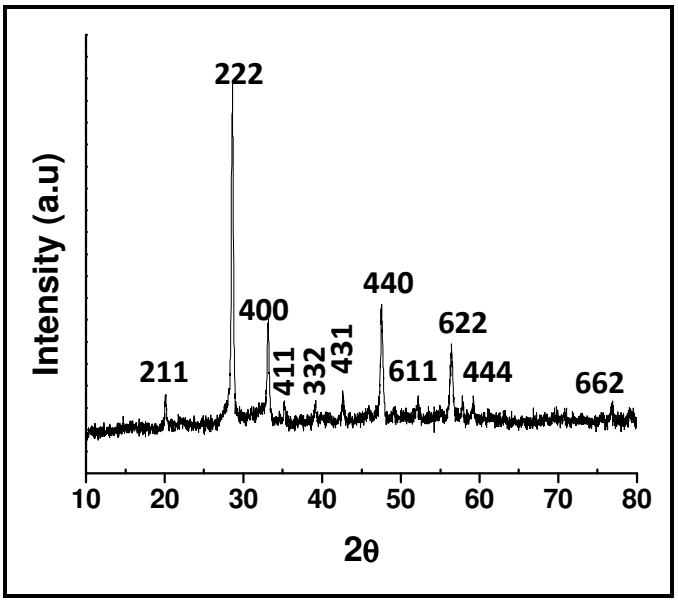

Figure 2.3: XRD measurements of biosynthesized Gd_2O_3 nanoparticles.

Fourier Transform Infrared (FTIR) spectroscopy

Figure 2.4 represents the Fourier Transform Infrared (FTIR) spectra of gadolinium chloride (curve 1), as synthesized gadolinium oxide nanoparticles (curve 2) and calcined gadolinium oxide nanoparticles at 300^{o}C for 3h (curve 3). Curve 2 in fig.2.4 shows sharp bands centered around 700, 828 and 998 cm^{-1}.The presence of these absorption bands are attributed to anti-symmetric Gd—O—Gd stretching mode of vibration [66] which is absent in curve 1 that belongs to $GdCl_3$. The two absorption bands at 1620 and 1670 cm^{-1} can be attributed to amide I and amide II of proteins present in the quasi-spherical Gd_2O_3 nanoparticles [67]. Increment in absorption bands in curve 3 (calcined Gd_2O_3 nanoparticles) clearly suggests that the calcination of Gd_2O_3 nanoparticles improves their crystallinity accompanying the disappearance of amide I and II bands of proteins which indicates the removal of protein from Gd_2O_3 nanoparticles after calcination. The sharp absorption band centered at 1770cm^{-1} in curve 3 may be attributed to C=O which is present in the capping protein that capped the Gd_2O_3 nanoparticles [67].

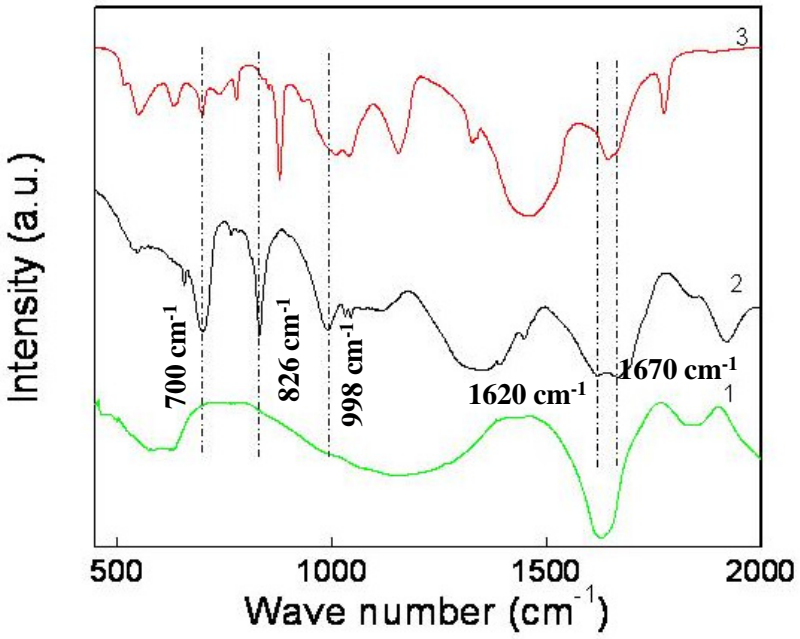

Figure 2.4: FTIR spectrum shows (1) Precursor (Gadolinium chloride), (2) As synthesized Gd_2O_3 nanoparticles and (3) Calcined biosynthesized Gd_2O_3 nanoparticles.

X-ray Photoemission Spectroscopy (XPS)

Figure 2.5 represents the XPS analysis of biosynthesized Gd_2O_3 nanoparticles. The Gd (3*d*) spectrum of Gd_2O_3 nanoparticles coated onto a Si substrate is shown in figure 2.5(A). The Gd (3*d*) level consists of a spin orbit split doublet, with the Gd (3*d*5/2) and Gd (3*d*3/2) peaks at 1188.25 and 1219.98 eV respectively. The line shape and peak positions are in good agreement with earlier published data on Gd_2O_3 nanoparticles, confirming that the sample consists of Gd_2O_3 [68]. The C (1s) spectrum in figure 2.5 (B) shows three different peaks at 282.67, 285.03 and 287.01 eV and can be attributed to α-carbon, hydrocarbon chains and –COOH respectively of the proteins associated with Gd_2O_3 nanoparticles. Figure 2.5 (C) represents the O (1s) spectrum which shows three distinct peaks. The peak at 531.30 eV corresponds to the oxygen in the Gd_2O_3 nanoparticles [68], whereas peaks at 529.18 and 533.26 eV originates from the oxygen in the carboxyl groups of protein associated with Gd_2O_3 nanoparticles. Figure 2.5 (D) shows the N 1s core level spectra that could be decomposed into two chemically distinct components centered at 399.6 and 402.5 eV and can be attributed to neutral amino group NH_2 and N atoms present in amide bonds of capping protein of Gd_2O_3 nanoparticles [68]. These signatures of carbon and

oxygen arising from proteins have certainly exposed a prominent role of proteins and enzymes in the reduction and capping of Gd_2O_3 nanoparticles.

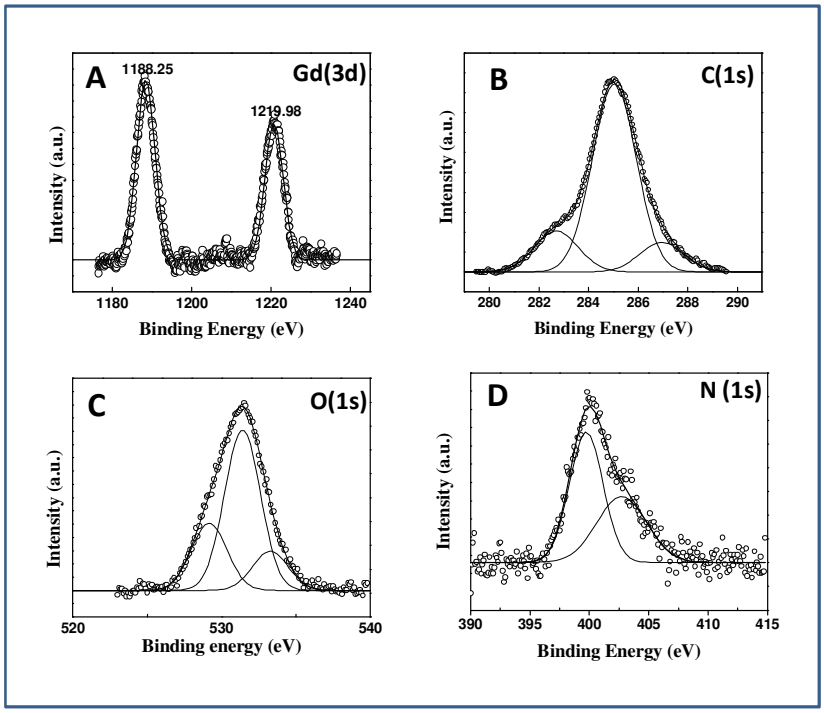

Figure 2.5: XPS data showing the (A) Gd 3d, (B) C 1s, (C) O 1s and (D) N 1s core level spectra recorded from biosynthesized Gd_2O_3 nanoparticles film cast onto a Si substrate. The raw data are shown in the form of symbols, while the chemically resolved components are shown as solid lines and are discussed in the text.

Energy Dispersive Analysis of X-rays (EDAX)

Figure 2.6 shows the Energy Dispersive Analysis of X-rays (EDAX) spectra recorded in the spot profile mode from one of the densely populated biosynthesized gadolinium oxide nanoparticles on the surface. Signals are observed from Gd, C, O and N. The signals for C, O and N are due to the proteins that are capped onto the surface of nanoparticles.

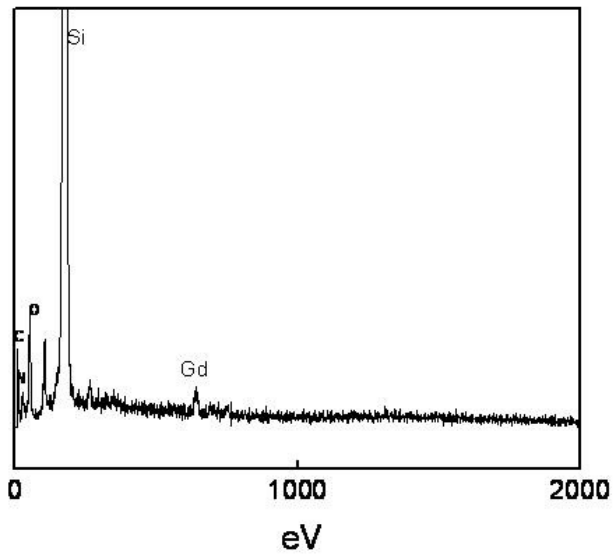

Figure 2.6: EDAX spectra recorded for biosynthesized gadolinium oxide nanoparticles

Complex formation study:

On the basis of chromatographic analysis, the radiolabeling efficiency was found to be more than 90% consistently.

Biodistribution & Gamma Scintigraphic imaging of 99mTc- Gd_2O_3 nanoparticles in normal rat:

Localization and biodistribution study of 99mTc- Gd_2O_3 nanoparticles in normal healthy rats over time was determined by gamma camera imaging, is shown in Figure. The study clearly indicates the biodistribution of the complex (99mTc-Gd nanoparticle), these Gd nanoparticles were taken up in the liver, heart, kidneys and cleared through urine within 45 minutes.

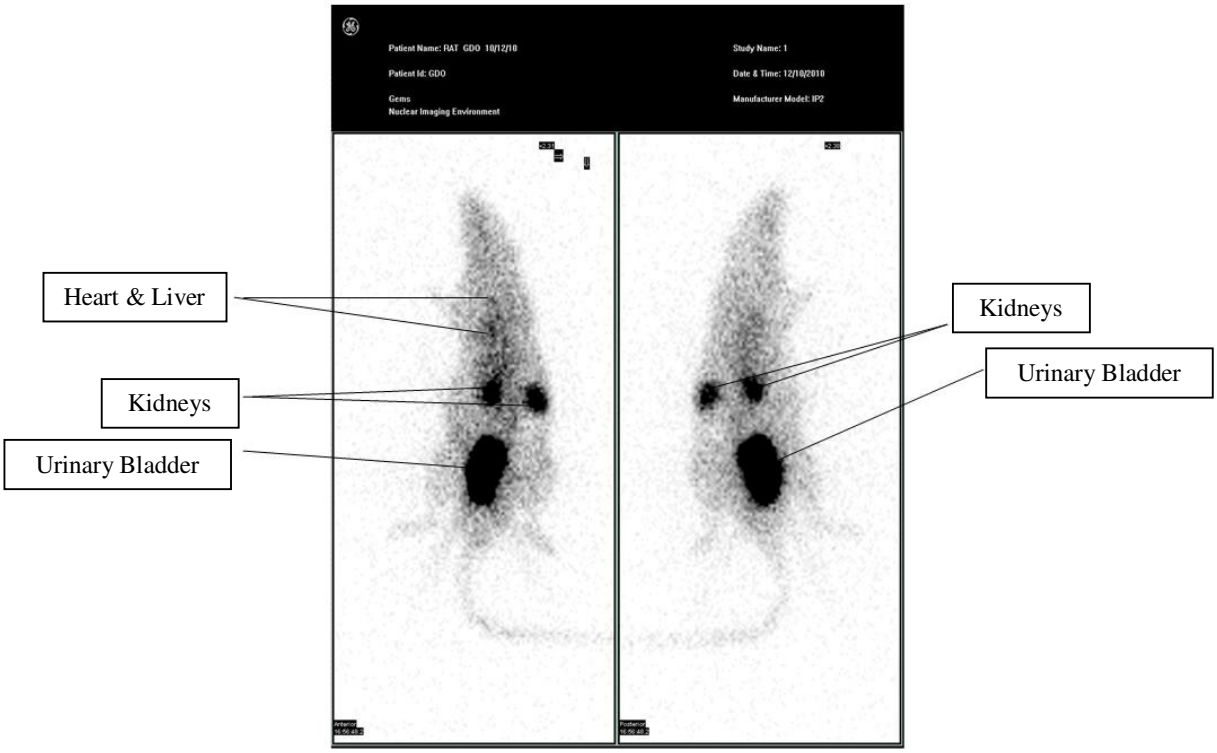

Figure 2.7: Gamma Scintigraphic image of biodistribution of Gd_2O_3 nanoparticles in rat

2.3 Synthesis of Gd_2O_3-Taxol conjugate

2.3.1 Materials and Methods

Glutaric anhydride, N,N'-Carbonyldiimidazole (CDI), t-butyldimethylsilyl chloride, Imidazole, Dimethyl formamide, Succinic anhydride, Dimethylamino-pyridine, 3-(4, 5-dimethylthiazol-2-yl)-2, 5-diphenyltetrazoliumbromide, 1-ethyl-3-(3 dimethyamin-opropyl) Carbodiimide (EDC), 1- Hydroxyl benzo-triazol, 2-(N-morpholino) ethanesulfonic acid (MES) and (4-(2-hydroxyethyl)-1-piperazineethane sulphonic acid (HEPES) were purchased from Sigma and HPLC grade solvents were purchased from Merck. THP- 1 cell lines were obtained from National Centre for Cell Sciences (NCCS), Pune (India).

2.3.2 Synthesis of 2'-Glutaryl taxol

2'-Glutaryl taxol was prepared by reacting 10 mg of taxol, dissolved in 1.2 ml of pyridine, with 140 mg of Glutaric anhydride [69]. The reaction was carried out at

room temperature for about 2h and was monitored on TLC using a mobile phase of chloroform: acetonitrile (7: 3). After the incubation period, the solvent was evaporated under high vacuum and the residue was washed twice with water. The product obtained was precipitated using acetone and further purified by preparative TLC using the mobile phase Chloroform: Acetonitrile (7: 3).

2.3.3 Synthesis of 2'-Glutaryl-hexanediamine taxol

The recovered 2'-Glutaryl taxol from the preparative TLC was solvent dried and dissolved in 100 µl of dry acetonitrile, 5 µmol of N, N'-Carbonyldiimidazole (CDI) was added to it and heated at 45^{o}C for about 15 min. After the reaction mixture comes to room temperature, 5 µmol of 1, 6-hexanediamine. 2HCl was added to it and left at room temperature for 1h. The reaction was monitored on TLC and purified as described above.

2.3.4 Synthesis of gadolinium oxide (Gd_2O_3)-taxol conjugates

Biologically synthesized gadolinium oxide nanoparticles have a natural protein coat; the carboxylic group present on these protein capped nanoparticles was targeted to couple with the free amino group present in 2'-Glutaryl-hexanediamine taxol.

2.3.5 Estimation of Free Carboxyl Group

The total reaction mixture of 3 ml containing 100 µg of Gd nanoparticles in 50 mM MES/HEPES buffer (75:25 v/v) pH 6.0, 50 mM EDC and 30 mM NTEE was incubated at 30^{o}C for 45 minutes. Subsequently, the reaction was arrested with the addition of 1 ml of 10% TCA and the precipitated Gd-peptide complex was collected by centrifugation, washed extensively with chilled acetone, air-dried and redissolved in 1 ml of 100 mM NaOH. The number of nitrotyrosyl group incorporated was determined spectrophotometrically at 430 nm using a molar absorption coefficient of 4600 M^{-1} cm^{-1}. 2'-glutaryl-hexanediamine taxol (400 µg) was dissolved in anhydrous DMF (300 µL), and EDC (1.2 µ mol, 1.1 eq) along with 1- Hydroxyl benzo-triazol (HBT) (4 µ mol, 2.2 eq) was added to it. The reaction mixture was stirred at room temperature for about 1 h and a solution of Gd nanoparticles in phosphate buffer pH 7.2 was added to it. After stirring for 12 h at room temperature, the reaction mixture was concentrated under high vacuum and further purification of the 2'-glutaryl-hexanediamine-taxol-Gd conjugate was done by HPLC.

2.3.6 Characterization of Gd_2O_3-taxol conjugate

UV-vis spectroscopy

UV-vis spectroscopy analysis of Gd_2O_3-taxol conjugate and nascent Gd was carried out on a Shimadzu dual-beam spectrophotometer (model UV-1601 PC) operated at a resolution of 1 nm.

Fluorescence microscopy

Fluorescence measurements were carried out using a Perkin Elmer LS-50B spectrofluorimeter, with slit width of 7 nm for both the monochromators and a scan speed of 100 nm/min.

2.3.7 Purification of Gd_2O_3-taxol conjugate by HPLC

The conjugate from other chemical contaminants was purified by HPLC (Waters model 2489 with UV/vis detector) using Acetonitrile 5% - 95% on a C_{18} symmetry column. The compounds eluted from the columns were detected at 227 nm and 330 nm using a dual wavelength detector.

2.3.8 Cytotoxicity of Gd_2O_3-taxol conjugate

Cytotoxicity of the Gd_2O_3-taxol conjugate was checked against THP-1 Acute monocyte leukemia cell lines by MTT assay.

2.3.9 Results and Discussions

Estimation of free carboxyl groups

The total number of free carboxyl groups present in the capping protein of gadolinium oxide nanoparticles was found to be 14; by using the protocol of Pho *et al*. [70]. Hence, these free carboxyl groups were exploited for the conjugation with free amino groups of the modified drug (Glutaryl-hexanediamine-taxol).

UV-vis spectroscopy

Figure 2.7 (A) and (B) show the UV-vis analysis of gadolinium oxide nanoparticles and Gd_2O_3-taxol conjugate respectively. Gadolinium oxide (Gd_2O_3) nanoparticles showed a broad shoulder at *ca* 330nm (A) which after conjugation with taxol red shifted to 350 nm (B).This type of red-shifting after conjugation has been explained

by several reports [70, 71]. Since conjugation of drug with nanoparticles made them slightly heavier, they tend to absorb at higher wavelengths.

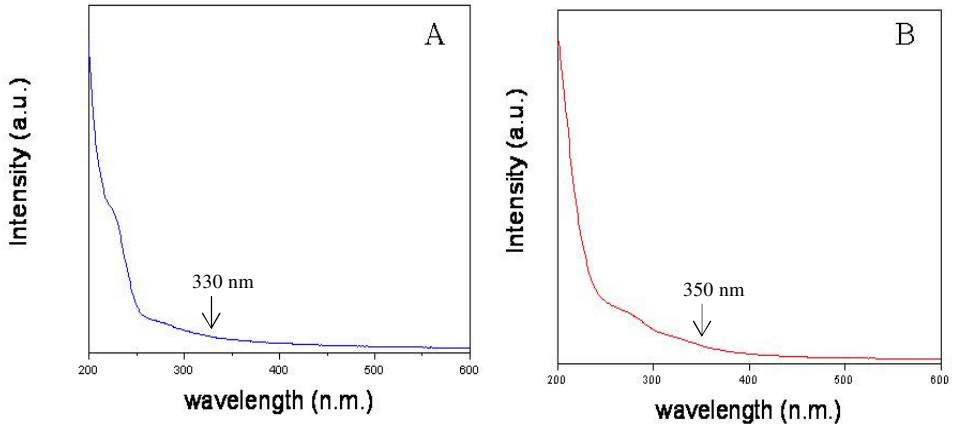

Figure 2.7: UV-vis spectroscopy of (A) Gd_2O_3 nanoparticles showing a shoulder at 330nm and (B) Gd_2O_3-taxol conjugate showing a shoulder at 350nm.

Fluorescence microscopy

Figure 2.8 (A) represents fluorescence spectra of Gadolinium oxide (Gd_2O_3) nanoparticles and (B) Gd_2O_3-taxol conjugate. Both the samples were excited at 320nm; gadolinium oxide (Gd_2O_3) nanoparticles give a sharp emission at 400nm whereas Gd_2O_3-taxol conjugate gives an emission spectrum with λ_{max} at 440 nm. This red-shifting in λ_{max} occurs because of the coupling of gadolinium oxide (Gd_2O_3) nanoparticle with taxol.

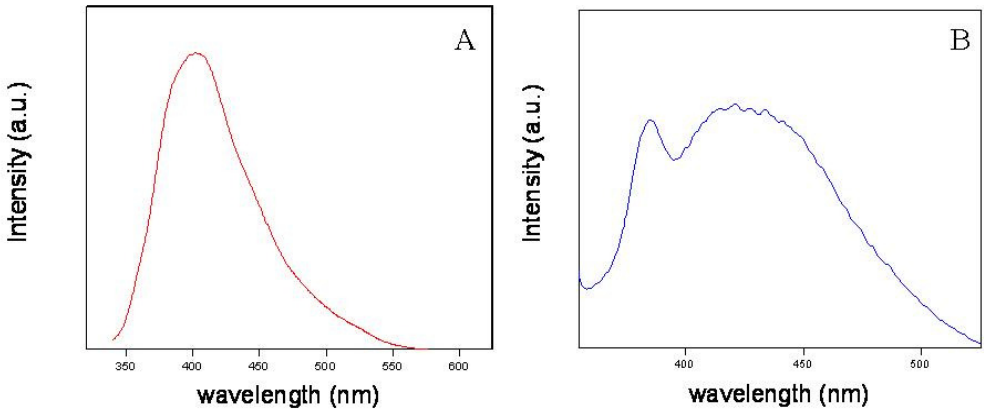

Figure 2.8: (A) Fluorescence spectra of Gd_2O_3 nanoparticles excited at 320nm giving emission at 400nm and (B) Gd_2O_3-taxol conjugate excited at 320nm giving emission at 440nm.

Purification of Gd_2O_3-taxol conjugate by HPLC

Figure 2.9 shows the HPLC profile of Gd_2O_3-taxol conjugate detected at 227nm and 330nm which are attributed to the absorption maxima of taxol and Gd nanoparticles respectively. From the figure, it is very clear that Gd_2O_3-taxol conjugate emerged as a single peak at both the wavelengths with same retention time, thus confirming conjugation of taxol with Gd_2O_3 nanoparticles.

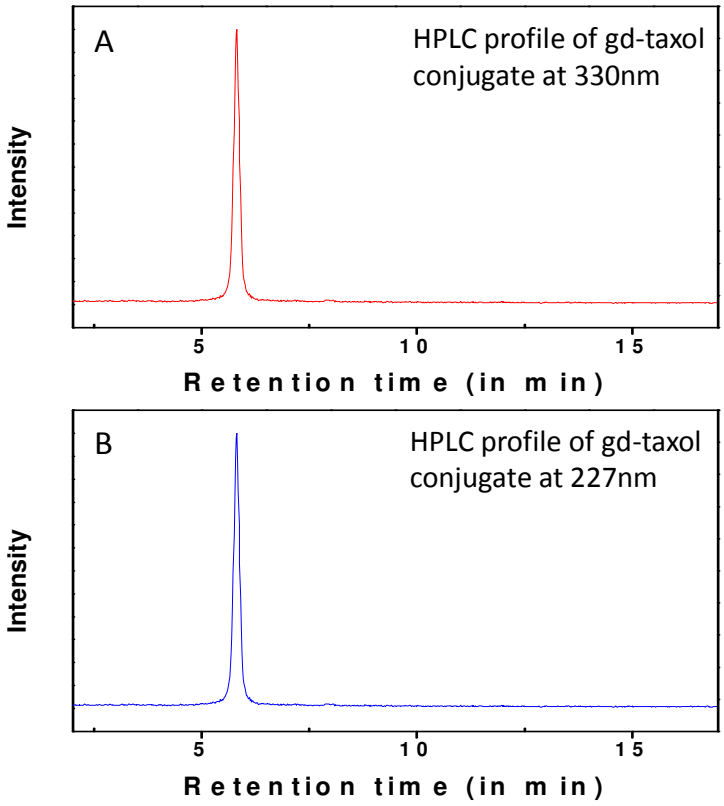

Figure 2.9: HPLC profile of Gd_2O_3-taxol conjugate showing absorbance at (A) 330nm and (B) 227nm.

Cytotoxicity of Gd_2O_3-taxol conjugate

Figure 2.10 shows the cytotoxicity data of (A) nascent taxol and (B) Gd_2O_3-taxol conjugate against THP-1 acute monocyte leukemia cell lines. IC_{50} of nascent taxol and Gd_2O_3-taxol conjugate was found to be 8.1µg/ml and 2.5µg/ml respectively. Hence, it is very clear that Gd_2O_3-taxol conjugate is more potent in inhibiting THP-1 cell lines than taxol alone. Conjugation of taxol to Gd nanoparticles lowers its hydrophobicity and facilitates its entry into the cells more easily, thereby killing more number of cells with less amount of drug. However, cytotoxicity of Gd nanoparticles

and internalization processes such as endocytosis of Gd_2O_3-taxol conjugate by the cells cannot be over-ruled for the more potent inhibitory activity of Gd_2O_3-taxol conjugate.

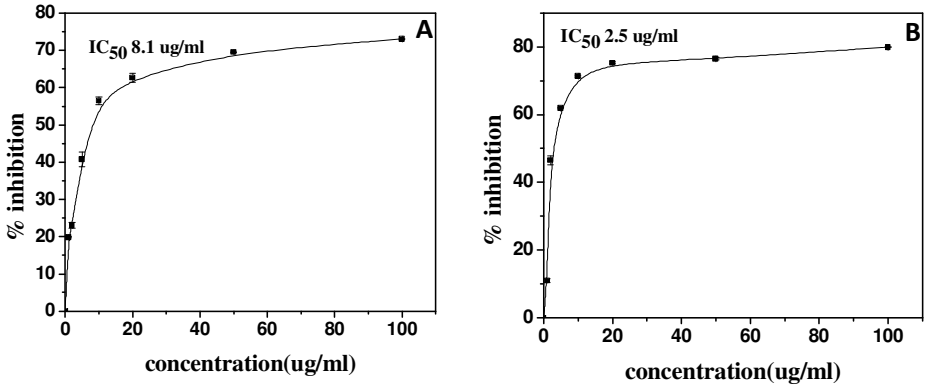

Figure 2.10: Cytotoxicity data of (A)nascent taxol and (B) Gd_2O_3-taxol conjugate against THP-1 acute monocyte leukemia cell lines.

2.4 Extracellular biosynthesis of Cerium oxide (CeO_2) nanoparticles using thermophilic fungus *Humicola* sp.

2.4.1 Materials and Methods

Cerium (III) nitrate hexahydrate ($CeN_3O_9.6H_2O$) was purchased from Fluka. Malt extract, yeast extract, glucose and peptone were obtained from HiMedia and used as-received.

2.4.2 Biosynthesis of cerium oxide (CeO_2) nanoparticles

The thermophilic fungus *Humicola* sp. was maintained on MGYP (malt extract, glucose, yeast extract, and peptone) agar slants. Stock cultures were maintained by subculturing at monthly intervals. After growing the fungus at pH 9 and 50°C for 96h, the slants were preserved at 15°C. From an actively growing stock culture, subcultures were made on fresh slants and, after 96h incubation at pH 9 and 50°C, were used as the starting material for fermentation experiments. For the synthesis of the cerium oxide nanoparticles, the fungus was grown in 250 ml Erlenmeyer flasks containing 100 ml of MGYP medium which is composed of malt extract (0.3%), glucose (1%), yeast extract (0.3%), and peptone (0.5%). Sterile 10% sodium carbonate was used to adjust the pH of the medium to 9. After the pH of the medium

was adjusted, the culture was grown with continuous shaking on a rotary shaker (200 rpm) at 50°C for 96h. After 96h of fermentation, mycelial mass were separated from the culture broth by centrifugation (5000 rpm) at 20°C for 20 min and then were washed thrice with sterile distilled water under sterile conditions. The harvested mycelial mass (20 g of wet mycelia) was then resuspended in 100 ml of 10^{-3} M aqueous Cerium (III) nitrate hexahydrate ($CeN_3O_9.6H_2O$) solution in 250 ml Erlenmeyer flask at pH 9. The whole mixture was put onto a shaker at 50°C (200 rpm) and maintained in the dark.

2.4.3 Characterization of cerium oxide (CeO_2) nanoparticles

UV-vis spectroscopy

The synthesis of cerium oxide nanoparticles in solution was monitored by periodic sampling of aliquots (2ml) of the aqueous component. The sample was scanned from 200 to 900 nm with deionized water as reference. The measurements were carried out on a Shimadzu dual-beam spectrophotometer (model UV-1601 PC) operated at a resolution of 1 nm.

Photoluminescence (PL)

Fluorescence measurements were carried out using a Perkin Elmer LS-50B spectrofluorimeter, with slit width of 7 nm for both the monochromators and a scan speed of 100 nm/min.

Transmission Electron Microscopy (TEM)

The shape and size analyses of cerium oxide nanoparticles were carried out on a JEOL model 1200 EX TEM operated at 80 KV. HR-TEM measurements were carried out on a TECHNAI G2 F30 S-TWIN instrument (Operated at an acceleration voltage of 300 kV with a lattice resolution of 0.14 nm and a point image resolution of 0.20 nm). For this purpose, carbon coated copper grids were prepared by drop-casting the particles suspended in aqueous medium. The Selected Area Electron Diffraction (SAED) pattern analysis was carried out on the same grids.

Fourier Transform Infrared (FTIR) spectroscopy

The FTIR spectroscopy measurement of as-synthesized cerium oxide nanoparticles powder (after 96h reaction with fungus) taken in KBr pellet was carried out using a

Perkin–Elmer Spectrum One instrument. Spectrometer was operated in the diffuse reflectance mode at a resolution of 2 cm^{-1}. To obtain good signal to noise ratio, 128 scans of the film were taken in the range of 450–4000 cm^{-1}.

X-Ray Diffraction (XRD) Measurements

To analyze the structure of the cerium oxide nanoparticles, X-Ray Diffraction (XRD) studies of the biosynthesized CeO_2 powder casted on glass substrates were carried out on a Philips X'PERT PRO instrument equipped X'celerator. The sample was scanned using X'celerator with a total number of active channels of 121. Iron-filtered Cu Kα radiation (λ=1.5406 Å) was used. XRPD patterns were recorded in the 2 theta range of 20°- 80° with a step size of 0.02° and a time of 5 seconds per step at 40 kV voltage and a current of 30 mA.

X-ray Photoemission Spectroscopy (XPS)

XPS of the biogenic CeO_2 nanoparticles was carried-out on a VG MicroTech ESCA 3000 instrument after depositing CeO_2 nanoparticles on Si substrate.

Energy Dispersive Analysis of X-rays (EDAX)

Energy Dispersive Analysis of X-rays (EDAX) measurements of the CeO_2 nanoparticles were carried out on a Leica Stereoscan-440 SEM equipped with a Phoenix EDAX attachment. EDAX spectra were recorded in the spot-profile mode by focusing the electron beam onto a region on the surface coated with CeO_2 nanoparticles.

Thermogravimetric Analysis (TGA) and Differential Thermo Analysis (DTA)

For this purpose, we dried the sample under IR-lamp to form powder. Thermogravimetric analysis of this dried powder of biogenic CeO_2 nanocrystals was carried-out using a Q5000 V2.4 Build 223 instrument by applying a scan rate of 10^oC min^{-1}.

2.4.4 Results and Discussions

Figure 2.11 shows the UV-vis spectrum of biosynthesized cerium oxide nanoparticles after 96h reaction with the fungus *Humicola* sp. The absorption spectrum of

biosynthesized CeO_2 nanoparticles revealed a strong absorption band and absorption edge at 300 and 400nm respectively. This is due to the charge-transfer transitions from O2p to Ce 4f [72]. The absorption edge of the CeO_2 nanoparticles is obviously blue-shifted with respect to that of bulk cerium oxide [73], suggesting the presence of strong size confinement owing to the molecular scale dimension of the nanoparticles. The appearance of absorption edge at *ca* 270nm can be assigned to the aromatic amino acid residues such as tyrosine, tryptophan and phenylalanine present in the protein, which is secreted in the solution by the fungus *Humicola* sp. [63]. The inset in figure 2.11 shows that direct band of CeO_2 nanoparticles was calculated to be 3.28eV obtained from UV-vis spectrum of CeO_2 nanoparticles by plotting $(\alpha h\nu)^2$ against $(h\nu)$. The reported band gap energy of bulk CeO_2 is roughly around 3.12eV [74]. This blue-shift in band gap energy in the case of biosynthesized CeO_2 is expected since band gap energy increases as particle size is reduced. Since CeO_2 is a direct band gap semiconductor, a decrease in particle size is exhibited to be manifested by a blue shift of the absorption edge [74]. This blue-shift in absorption spectrum is attributed to the quantum size effect [75].

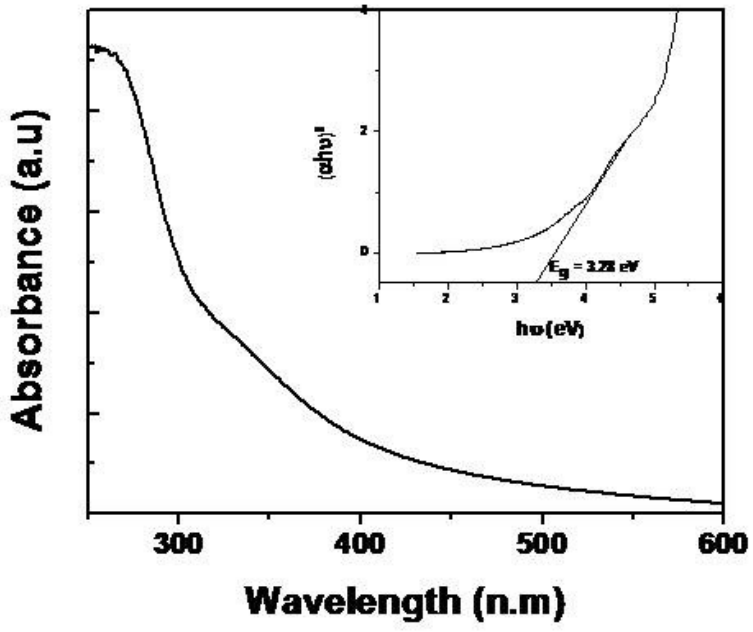

Figure 2.11 UV-visible spectrum of biosynthesized CeO_2 nanoparticles after 96h reaction with fungus Humicola sp. *Inset shows the direct band gap energy (tauc's plot) of biosynthesized CeO_2 nanoparticles obtained by plotting $(\alpha h\nu)^2$ against $(h\nu)$.*

Photoluminescence measurements

Figure 2.12 shows the room temperature Photoluminescence (PL) spectrum of a biosynthesized CeO_2 nanoparticles excited at 300nm. The PL spectrum shows a strong and sharp emission centered at 396 nm, and a weak shoulder at 335 nm. The emission from cerium oxide nanoparticles is associated with the defects localized between the Ce 4f band and the O2p band [72].

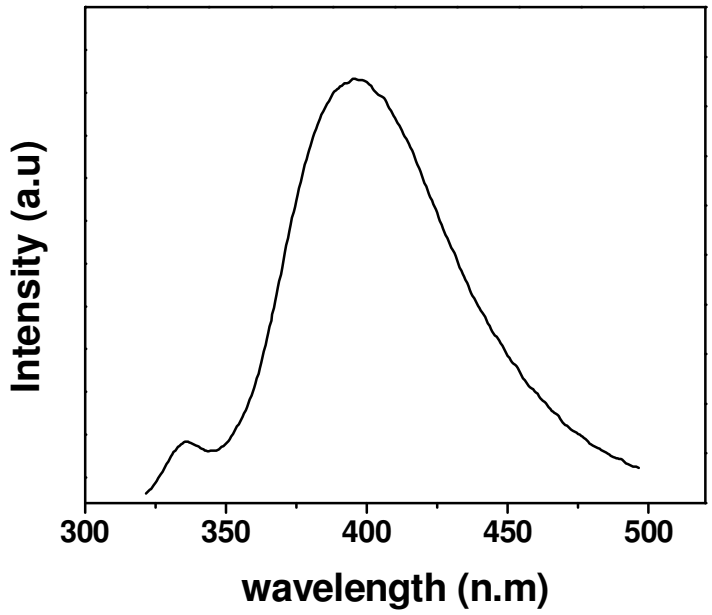

Figure 2.12: Photoluminescence spectrum of biosynthesized CeO_2 nanoparticles excited at 300nm.

Transmission Electron Microscopy (TEM)

Figure 2.13(A) represents the Transmission Electron Microscopic (TEM) analysis of biosynthesized cerium oxide nanoparticles after 96h reaction between Cerium (III) nitrate hexahydrate ($CeN_3O_9.6H_2O$) and the fungus *Humicola* sp. From the figure it is very clear that the particles are poly dispersed and spherical in shape. Particle size distribution analysis in figure 2.13 (B) reveals that the particles are in the range of 12-20nm with 16nm as an average diameter. Figure 2.13 (C) represents the HR-TEM image of one of the CeO_2 nanoparticles showing inter planar distance or 'd' value which was estimated to be 1.90 Å and corresponds to the {220} plane of CeO_2 nanoparticles. Selected Area Electron Diffraction pattern in figure 2.13(D) indicates that the CeO_2 nanoparticles are polycrystalline in nature. The electron diffraction

pattern of the CeO_2 nanoparticles was also consistently indexed as that of cubic cerium (IV) oxide with fluorite structure [76].

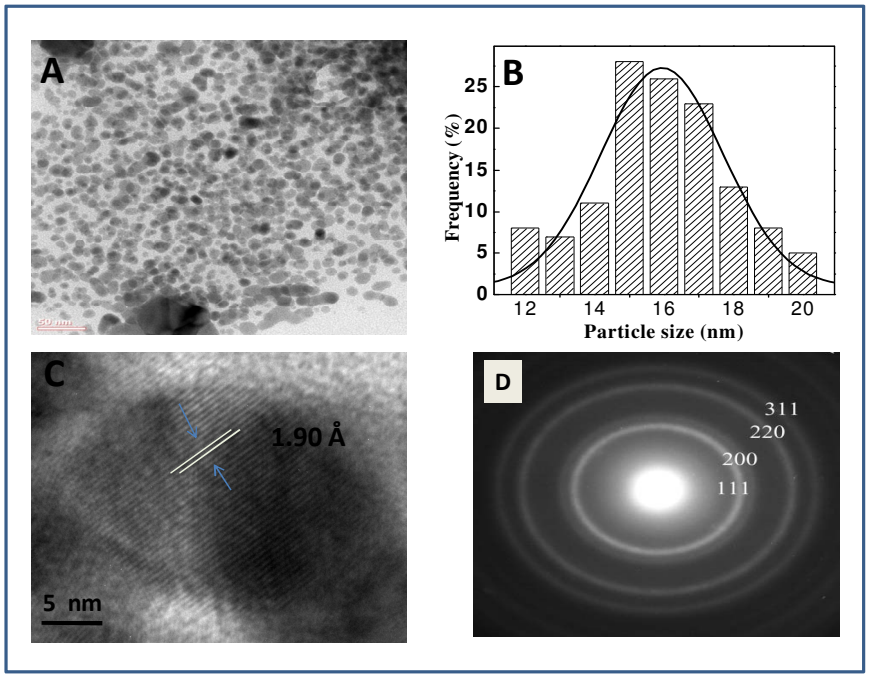

Figure 2.13: (A) TEM micrograph recorded from drop-cast films of CeO_2 nanoparticle solution formed by the reaction of cerium nitrate with the fungal biomass of Humicola sp. *for 96 h. (B) Particle size distribution determined from TEM micrograph. (C) HR-TEM image of CeO_2 nanoparticles showing inter planar distance. (D) Selected Area Electron Diffraction (SAED) pattern recorded from the CeO_2 nanoparticles.*

X-Ray Diffraction (XRD) measurements

Figure 2.14 represents the powder X-Ray Diffraction (XRD) pattern of the biosynthesized CeO_2 nanoparticles. The well resolved peaks in the XRD pattern can be indexed to {111}, {200}, {220}, {311}, {222}, {400}, {331} and {420} crystal planes of CeO_2 nanoparticles. The apparent broadening of the diffraction peaks is ascribed to the small size of cerium oxide nanoparticles [76].

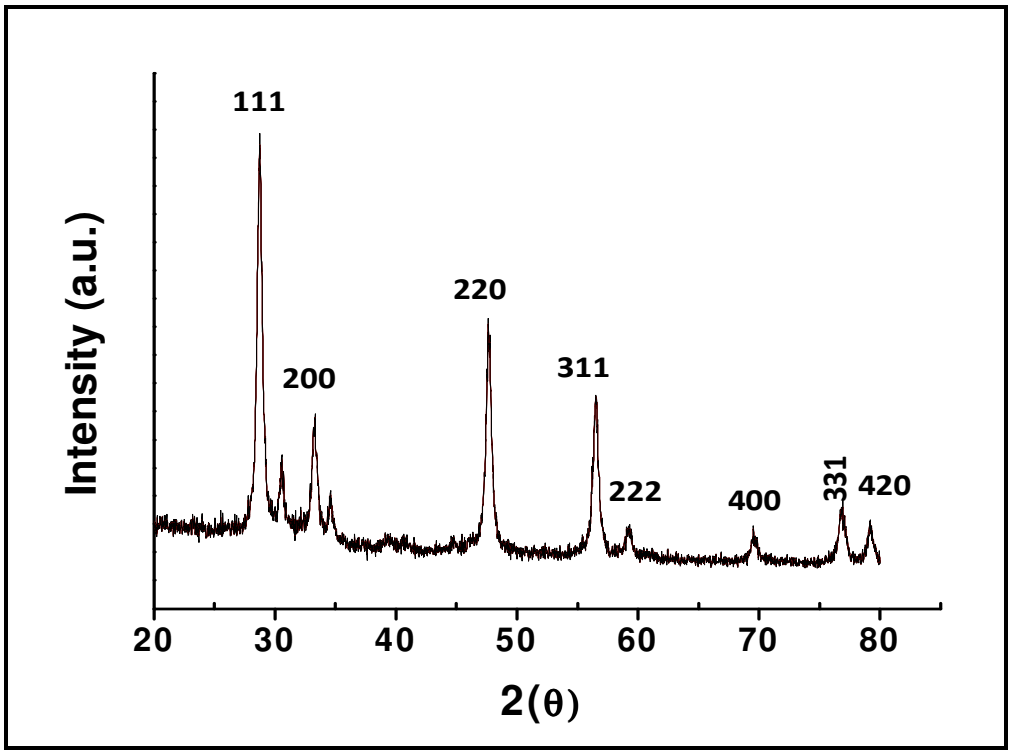

Figure 2.14: XRD pattern of biosynthesized Cerium oxide (CeO_2) nanoparticles

Fourier Transform Infrared Spectroscopy (FTIR) measurements

Figure 2.15 shows Fourier Transform Infrared Spectroscopy (FTIR) measurement for precursor cerium nitrate (curve 1) and CeO_2 nanoparticles [as – synthesized (curve 2) and calcined at 300^oC for 3h (curve 3)]. In curve 2, cerium oxide nanoparticles (as – synthesized) shows sharp vibrations centered at 500,725,825 and 962 cm^{-1}. The peak at 500 and 962 cm^{-1} may be attributed to Ce—O vibrations whereas peaks at 725 and 825 cm^{-1} may arise from Ce—O—Ce vibrations. [66]. Also, vibration bands at 1620 and 1690 cm^{-1} in curve 2 may be attributed to amide I and amide II bands respectively arising from protein moieties present in the biosynthesized CeO_2 nanoparticles [67].

Calcination of CeO_2 nanoparticles (curve 3) accompanied by the disappearance of amide bands also improves the crystallinty of CeO_2 nanoparticles.

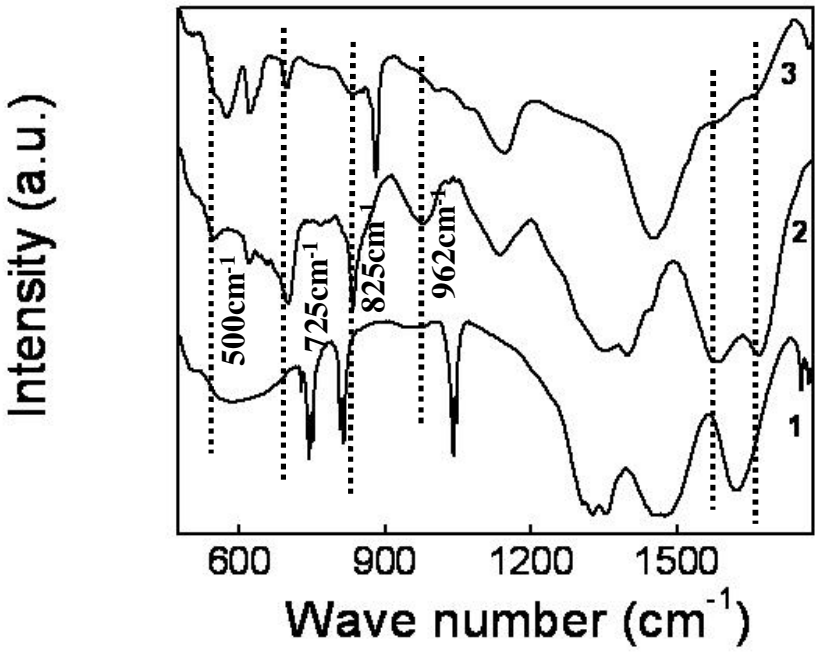

Figure 2.15: (1) FTIR spectra recorded from powder of Cerium nitrate hexahydrate ($CeN_3O_9.6H_2O$) (2) CeO_2 nanoparticles synthesized using Humicola sp. *before and (3) after calcination at 300^oC for 3h.*

X-ray Photoemission Spectroscopy (XPS)

Figure 2.16 shows the XPS spectra of biosynthesized cerium oxide (CeO_2) nanoparticles. The Ce (3d) XPS spectrum (Figure 2.16 A) consists of a spin orbit split doublet, with the Ce (3*d*5/2) and Ce (3*d*3/2) peaks at 883.34, 886.43, 897.90 and 903.20 eV. The peaks at 883.34 and 897.90 eV can be attributed to Ce^{+4} oxidation states while the peaks at 886.43 and 903.20 eV emanate from Ce^{+3} oxidation states of cerium [77]. Hence, from the XPS spectrum it is confirmed that the cerium sample contains mixed oxidation states (Ce^{+4} and Ce^{+3}) which can be very useful in free radical quenching and in various biological applications [78]. The C (1s) XPS spectrum is shown in Figure 2.16 (B) showing three peaks at 284.04, 285.13 and 286.42 eV and can be attributed to α-carbon, hydrocarbon chains and –COOH respectively of the proteins associated with CeO_2 nanoparticles. The O (1s) XPS spectrum (Figure 2.16 C) is represented by two distinct peaks at 530.23 and 531.40 eV which can be assigned to Ce^{+4} and Ce^{+3} oxidation states of cerium [78]. Figure

2.16 (D) presents the N (1s) XPS spectrum of CeO_2 nanoparticles showing two peaks at 399.7 and 401.6 eV and can be attributed to amino group NH_2 and ammonium group NH^{3+} respectively which are present in the capping protein of CeO_2 nanoparticles [78]. The signals emanating from carbon and oxygen in CeO_2 samples are a clear indication of the presence of proteins and confirms their role in biosynthesis of CeO_2 nanoparticles and subsequent capping.

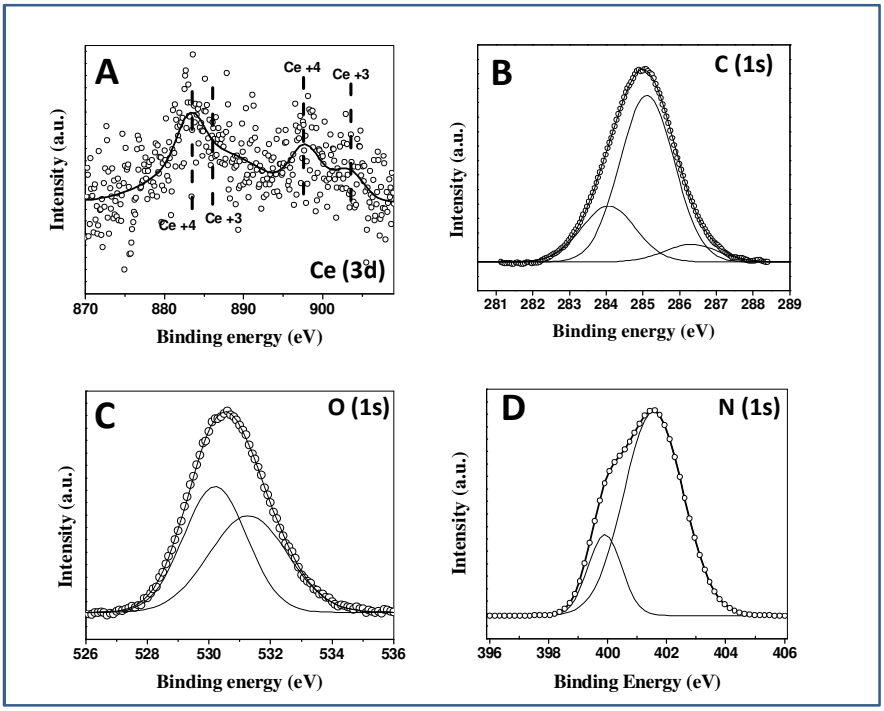

Figure 2.16: XPS data showing the (A) Ce 3d, (B) C 1s (C) O 1s and (D) N1s core level spectra recorded from biosynthesized CeO_2 nanoparticles film - cast onto a Si substrate. The raw data are shown in the form of symbols, while the chemically resolved components are shown as solid lines and are discussed in the text.

Thermogravimetric Analysis (TGA) and Differential Thermo Analysis (DTA)

Figure 2.17 shows the Thermogravimetric Analysis (TGA) and Differential Thermo Analysis (DTA) of the biosynthesized cerium oxide nanoparticles in air.TGA curve indicates a slight weight loss of 15 % below 200^oC at around 150^oC accompanying a slight endothermic peak in DTA curve. This decomposition of mass and endothermic peak may be attributed to the removal of adsorbed water from CeO_2 nanoparticles. A further 45% weight loss was seen at ca 320^oC which is mainly due to the loss of biomolecules (unbound proteins) from CeO_2 nanoparticles, thus causing a sharp

exothermic peak. Further heating of the sample results in more weight loss of around 60% at 600°C. This weight loss can be attributed to the removal of capping molecules involved in the capping of CeO_2 nanoparticles with the accompanied appearance of a very sharp exothermic peak. Further heating of the sample above 600°C did not show any weight loss which can be confirmed by the appearance of a plateau. This corresponds most likely to the crystallization of CeO_2 nanoparticles.

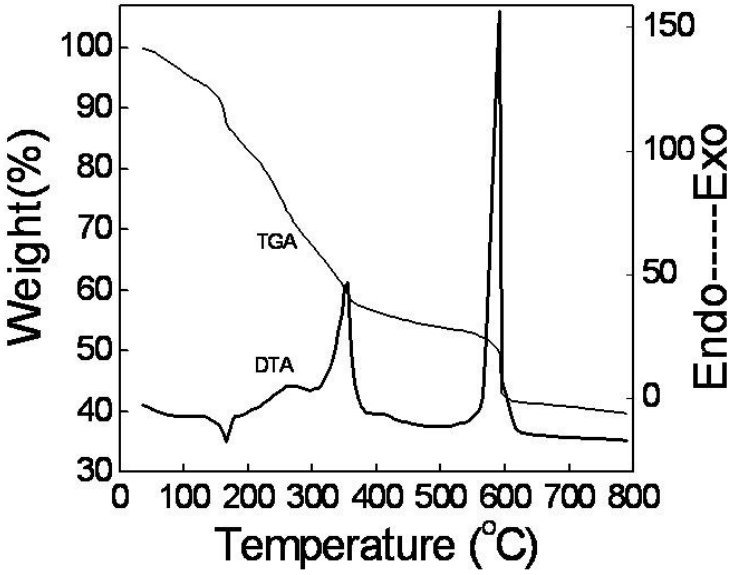

Figure 2.17 TGA and DTA curves for biologically synthesized CeO_2 nanoparticles.

Energy Dispersive Analysis of X-rays (EDAX) measurements

Figure 2.18 shows the Energy Dispersive Analysis of X-rays (EDAX) measurement of biosynthesized cerium oxide nanoparticles which show cerium in small amounts, since biosynthetic protocols of nanoparticles account for a low yield. Signals are also observed for C, O and N. The signals for C, O and N are due to the proteins that are capped onto the surface of the nanoparticles. The highest peak corresponds to silica which is used as a template for analyzing the sample.

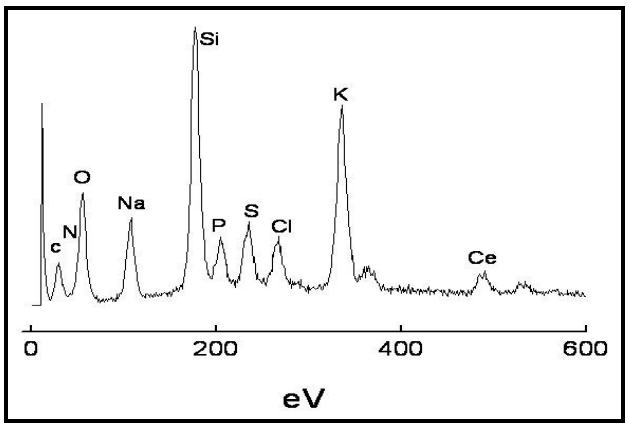

Figure 2.18 EDAX spectrum of cerium oxide (CeO_2) nanoparticles.

2.5 References

[1] A. Ahmad, P. Mukherjee, S. Senapati, D. Mandal, M. Islam Khan, R. Kumar, M. Sastry, *Colloids and Surfaces B: Biointerfaces* **2003**, 28 , 313.

[2] A. Ahmad, S. Senapati, M. I. Khan, R. Kumar, R. Ramani, V. Srinivas, M. Sastry, *Nanotechnol*. **2003**, 14, 824.

[3] A. Ahmad, S. Senapati, M. I. Khan, R. Kumar, M. Sastry, *Langmuir* **2003**, 19, 3550.

[4] A. Ahmad, P. Mukherjee, D. Mandal, S. Senapati, M. I. Khan, R. Kumar, M. Sastry, *J. Am. Chem. Soc*. **2002**, 124, 12108.

[5] A.Ahmad, T. Jagadale, V. Dhas, S. Khan, S. Patil, R. Pasricha, V. Ravi, S. Ogale, *Advanced Materials* **2007**, 19, 3295.

[6] S. S. Shankar, A. Rai, B. Ankamwar, A. Singh, A. Ahmad, M. Sastry, *Nat. Mater.* **2004**, 3, 482.

[7] S. Senapati, A. Ahmad, M. I. Khan, M. Sastry, R. Kumar, *Small* **2005**, 1, 517.

[8] J. A. Ascencio, Y. Mejia, H. B. Liu, C. Angeles, G. Canizal, *Langmuir* **2003**, 19, 5882.

[9] P. S. Schabes-Retchkiman, G. Canizal, R. Herrera-Becerra, C. Zorrilla, H. B. Liu, J. A. Ascencio, *Opt. Mater.* **2006**, 29, 88.

[10] E. Juarez-Ruiz, U. Pal, J. A. Lombardero-Chartuni, A. Medina, J. A. Ascencio, *Appl. Phys. A* **2007**, 86, 441.

[11] G. Canizal, J. A. Ascencio, J. Gardea-Torresday, M. Jose´-Yacaman, *J. Nanopart. Res.* **2001**, 3, 475.

[12] M. Jose-Yacaman, J. A. Ascencio, G. Canizal, *Surf. Sci.* **2001**, 486, L449.

[13] G. Canizal, P. Schabes-Retchkiman, U. Pal, H. B. Liu, J. A. Ascencio, *Mater. Chem. Phys.* **2006**, 97, 321.

[14] V. Bansal, A. Syed, S. K. Bhargava, A. Ahmad, A. Sastry, *Langmuir* **2007**, 23, 4993.

[15] V. Bansal, P. Poddar, A. Ahmad, M. Sastry, *J. Am. Chem. Soc.* **2006**, 128, 11958.

[16] J. C. G. Bunzli, *Acc. Chem. Res.* **2006**, 39, 53.

[17] D. Dosev, M. Nichkova, I. M. Kennedy, *J. Nanosci. Nanotechnol.* **2008**, 8, 1052.

[18] J. Georges, *Analyst* **1993**, 118, 1481.

[19] J. Shen, L. D. Sun, C. H. Yan, *Dalton Trans.* **2008**, 5687.

[20] H. Siitari, I. Hemmila, E. Soini, T. Lovgren, V. Koistinen, *Nature* **1983**, 301, 258.

[21] F. Vetrone, J. A. Capobianco, *Int. J. Nanotechnol.* **2008**, 5, 1306.

[22] J. L. Yuan, G. L. Wang, *Trends Anal. Chem.* **2006**, 25, 490.

[23] G. A. M. Hussein, *J. Phys. Chem.* **1994**, 98, 9657.

[24] G. Gunduz, I. Uslu, *J. Nucl. Mater.* **1996**, 231, 113.

[25] S. Bhattacharyya, D. C. Agrawal, *J. Mater. Sci.* **1995**, 30, 1495.

[26] Z. Chen, J. Am. *Ceram. Soc.* **1996**, 79, 530.

[27] J. L. Bridot, A. C. Faure, S. Laurent, C. Riviere, C. Billotey, B. Hiba, M. Janier, V. Josserand, J. L. Coll, L. V. Elst, R. Muller, S. Roux, P. Perriat, O. Tillement, *J. Am. Chem. Soc.* **2007**, 129, 5076.

[28] R. F. Barth, A. H. Soloway, *Mol. Chem. Neuropathol.* **1994**, 21, 139.

[29] Y. Akine, N. Tokita, T. Matsumoto, H. Oyama, S. Egawa, O. Aizawa, *Strahlenther. Onkol.* **1990**, 166, 831.

[30] E. Matijevic, W. P. Hsu, *J. Colloid Interface Sci.* **1987**, 118, 506.

[31] K. S. Mazdiyasni, L. M. Brown, *J. Am. Ceram. Soc.* **1971**, 54, 479.

[32] F. Imoto, T. Nanatani, S. Kaneko, *Ceram. Trans*. **1988**, 1, 204.

[33] A. T. Rowley, I. P. Parkin, *Inorg. Chim. Acta*. **1993**, 211, 77.

[34] P. G. McCormick, J. Ding, H. Yang, T. Tsuzuki, *Materials Research* **1996**, 1, 85.

[35] J. Dubois, *Expert Opin. Ther. Pat.* **2006**, 16, 1481.

[36] N. I. Marupudi, J. E. Han, K. W. Li, V. M. Renard, B. M. Tyler, H. Brem, *Expert Opin. Drug Saf.* **2007**, 6, 609.

[37] P. B. Schiff, S. B. Horwitz, *Proc. Natl. Acad. Sci. U.S.A.* **1980**, 77, 1561.

[38] I. Ojima, *Acc. Chem. Res.* **2008**, 41, 108.

[39] J. D. Gibson, B. P. Khanal, E. R. Zubarev, *J. Am. Chem. Soc.* **2007**, 129, 11653.

[40] J. R. Hwu, Y. S. Lin, T. Josephrajan, M. H. Hsu, F. Y. Cheng, C. S. Yeh, W. C. Su, D. B. Shieh, *J. Am. Chem. Soc.* **2009**, 131, 66.

[41] A. Trovarelli, *Catal. Rev. Sci. Eng.* **1996**, 38, 439.

[42] P. Patsalas, S. Logothetidis, L. Sygellou, S. Kennou, *Phys. Rev.* B **2003**, 68, 035104.

[43] T. Suzuki, I. Kosacki, H. Anderson, P. Colomban, *J. Am. Ceram. Soc.* **2001**, 84, 2007.

[44] S. Tsunekawa, J. T. Wang, Y. Kawazoe, *J. Alloys and Compound* **2006**, 408, 1145.

[45] F. Zheng, S. W. Chan, J. E. Spanier, E. Apak, Q. Jin, R. D. Robinson, I. P. Herman, *Appl. Phys. Lett.* **2002**, 80, 127.

[46] T. Sakata, H. Mori, *Chem. Mater.* **1997**, 9, 2197.

[47] L. Tye, N. A. El-Masry, *Appl. Phys. Lett.* **1994**, 65, 3081.

[48] B. Rzigalinski, *Tech. Canc. Resea. & Treatm.* **2005**, 4, 651.

[49] S. Tsunekawa, R. Sivamohan, T. Ohsuna, A. Kasuya, H. Takahashi, K. Tohji, *Mater. Sci. Forum*. **1999**, 315, 439.

[50] M. Das, S. Patil, N. Bhargava, J. F. Kang, L. M. Riedel, S. Seal, J. J. Hickman, *Biomaterials* **2007**, 28, 1918.

[51] J. C. Yu, L. Zhang, J. Lin, *J. Colloid Interface Sci.* **2003**, 260, 240.

[52] C. Korsvik, S. Patil, S. Seal, W. T. Self, *Chem. Commun*. **2007**, 10, 1056.

[53] J. P. Chen, S. Patil, S. Seal, J. F. McGinnis, *Nat. Nanotechnol.* **2006**, 1, 142.

[54] J. Chen, S. Patil, S. Seal, J. F. McGinnis, *Adv. Exp. Med. Biol.* **2008**, 613, 53.

[55] R. W. Tarnuzzer, J. Colon, S. Patil, S. Seal, *Nano Lett.* **2005**, 5, 2573.

[56] M. F. Hochella, S. K. Lower, P. A. Maurice, R. L. Penn, N. Sahai, D. L. Sparks, B. S. Twining, *Science* **2008**, 319, 1631.

[57] M. Nolan, S. C. Parker, G. W. Watson, *J. Phys. Chem.* B **2006**, 110, 2256.

[58] B. A. Rzigalinski, K. Meehan, R. M. Davis, Y. Xu, W. C. Miles, C. A. Cohen, *Nanomedicine* **2006**, 1, 399.

[59] B. A. Rzigalinski, *Technol. Cancer Res. Treat.* **2005**, 4, 651.

[60] J. Niu, A. Azfer, L. M. Rogers, X. Wang, P. E. Kolattukudy, *Cardiovasc. Res.* **2007**, 73, 549.

[61] Z. Markovic, V. Trajkovic, *Biomaterials* **2008**, 29, 3561.

[62] O. I. Shadyro, I. L. Yurkova, M. A. Kisel, *Int. J. Radiat. Biol*. **2002**, 78, 211.

[63] (a) M. R. Eftink, C. A. Ghiron, *Anal. Biochem*. **1981**, 114, 199. (b) Cantor, Schimmel, (Eds.) *Biophysical Chemistry, Part II*: Techniques for the Study of Biological Structure and Function, H. Freeman and Co., San Francisco. **1980**, Ch 7, 377.

[64] Basic solid state chemistry (second edition, john wiley and sons) by A. R. West, **1999**, 182-183.

[65] The XRD, SAED patterns and *d* vaules were indexed with reference to the crystal structures from the PCPDF files (PCPDF card no.00-012-0797).

[66] D. W. Sheibley, M. H. Flower, *National Aeronautics and Space Administration*, 1966.

[67] (a) I. D. G. Macdonald, W. E. Smith, *Langmuir* **1996**, 12, 706. (b) C. D. Keating, K. K. Kovaleski, M. J. Natan, *J. Phys. Chem. B* **1998**, 102, 9414. (c) C. V. Kumar, G. L. McLendon, *Chem. Mater.* **1997**, 9, 863. (d) A. Gole, C. Dash, S. R. Sainkar, A. B. Mandale, M. Rao, M. Sastry, *Anal. Chem.* **2000**, 72, 1401.

[68] D. Raiser, J. P. Deville, *Journal of Electron Spectroscopy and Related Phenomena* **1991**, 57, 91.

[69] C. Bicamumpaha, M. Page, *J. Immun.Meth.* **1998**, 212, 1.

[70] D. B. Pho, C. Roustan, A. N. T. Tot, L. A. Pradel, *Biochem.* **1997**, 16, 4533.

[71] S. A. Kumar, Y. A. Peter, J. L. Nadeau, *Nanotechnology* **2008**, 19, 495101.

[72] F. Marabelli, P. Wachter, *Physical Rev.* B **1987**, 36, 1238.

[73] S. Tsunekawa, J. T. Wang, Y. Kawazoe, A. Kasuya, *Journal of Applied Physics* **2003**, 94, 3654.

[74] L. E. Brus, *J. Phys. Chem.* **1986**, 90, 2555.

[75] L. Yin, Y. Wang, G. Pang, Y. Koltypin, A. Gedanken, *J. Colloid Interface Sci.* **2002**, 246, 78.

[76] (a) R. Srinivasan, A. Chandra Bose, *Mater Lett*. **2010**, 64, 1954. (b) The XRD, SAED patterns and *d* vaules were indexed with reference to the crystal structures from the PCPDF files (PCPDF card no.001-0800).

[77] S. M. Hirst, A. S. Karakoti, R. D. Tyler, N. Sriranganathan, S. Seal, C. M. Reilly, *small* **2009**, 5, 2848.

[78] S. Patil, S. Reshetnikov, M. K. Haldar, S. Seal, S. Mallik *J. Phys. Chem. C* **2007**, 111, 8437.

CHAPTER 3

Fungus-mediated bioleaching of fly ash as a means of producing extracellular protein capped silica nanoparticles.

Summary

In this chapter we have shown that the mesophilic fungus *Fusarium oxysporum* can be used for the bioleaching of waste material such as fly-ash in order to produce crystalline protein capped silica nanoparticles extracellularly at ambient temperature. When the fungus *Fusarium oxysporum* is exposed to flyash, it is capable of leaching out silica nanoparticles of quasi-spherical morphology within 24h of reaction. These silica nanoparticles were then characterized by UV-vis spectroscopy, Photoluminescence (PL), Transmission electron microscopy (TEM), X-ray diffraction (XRD), Fourier transform infrared spectroscopy (FTIR) and Energy dispersive analysis of X-rays (EDAX).

3.1 Introduction

Bioleaching may be described as an interaction between metals and microorganisms that causes the solubilization of metal and is based on the ability of microorganisms to transform solid compounds, thus resulting in soluble and extractable elements which can be recovered [1]. The ability of a variety of microorganisms to mobilize and leach metals from solid materials is based on three principles, namely (i) the transformation of organic or inorganic acids (protons); (ii) oxidation and reduction reactions; and (iii) the excretion of complexing agents. Metals can be leached either directly (i.e., physical contact between microorganisms and solid material) or indirectly (e.g., bacterial oxidation of Fe^{2+} to Fe^{3+} which catalyses metal solubilization as an electron carrier) [1]. Microbial leaching technologies have been used on an industrial scale for the recovery of copper, gold, uranium and zinc from low-grade ores or from low-grade mineral resources [2]. Several groups of microorganisms, plants and animals are used in bioleaching: autotrophic bacteria, heterotrophic bacteria, actinomycetes, lichens, algae, mosses and fungi. The use of autotrophic *Acidithiobacilli* is advantageous because no organic carbon source is needed for their growth. On the other hand, heterotrophic bacteria and fungi can be used with higher pH (i.e., alkaline and acid-consuming materials) [3]. The most effective and common bacteria for metal solubilization belong to the genus *Acidithiobacillus,* of which the two chemolithoautotrophs *Acidithiobacillus ferrooxidans* and *A. thiooxidans* are of industrial importance. In addition, the *Aspergillus* and *Penicillium* genera are the most well studied fungi used in bioleaching studies.

The unexpected spurt in global industrial activities, which was in a way essential to sustain the phenomenal rise in population, resulted in progressive deterioration of the ecosystem due to discharge of highly polluted effluents in the forms of liquids, solids and gases. Technologists have been striving to develop eco-friendly and sustainable processes in order to arrest the rapid degradation in the ecosystem. Therefore, concerted efforts are put to develop eco-friendly processes especially in the fields of mineral processing and extraction of metals, which have been the mainstay of world economy [4]. Usually, metal values are recovered from the respective ores through pyro- and hydro-metallurgical routes or a combination of both. But due to gradual depletion of high-grade ores, efforts are now being directed to recover metal values from wastes, complex and lean ores, which otherwise cannot be treated by conventional routes economically [5, 6]. The reuse of such materials not only

conserves the non-renewable resources but also solves the problem of environmental degradation, which would otherwise have polluted the environment.

Fly- ash is the finest coal combustion product generated during the burning of pulverized coal for power generation. Consisting of small particles of inorganic minerals, with some carbon, it is characterized by high flow ability due to its near-spherical particle shape. Because of its mineral chemistry, particularly rich in silica, it normally exhibits pozzolanic and sometimes cementitious behavior. It is therefore an important (cost-reducing) additive in cement and can also be used to stabilize loose soils for geotechnical engineering. One common type of fly ash is generally composed of crystalline compounds such as quartz, mullite and haematite, glassy compounds such as silica glass and other oxides. Hence, bioleaching of fly-ash can result in an economical recovery of these commercially important compounds. From this point of view, the fly-ash could be considered as an "artificial ore". In this work, we have demonstrated that the fungus *Fusarium oxysporum* can be used for bioleaching of fly-ash to obtain highly crystalline silica nanoparticles. Silica nanoparticles have always been a center of attraction for researchers due to their innumerable technological applications and biological importance. Silica finds its application in various industrial processes such as catalysis, pigments, pharmacy, electronic and thin film substrates, electronic and thermal insulators and humidity sensors [7]. Nano silica also plays an important role in silica-based materials such as resins, catalysts and molecular sieves [8]. Silica nanoparticles have started gaining their importance in biology and medicine also. Bioconjugated and doped silica nanoparticles in particular are very important in cancer cell imaging [9], ultrasensitive single bacterium detection [10], DNA and microarray detection [11], bar-coding tags [12], separation and purification of biological molecules and cells [13] and gene/drug delivery [14]. Biological synthesis of silica nanoparticles has been reported mainly by the activities of simple aquatic life forms including unicellular organisms like radiolarians, diatoms and synurophytes and also multicellular sponges [15]. Three families of cell wall proteins (frustulins, pleuralins and silaffins) from the diatom *Cylindrotheca fusiformis* have been isolated and characterized [16]. Also, extremely long chain polyamines have been discovered as an important constituent of silica [17]. It has been revealed that frustulins and pleuralins are not involved in silica formation because they become associated with the silica only after its deposition on cell wall [18]. In contrast, silaffins and polyamines exert a drastic influence on *in vitro* silica

formation and thus show direct involvement in silica nanoparticle synthesis [19]. Although there have been huge number of reports mentioning biological synthesis of amorphous and crystalline silica that uses chemical precursors which biotransformed into silica nanoparticles, the concept of silica bioleaching is very rarely encountered in literature. Bansal and co-workers have demonstrated that the fungus *Fusarium oxysporum* could be used for selective bioleaching of crystalline silica nanoparticles from white sand and zircon sand [20, 21]. In another experiment carried out by the same group, it has been shown that *F. oxysporum* when exposed to rice husk, is not only capable of leaching out huge amounts of amorphous silica present in the rice husk in the form of flat, porous silica nanostructures; but more interestingly, the fungus also biotransforms this amorphous silica into crystalline silica particles at room temperature [22]. Similarly, Kulkarni and co-workers have obtained silicate nanoparticles using fungus *Humicola* sp. at 50^{o}C by bioleaching of glass with the accompanied modification of the glass surface [23]. Bioleaching has become a potential tool for eco-friendly, low-cost synthesis of various metals from their precursors. Inorganic materials produced by organisms via bioleaching at commercial level include various metals like copper, iron and gold. In this chapter, we have extended this issue of fungal bioleaching and describe our efforts to set up a biological model system for the extracellular bioleaching of silica nanoparticles from waste material such as fly-ash obtained from thermal power plants. The replacement of chemical precursors with naturally available materials, in turn, makes the process completely biogenic, economical and eco-friendly.

We show that the fungus *F. oxysporum*, when exposed to fly-ash, is capable of leaching out silica nanoparticles of quasi-spherical morphology within 24h of reaction.

3.2 Materials and Methods

Fly-ash was obtained from thermal power plant (Chandrapur, Maharashtra, India), malt extract, yeast extract, glucose and peptone were obtained from HiMedia and used as-received.

3.3 Bioleaching of fly-ash for the production of silica nanoparticles

The mesophilic fungus *Fusarium oxysporum* was isolated from plant material and maintained on MGYP (malt extract, glucose, yeast extract and peptone) agar slants.

Stock cultures were maintained by sub culturing at monthly intervals. After growing the fungus for 96h, the slants were preserved at 15°C. From an actively growing stock culture, subcultures were made on fresh slants and after 96h of incubation were used as the starting material for fermentation experiments. For the bioleaching of fly-ash and subsequent production of silica nanoparticles, the fungus was grown in 250 ml Erlenmeyer flasks containing 100 ml of MGYP medium which is composed of malt extract (0.3%), glucose (1%), yeast extract (0.3%) and peptone (0.5%). The culture was grown with continuous shaking on a rotary shaker (200 rpm) at 25°C for 96h. After 96h of fermentation, mycelial mass were separated from the culture broth by centrifugation (5000 rpm) at 20°C for 20 min and then the mycelia were washed thrice with sterile distilled water under sterile conditions. The harvested mycelial mass (60 g of wet mycelia) was then resuspended in 10g of flyash in 500 ml Erlenmeyer flask. The whole mixture was put onto a shaker at 25°C (200 rpm) and maintained in the dark.

3.4 Characterization of bioleached silica nanoparticles

UV-visible spectroscopy measurement

Aliquots of the bioleached silica nanoparticles were removed at regular intervals and UV-vis spectrophotometric measurements were carried out on a Perkin Elmer dual-beam spectrophotometer (Model lambda 750) operated at a resolution of 1 nm.

Photoluminescence (PL) measurements

Aliquots of the reaction mixture were removed at regular intervals and subjected to the fluorescence measurements, which were carried out using a Perkin-Elmer LS 50B luminescence spectrophotometer.

Transmission Electron Microscopy (TEM) measurements

The size and shape analysis of bioleached silica nanoparticles was done on a TECHNAI G2 F20 S-TWIN instrument operated at voltage of 200 KV. HR-TEM measurements were carried out on a TECHNAI G2 F30 S-TWIN instrument (Operated at an acceleration voltage of 300 kV with a lattice resolution of 0.14 nm and a point image resolution of 0.20 nm).For this purpose, the samples were prepared by drop-coating the particles suspended in aqueous medium on carbon coated copper grids. Selected area electron diffraction (SAED) analysis was carried-out on the same grids.

X - Ray Diffraction pattern (XRD) measurements

XRD patterns were recorded using a PHILIPS X'PERT PRO instrument equipped X'celerator, a fast solid-state detector on drop-coated sample on glass substrate. The sample was scanned using X'celerator with a total number of 121 active channels. Iron-filtered Cu Kα radiation (λ=1.5406 Å) was used. XRD patterns were recorded in the 2θ range of 20°- 80° with a step size of 0.02° and a time of 5 seconds per step at 40 kV voltage and a current of 30 mA.

Fourier Transform Infrared Spectroscopy (FTIR)

FTIR spectroscopy measurements on bioleached silica nanoparticles powder taken in KBr pellet were carried out using a Perkin–Elmer Spectrum One instrument. Spectrometer was operated in the diffuse reflectance mode at a resolution of 2 cm^{-1}. To obtain good signal to noise ratio, 128 scans of the film were taken in the range of 450 – 4000 cm^{-1}.

Energy Dispersive Analysis of X-rays (EDAX)

Energy Dispersive Analysis of X-rays (EDAX) measurements of the bioleached silica nanoparticles were carried out on a Leica Stereoscan-440 SEM equipped with a Phoenix EDAX attachment. EDAX spectra were recorded in the spot-profile mode by focusing the electron beam onto a region on the surface coated with bioleached silica nanoparticles.

3.5 Results and Discussions

UV-vis Spectroscopy measurement

Figure 3.1 shows the UV-visible spectroscopy measurements of the bioleached silica nanoparticles after a reaction of 24h between the fungus *Fusarium oxysporum* and fly-ash. The UV-visible spectrum shows a prominent absorption at *ca* 275 nm and a slight absorption edge at *ca* 350 nm. Absorption at 275 nm can be assigned to the presence of aromatic amino acids such as tryptophan, tyrosine and phenylalanine [24]. These amino acids are present in the proteins and enzymes secreted by the fungus while leaching of fly-ash, thus confirming the role of certain biomolecules in the bioleaching process. When the fungal biomass reacts with fly-ash, the specific proteins and enzymes secreted by the fungus in response to stress conditions act

predominantly on the silica component of fly-ash, since it has been reported that *Fusarium oxysporum* is having more affinity towards silica [21]. This interaction of proteins and enzymes results in the formation of an enzyme-silicic acid complex (initial bioleached product). This siliceous complex will be hydrolyzed by the action of specific hydrolyzing enzymes again secreted by the fungus. This siliceous complex which is present within biomass will be then released into the solution in the form of silica nanoparticles. Since fly-ash comprises mainly of silica, mullite and silimanite (SiO_2, $Al_6Si_2O_{13}$ and Al_2SiO_5 respectively), at this point of time we are not sure about the silica component on which the enzymes are acting upon. The source of bioleached silica nanoparticles, which are released into the solution, may be of the nascent silica or mullite/silimanite or all the silica constituents present in the fly-ash. The absorption edge at *ca* 350nm thus can be attributed to bioleached silica nanoparticles which are released into the solution extracellularly.

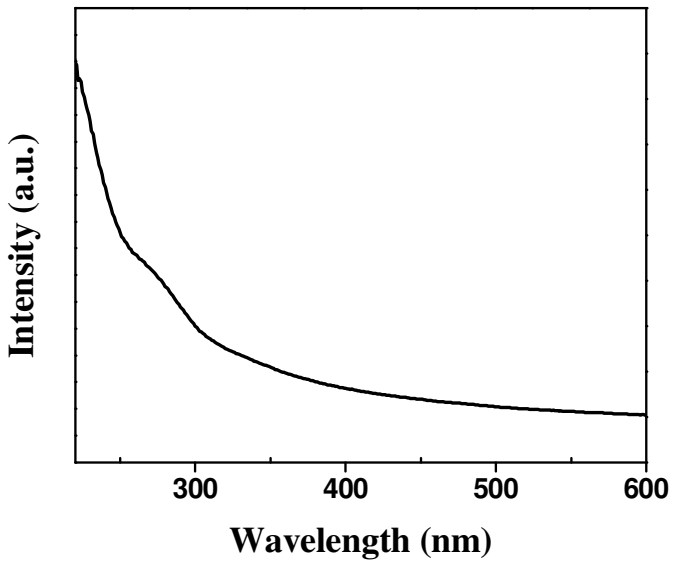

Figure 3.1: UV-visible spectroscopy measurements of the bioleached silica nanoparticles after a reaction of 24h between the fungus Fusarium oxysporum and fly-ash.

Photoluminescence measurements (PL)

Figure 3.2 shows the photoluminescence (PL) spectrum of bioleached silica nanoparticles after reaction of 24h between the fungus *Fusarium oxysporum* and fly-ash. When extracellular solution of bioleached silica nanoparticles is excited at

360nm, an emission band at 442 nm is observed. This phenomenon of photoluminescence occurs when there is interface between Si nanocrystals in SiO_2 matrix at nanoscale size regime [25].

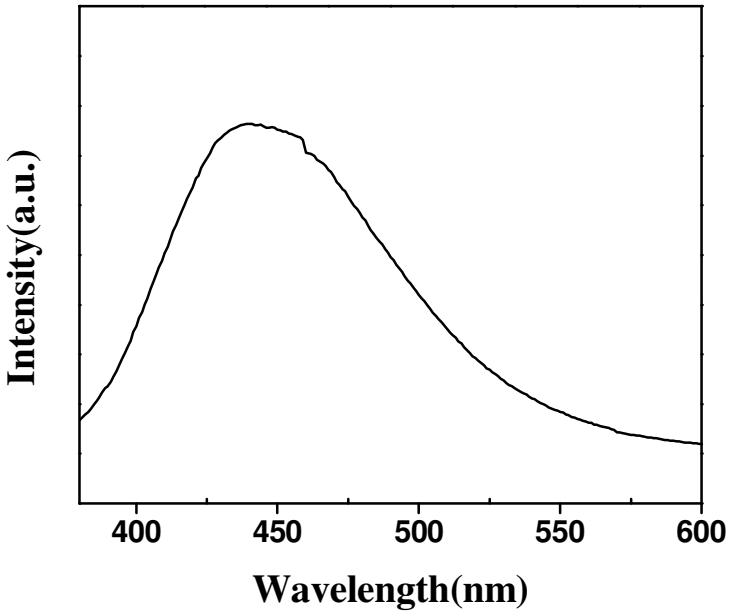

Figure 3.2: Photoluminescence spectrum of bioleached silica nanoparticles obtained after 24h reaction between Fusarium oxysporum and fly-ash. (λ excitation = 360nm and λ emission = 442nm).

Transmission Electron Microscopy (TEM) measurements

Figure 3.3 (A) shows a representative TEM image of fly-ash (control) showing bigger particles. Figure 3.3 (B) shows a representative TEM image of bioleached silica nanoparticles obtained after reacting fly-ash with *Fusarium oxysporum* for 24h.The particles are polydispersed and irregular in shape. Inset in figure 3.3 (B) shows Selected Area Electron Diffraction (SAED) analysis of bioleached silica nanoparticles. The diffraction spots in the SAED pattern could be well indexed based on the silica structure [26]. Figure 3.3 (C) represents a particle size distribution histogram of bioleached silica nanoparticles showing that the particles are in the range of 22-28 nm with an average diameter of 24 nm. HR-TEM analysis of bioleached silica nanoparticles (figure 3.3 D) revealed the inter planar distance to be 2.20 Å which corresponds to the plane {048} of

SiO_2. The TEM and SAED results clearly show that silica nanoparticles are leached out from the fly-ash by the fungus *Fusarium oxysporum.*

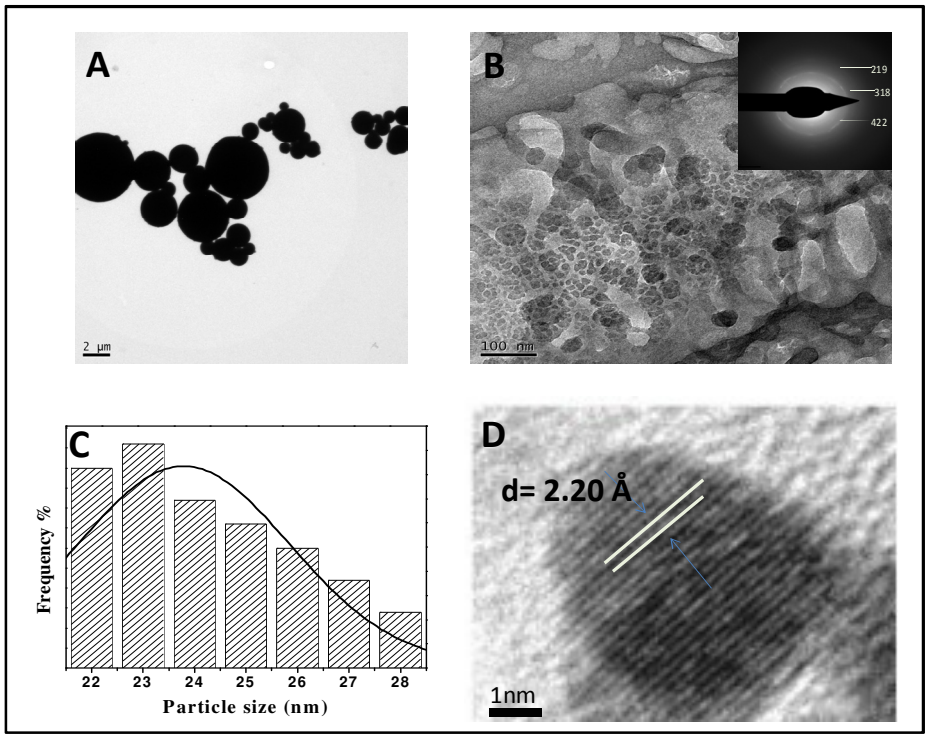

Figure 3.3: (A) represents the TEM image of fly-ash (control) (B) represents the TEM image of bioleached silica nanoparticles obtained after reacting fly-ash with Fusarium oxysporum for 24h. Inset shows Selected Area Electron Diffraction (SAED) analysis of bioleached silica nanoparticles (C) Particle size distribution analysis calculated from TEM image. (D) HR-TEM image of bioleached silica nanoparticles.

X - Ray Diffraction (XRD) measurements

Figure 3.4 represents the X-ray diffraction analysis of bioleached silica nanoparticles obtained after reacting fly-ash with *Fusarium oxysporum* for 24h.The XRD pattern of silica nanoparticles showed peaks at {031},{219}, {318}, {042},{3110}, {422}, {048}, {051}, {514}, {057}, {622} and {631} in the 2θ range 20–80^o and agree well with crystalline polymorph of silica [26]. The broadened XRD peaks reflect the small size of silica nanoparticles. It is important to note here that even though the particles are capped by proteins, presence of proteins does not compromise with the crystallinity of the bioleached silica nanoparticles which can be confirmed by the occurrence of sharp Bragg reflections even without calcinations of as-bioleached silica particles.

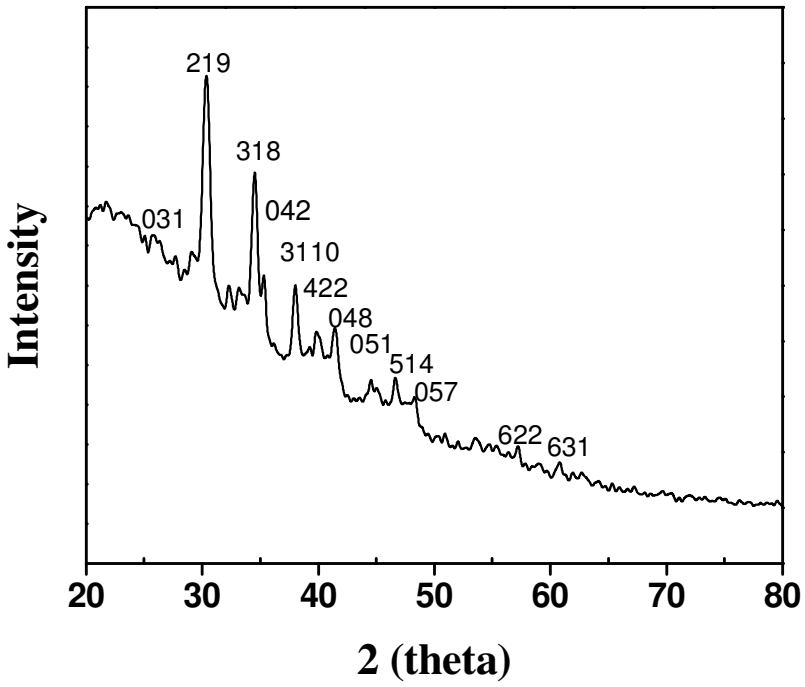

Figure 3.4: X-ray diffraction (XRD) analysis of bioleached silica nanoparticles obtained after reacting fly-ash with Fusarium oxysporum for 24h.

Fourier transform infrared spectroscopy (FTIR) analysis

Figure 3.5 (A) represents the fourier transform spectroscopy analysis of bioleached silica nanoparticles obtained after reacting fly-ash with *Fusarium oxysporum* for 24h.The FTIR spectrum shows a sharp peak at *ca* 1100cm^{-1}. This peak can be assigned to the Si–O–Si antisymmetric stretching mode of silica [27]. Thus; it is made very clear that the silica nanoparticles are leached out by the fungus in the extracellular solution. The FTIR spectrum given in figure 3.5 (B) shows the presence of two peaks at *ca* 1641 and 1540 cm^{-1} which can be assigned to amide I and amide II bands respectively. These amide bands may emanate from the proteins present in the silica particles which have been released in the solution by the fungus during the reaction with fly-ash.

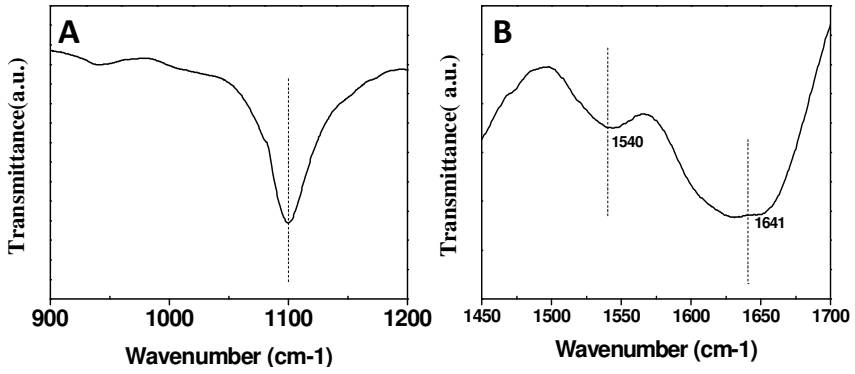

Figure 3.5: (A) FTIR spectrum of bioleached silica nanoparticles obtained after reacting fly-ash with Fusarium oxysporum for 24h.(B) FTIR spectrum of bioleached silica nanoparticles showing amide bands.

Energy Dispersive Analysis of X-rays (EDAX)

Figure 3.6 represents the Energy Dispersive Analysis of X-rays (EDAX) spectrum of bioleached silica nanoparticles obtained after reacting fly-ash with *Fusarium oxysporum* for 24h. The spectrum shows a sharp peak at 1.74 KeV and at 0.51 KeV corresponding to Si and O respectively. The presence of Si and O in the bioleached sample confirms the presence of silica nanoparticles. These results are in good agreement with the XRD analysis (figure 3.4) confirming the bioleaching of fly-ash by the fungus accompanied by the predominant release of silica nanoparticles in the solution (filtrate).The spectrum also shows the signals of C, N, and S confirming the presence of proteins in the silica nanoparticles. Signals of Cu can be assigned to the copper (substrate) used for the analysis of sample.

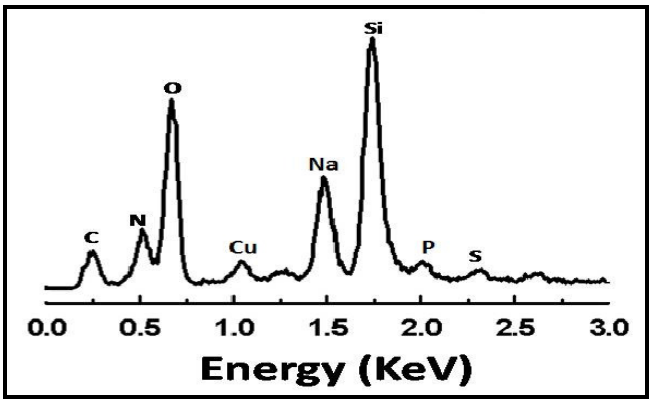

Figure 3.6: EDAX spectrum of bioleached silica nanoparticles obtained after reacting fly-ash with Fusarium oxysporum for 24h.

3.6 References

[1] H. Brandl, W. Krebs, C. Brombacher, P. P. Bosshard, R. Bachofen, Microbiological Systems for Metal Recycling. *In Proceedings of R'97-Recovery, Recycling, Re-Integration Geneva*, **1997** Vol IV, pp. 16.

[2] C. Brombacher, R. Bachofen, H. Brandl, *Applied Microbiology and Biotechnology*, **1997**, 48, 577.

[3] F. Schinner, W. Burgstaller, *Applied Environmental Microbiology*, **1989,** 55, 1153.

[4] W. Verstrate, *Journal of Biotechnology* **2002**, 94, 93.

[5] J. D. Miller, J. Li, J. C. Davidtz, F. Vos, *Minerals Engineering* **2005**, 18, 855.

[6] J. Cui, L. Zhang, *Journal of Hazardous Materials* **2008**, 158, 228.

[7] G. Herbert, *J. Eur. Ceram. Soc*. **1994**, 14, 205.

[8] A. Corma, *Chem. Rev*. **1997**, 97, 2373.

[9] S. Santra, K. M. Wang, R. Tapec, W. H. Tan, *J. Biomed. Opt*. **2001**, 6, 160.

[10] X. J. Zhao, L. R. Hilliard, S. J. Mechery, Y. Wang, R. P. Bagwe, S. Jin, W. H. Tan, *P. Natl. Acad. Sci. USA* **2004**, 101, 15027.

[11] X. J. Zhao, R. Tapec-Dytioco, W. H. Tan, *J. Am. Chem. Soc*. **2003**, 125, 11474.

[12] L. Wang, W. H. Tan, *Nano Lett*. **2006**, 6, 84.

[13] X. J. Zhao, R. Tapec-Dytioco, K. M. Wang, W. H. Tan, *Anal. Chem*. **2003**, 75, 3476.

[14] M. N. V. Ravi Kumar, M. Sameti, S. S. Mohapatra, X. Kong, R. F. Lockey, U. Bakowsky, G. Lindenblatt, H. Schmidt, C. M. Lehr, *J. Nanosci. Nanotechnol.* **2004**, 4, 876.

[15] H. A. Lowenstam, S. Weiner, *On Biomineralization*, Oxford University Press, Oxford, **1989**.

[16] (a) N. Kroger, C. Bergsdorf, M. Sumper, *EMBO J.* **1994**, 13, 4676. (b) N. Kroger,G. Lehmann, R. Rachel, M. Sumper, *Eur. J. Biochem*. **1997**, 250, 99. (c) N. Kroger,R. Deutzmann, M. Sumper, *Science* **1999**, 286, 1129.

[17] N. Kroger, R. Deutzmann, C. Bergsdorf, M. Sumper, *Proc. Natl. Acad. Sci. USA*, **2000**, 97, 14133.

[18] (a) W. H.van de Poll, E. G. Vrieling, W. W.C. Gieskes, *J. Phycol.* **1999**, 35, 1044. (b) N. Kroger, R. Wetherbee, *Protist* **2000**, 151, 263.

[19] M. Sumper, N. Kroger, *J. Mater. Chem.* **2004**, 14, 2059.

[20] V. Bansal, A. Sanyal, D. Rautaray, A. Ahmad, M. Sastry, *Adv. Mater.* **2005**, 17, 889.

[21] V. Bansal, A. Syed, S. K. Bhargava, A. Ahmad, M. Sastry *Langmuir* **2007,** 23, 4993.

[22] V. Bansal, A. Ahmad, M. Sastry, *J. Am. Chem. Soc.* **2006**, 148,14059.

[23] S. Kulkarni, A. Syed, S. Singh, A. Gaikwad, K. Patil, K. Vijayamohanan, A. Ahmad, S. Ogale, **2008,** 354, 3433.

[24] (a) M. R. Eftink, C. A. Ghiron, *Anal. Biochem*. **1981**, 114, 199. (b) Cantor, Schimmel, (Eds.) *Biophysical Chemistry, Part II*: Techniques for the Study of Biological Structure and Function, H. Freeman and Co., San Francisco. **1980**, Ch 7, 377.

[25] L. Pavesi, L. D. Negro, C. Nazzoleni, G. Franzo, P. Priolo, *Nature* **2000**, 408, 440.

[26] The XRD pattern and SAED spots were indexed with reference to the crystal structure from the *PCPDF* chart: silica (*PCPDF* card no. 040–1498).

[27] P. Innocenzi, P. Falcaro, D. Grosso, F. Babonneau, *J. Phys. Chem B.* **2003**,107, 4711.

CHAPTER 4

Phase, Size and Shape Transformation by Fungal Biotransformation of TiO_2 Nanoparticles.

Summary

In this chapter, we have shown that the thermophilic fungus *Humicola* sp. can be used not only for the production of technologically viable large scale synthesis of TiO_2 nanoparticles but also for the transformation of shape, phase and size of bulk anatase TiO_2 powder. When the fungus *Humicola* sp. was incubated with disc shaped micron size anatase TiO_2 powder at 50^oC for 96h, the fungus biotransformed the disc shaped micron sized anatase powder into circular nanosized brookite phase of TiO_2. The biotransformed protein capped TiO_2 nanoparticles were having diameter of 2-4nm and were characterized by UV-vis spectroscopy, Photoluminescence measurements (PL), Transmission Electron Microscopy (TEM), X-Ray Diffraction (XRD), Fourier Transform Infrared (FTIR) spectroscopy, X-ray Photoemission Spectroscopy (XPS), and Energy Dispersive Analysis of X-rays (EDAX).

4.1 Introduction

Titanium dioxide i.e. TiO_2 or titania exists in both crystalline and amorphous forms. Titanium dioxide mainly exists in three crystalline polymorphs namely anatase, rutile and brookite. These three polymorphs have different crystalline structures. Anatase and rutile have tetragonal structure, whereas brookite is orthorhombic [1-8]. Anatase and brookite are meta stable phases, whereas rutile is the most stable phase. Brookite and anatase convert to rutile when they are calcined at higher temperatures [9, 10]. The phase transition temperature varies with the method of preparation of the powders. Brightness and high refractive index of the titanium dioxide powder makes it useful in applications like paints and pigments. It is being employed as a pigment to provide whiteness and opacity to products like paints, coatings, plastics, papers, inks, foods and toothpastes [11-13]. It is also being used as a pigment and thickener in cosmetic and skin care products. Almost every sun-block contains titanium dioxide because of its high refractive index and its resistance to discoloration under ultraviolet light. This enhances its ability to protect the skin from ultraviolet light. Hence, this pigment is being used extensively in plastics and other applications for its UV resistant properties where it acts as a UV reflector [13-16]. Titanium dioxide is the most promising compound for photocatalysis applications. TiO_2 is stable in aqueous media and is tolerant to both acidic and alkaline solutions. It is inexpensive, recyclable, reusable and is relatively simpler to produce. Most importantly, its band gap is appropriate to initiate a variety of organic reactions as the redox potential of H_2O/OH^- lies within the band gap. The large band gap of TiO_2, 3.2 eV, lies in the UV range of the electromagnetic spectrum. This allows only 5-8% of sunlight that has the required energy to be useable for photocatalysis. Therefore, a visible-light activated catalyst would be much more efficient and effective. There are several known ways to increase the efficiency of a photocatalyst. Tailoring the band gap of TiO_2 to allow for visible light photocatalysis may be accomplished by reducing the particle size [17], metal - ion doping [18–20], or electronegative atom doping [21, 22]. Anatase and rutile have been of interest to many researchers for a long time [23, 24]. The properties and applications of brookite phase are comparatively new. Much less attention has been given to the properties and applications of this phase due to the difficulty in producing pure brookite particles. Commercially available anatase phase TiO_2 nanoparticles can serve as antimicrobial agents via UV light activation. However, brookite phase nanoparticles, due to their smaller particle size may increase

the efficiency of TiO_2 nanoparticles to inhibit bacterial growth by promoting a greater surface area contact ratio which subsequently causes cell death in less time than anatase phase nanoparticles.

To date, much effort is focused on the chemical and physical synthesis of titania nanomaterials; while there are only a few efforts concerning their bio-inspired synthesis [25-32]. For example, Morse *et al.* found that silicatein, an enzymatic biocatalyst purified from the glassy skeletal elements of a marine sponge is also capable of catalyzing and templating the hydrolysis and subsequent polycondensation of a water-stable alkoxide-like conjugate of titanium to form titanium dioxide at low temperature and pressure and neutral pH. Sewell and Wright reported that the R5 peptide, a bio-inspired analogue derived from the NatSil protein in *Cylindrotheca fusiformis* can form titanium dioxide in a concentration-dependent manner from the non natural substrate titanium bis (ammonium lactato) dihydroxide. Yajun *et al.* have shown that Protamine, a kind of cationic protein extracted from sperm nuclei, was employed for the first time *in vitro* to induce the formation of a titania/protamine nanoparticle composite from a water-stable titanium precursor, titanium (IV) bis (ammonium lactato) dihydroxide (Ti-BALDH). Inspite of all these reports on the biological synthesis of TiO_2 nanoparticles, brookite phase still remains the least studied and explored one. In this work, we have examined a different fungus based approach to the synthesis of brookite TiO_2 nanoparticles wherein we start with micron sized particles of the parent material instead of soluble precursors. Remarkably, we found that fungal processing of such large sized powders bioleaches them and transforms them into nanoparticles which are of a different phase (brookite) and shape (circular) as compared to the parent materials (anatase, disc shaped powder). Since processing of bulk powders is a relatively easy process, using such powders directly for top-down nanosynthesis may be an attractive alternative for the technology as compared to scaling-up of precursor based bottom-up nanosynthesis [33]. Bioleaching is a well known process in the context of metal extraction from minerals [34-36]. Although bioleaching is accomplished by several bio-organisms such as bacteria and fungi, its effectiveness varies for different organisms and different conditions [37, 38]. Several mechanisms such as acidolysis, complexolysis, redoxolysis and bioaccumulation are suggested to be involved in bioleaching [39]. As compared to bacterial leaching, fungal leaching has the advantages of the ability to grow under higher pH, thereby being more suitable for bioleaching of alkaline solids and enabling

relatively faster leaching [40]. Nanosynthesis is an ever expanding frontier in recent years in view of its implications to many future technologies covering diverse fields. Considerable progress has been made realizing high quality synthesis of elemental nanomaterials as well as compounds as chemical, biological and physical routes. The issue of technologically viable large scale synthesis still continues to be a challenge. Here we demonstrate a novel environmentally friendly top down approach to nanosynthesis which exploits the strength and peculiarities of fungus based bioleaching in extracting radicals from compounds and then providing them with a reactive as well as capping environment. Thus protein capped nanoparticles of TiO_2 (2-4 nm, circular and brookite phase) are formed directly from micron size (150-250 nm, disc shape, anatse phase) powder by exposing them to a medium of fungus *Humicola* sp. at just 50^{o}C. The fungus *Humicola* sp. is not only useful for the synthesis of nanoparticles but also for the transformation of shape, phase and size of TiO_2.

4.2 Materials and Methods

Materials: Micron size (TiO_2) Anatase Phase was purchased from Fluka**,** malt extract, yeast extract, glucose and peptone were obtained from HiMedia and used as-received.

4.3 Biotransformation of Micron sized Anatase TiO_2 to Nano sized Brookite TiO_2

The fungus *Humicola* sp. was maintained on MGYP (malt extract, glucose, yeast extract, and peptone) agar slants. Stock cultures were maintained by subculturing at monthly intervals. After growing the fungus at pH 9 and 50°C for 96h the slants were preserved at 15°C. From an actively growing stock culture, subcultures were made on fresh slants and after 96h of incubation at pH 9 and 50°C, were used as the starting material for fermentation experiments. For the biotransformation of TiO_2 nanoparticles, the fungus was grown in 250 ml Erlenmeyer flasks containing 100 ml of MGYP medium which is composed of malt extract (0.3%), glucose (1%), yeast extract (0.3%) and peptone (0.5%). Sterile 10% sodium carbonate was used to adjust the pH of the medium to 9. After the pH of the medium was adjusted, the culture was grown with continuous shaking on a rotary shaker (200 rpm) at 50°C for 96h. After 96h of fermentation, mycelial mass was separated from the culture broth by centrifugation (5000 rpm) at 20°C for 20 min and then the mycelia were washed

thrice with sterile distilled water under sterile conditions. The harvested mycelial mass (20 g of wet mycelia) was then resuspended in 100 ml of 10^{-3} M aqueous micron sized anatase TiO_2 powder solution in 250 ml Erlenmeyer flasks at pH 9. The whole mixture was put onto a shaker at 50°C (200 rpm) and maintained in the dark.

4.4 Characterization of biotransformed TiO_2 nanoparticles

UV-visible spectroscopy measurements

Aliquots of the biotransformed TiO_2 were removed at regular intervals and UV-vis spectrophotometric measurements were carried out on a Shimadzu dual-beam spectrophotometer (model UV-1601 PC) operated at a resolution of 1 nm.

Photoluminescence (PL) measurements

Aliquots of the reaction mixture were removed at regular intervals and subjected to fluorescence measurements, which were carried out using a Perkin-Elmer LS 50B luminescence spectrophotometer.

Transmission Electron Microscopy (TEM) measurements

The size and shape analysis of TiO_2 nanoparticles was done by a JEOL model 1200EX TEM operated at a voltage of 80 KV. For this purpose, the samples were prepared by drop-coating the particles suspended in aqueous medium on carbon coated copper grids. HR-TEM measurements were carried out on a TECHNAI G2 F30 S-TWIN instrument (Operated at an acceleration voltage of 300 kV with a lattice resolution of 0.14 nm and a point image resolution of 0.20 nm). Selected area electron diffraction (SAED) analysis was carried out on the same grids.

X - Ray Diffraction pattern (XRD) measurements

XRD patterns were recorded using a PHILIPS X'PERT PRO instrument equipped X'celerator, a fast solid-state detector on drop-coated sample on glass substrate. The sample was scanned using X'celerator with a total number of 121 active channels. Iron-filtered Cu Kα radiation (λ=1.5406 Å) was used. XRD patterns were recorded in the 2θ range of 20°- 80° with a step size of 0.02° and a time of 5 seconds per step at 40 kV voltage and a current of 30 mA.

Fourier Transform Infrared Spectroscopy (FTIR)

FTIR spectroscopy measurements on biotransformed TiO_2 nanoparticles powder taken in KBr pellet were carried out using a Perkin–Elmer Spectrum One instrument. The Spectrometer was operated in the diffuse reflectance mode at a resolution of 2 cm^{-1}. To obtain good signal to noise ratio, 128 scans of the film were taken in the range of 450 – 4000 cm^{-1}.

Energy Dispersive Analysis of X-rays (EDAX)

Energy Dispersive Analysis of X-rays (EDAX) measurements of the biotransformed TiO_2 nanoparticles were carried out on a Leica Stereoscan-440 SEM equipped with a Phoenix EDAX attachment. EDAX spectra were recorded in the spot-profile mode by focusing the electron beam onto a region on the surface coated with biotransformed TiO_2 nanoparticles.

X-ray Photoemission Spectroscopy (XPS)

XPS of the biotransformed TiO_2 nanoparticles cast on the Si substrate was carried out on a VG MicroTech ESCA 3000 instrument.

4.5 Results and Discussions

UV-visible spectroscopy

Figure 4.1 shows the UV-visible spectroscopic measurements of biotransformed TiO_2 nanoparticles after 96h of reaction with the fungus *Humicola* sp. The spectrum shows first absorption maxima at *ca* 270 nm which is attributed to the presence of aromatic amino acids secreted by the fungus in the reaction mixture while biotransforming TiO_2 nanoparticles. These aromatic amino acids may be present in the capping molecule which is supposed to play a vital role in capping of biotransformed TiO_2 nanoparticles [41]. The absorption edge at *ca* 380 nm corresponds to the well known signature of self-trapped exciton in TiO_2 matrix [42]. For semiconductor materials, the quantum confinement effect is expected if the semiconductor dimension becomes smaller than the Bohr's radius of the exciton and the absorption edge will be shifted to a higher energy [43]. The high absorption of visible light of biotransformed brookite TiO_2 nanoparticles can be due to higher surface area and smaller particles [44] and suggests photoactivity of these nanoparticles in the visible light region. The inset in figure 4.1 shows the optical band-gap energy for biotransformed TiO_2 nanoparticles

which was estimated from a plot of $(\alpha h\nu)^2$ versus $(h\nu)$, where α is the molar extinction coefficient and $h\nu$ is photon energy. The band gap energy of biotransformed brookite TiO_2 nanoparticles was calculated to be 3.28 eV which is in very good agreement with reported band gap energy for brookite TiO_2 nanoparticles [45].

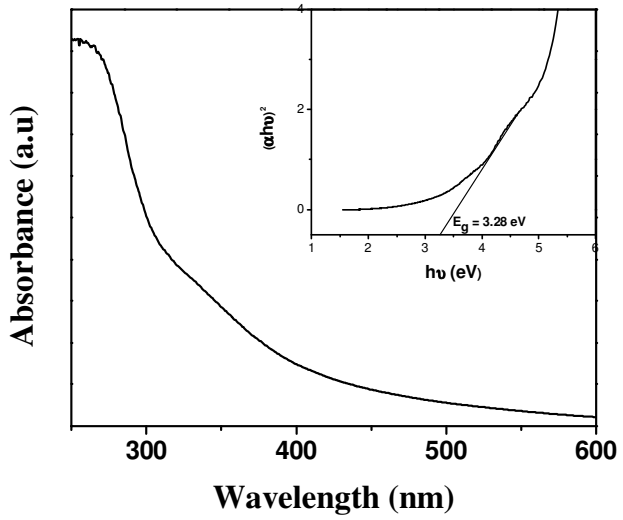

Figure 4.1: UV-vis spectrum of biotransformed brookite TiO_2 nanoparticles. Inset shows the corresponding plot of $(\alpha h\nu)^2$ versus photon energy (hν)(taucsplot) for the biotransformed brookite TiO_2 nanoparticles.

Photoluminescence (PL) measurements

Figure 4.2 shows the Photoluminescence spectrum of biotransformed brookite TiO_2 nanoparticles excited at 330nm and showed an emission peak at *ca* 413 nm.

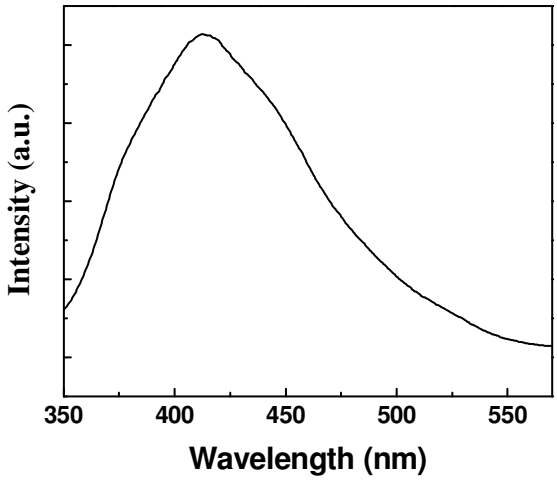

Figure 4.2: Photoluminescence spectrum of the biotransformed brookite TiO_2 nanoparticles excited at 330 nm.

Transmission Electron Microscopy (TEM) measurements

Figure 4.3 shows the TEM images of parent anatase type TiO_2 and biotransformed brookite type TiO_2 nanoparticles. From figure 4.3 (A), it is very clear that the parent anatase type TiO_2 are micron size disc shaped particles. Inset in figure 4.3 (A) confirms their disc shaped morphology. The micron size of anatase type TiO_2 nanoparticles is further confirmed by particle size distribution analysis. Figure 4.3 (B) clearly indicates that the anatase type TiO_2 particles are 0.1-0.25 µm in diameter with 0.15 µm as the average size. Figure 4.3 (C) represents the TEM image of biotransformed brookite type TiO_2 particles obtained after reacting anatase type TiO_2 particles with fungus *Humicola* sp. for 96h. Dense population of TiO_2 nanoparticles was found distributed over a large area of TEM grid. The biotransformed TiO_2 nanoparticles (Figure 4.3 C) show nearly uniform shape and size. Particles are nearly spherical in shape and are of 2.0-4.0 nm in size. As can be seen from TEM images the nanodisc start fragmenting and formed spherical particles to smaller size due to the reaction with fungal biomass. Now it is clear, this process carries huge technical advantages over traditional top down methods, which are quite expensive and the biomilling process provides a very simple and economical route to form smaller particles. SAED pattern from biotransformed TiO_2 nanoparticles (inset, Figure 4.3C) shows a poly crystalline ring pattern, which has been indexed on the basis of brookite phase. Three rings were indexed to {121}, {111} and {120} planes, which match well with the reported values of brookite phase [46]. Particle size distribution from biotransformed TiO_2 nanoparticles (Figure 4.3 D) was performed over 100 particles and average particle size was found to be 2.0 nm. Figure 4.3 (E) and (F) show the HR-TEM images of biotransformd brookite type TiO_2 nanoparticles. Clearly resolved lattice fringes of TiO_2 nanoparticles are observed in the image indicating the crystalline nature of TiO_2 nanoparticles. The inter planer spacing (d-spacing) of 3.47 Å and 2.88 Å was assigned to {120} and {121} planes of brookite phase of TiO_2 respectively [46].

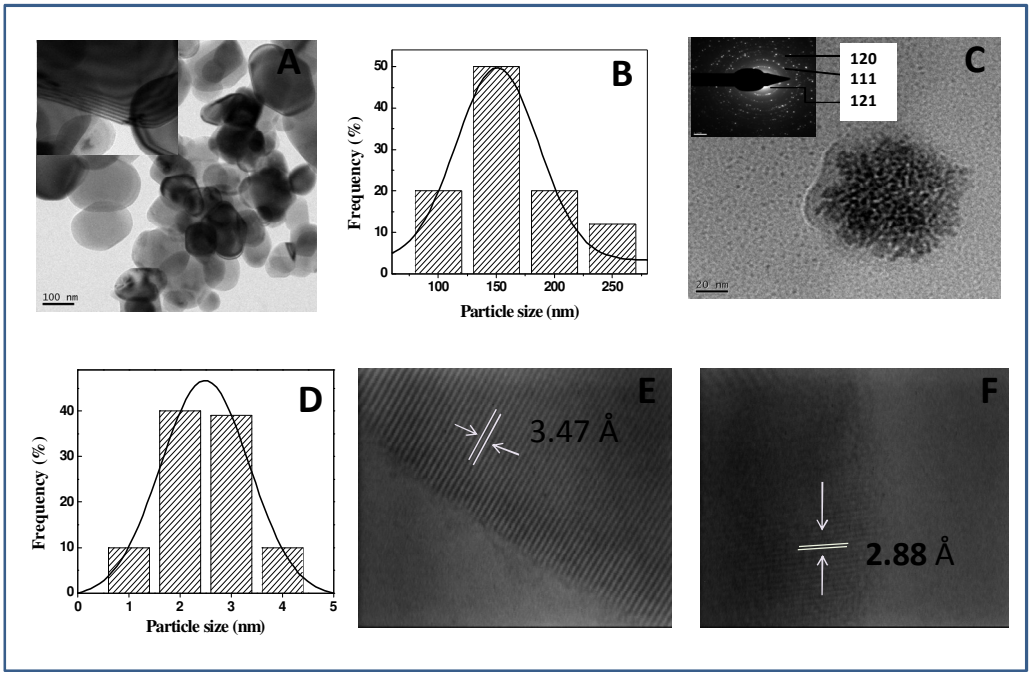

Figure 4.3: (A) TEM image of parent anatase type TiO_2 particles showing their micron size and disc shaped morphology. (B)Particle size distribution of anatase type TiO_2 particles obtained from TEM image.(C)TEM image of biotransformed brookite type TiO_2 nanoparticles obtained after 96h of reaction between anatase type TiO_2 particles and fungus Humicola sp. ,inset shows SAED pattern of biotransformed brookite type TiO_2 nanoparticles. (D)Particle size distribution of biotransformed brookite type TiO_2 nanoparticles obtained from TEM image. (E) and (F) HR-TEM images of biotransformed brookite type TiO_2 nanoparticles showing inter planer distance (d spacing).

X-Ray Diffraction (XRD) measurements

Figure 4.4 shows the comparison between parent (precursor) anatase type TiO_2 (A) and biotransformed brookite-type TiO_2 (B). The anatase powder shows sharp peaks reflecting their micron size and identified as anatase phase (JCPDF # 21-1272).This anatase type TiO_2 after reacting with fungus *Humicola* sp. for 96h at 50^oC completely biotransformed into brookite type TiO_2 nanoparticles. Biotransformed brookite-type TiO_2 nanoparticles peaks show considerable broadening suggesting the particle size in nanometer range (2-4 nm) which corresponds well with TEM images and identified as brookite phase. All the planes {120}, {111}, {121}, {012}, {201}, {231} and {320} can be well indexed to the brookite type TiO_2 (JCPDF#card no 29-1360) [46]. Katagiri and co-workers have also reported the formation of brookite type TiO_2 nanoparticles using lipase enzyme at pH 10 under ambient conditions [31]. Some

researchers claimed that the presence of sodium cations are essential, [47, 48, 49] while some others argued that low solution pH and Cl^- ions favor brookite formation [50]. Our results seem to support the former claim, since sodium carbonate has been used to adjust the pH of the reaction mixture.

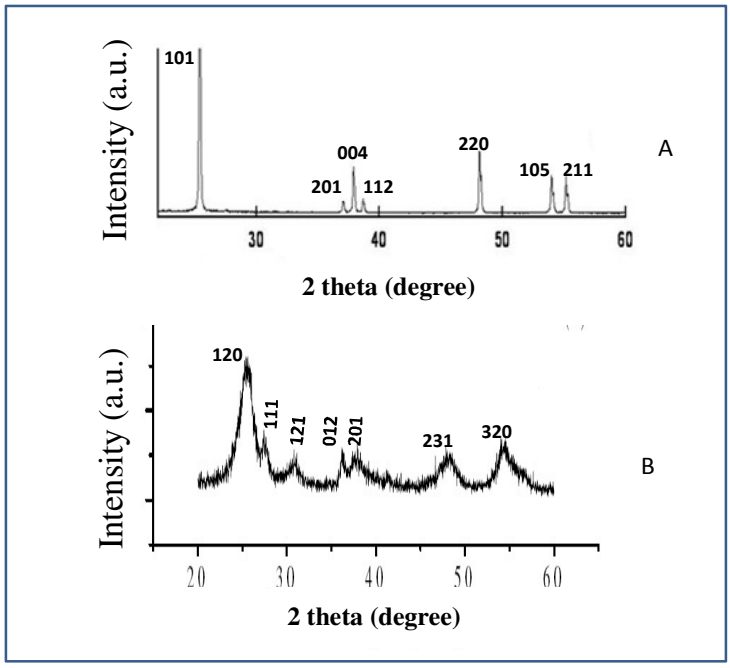

Figure 4.4: showing X-ray diffraction (XRD) measurements of (A) Micron sized anatase- type TiO_2 and (B) Biotransformed nanosized brookite-type TiO_2.

Fourier Transform Infrared Spectroscopy (FTIR)

Figure 4.5 shows the FTIR spectra of biotransformed brookite TiO_2 nanoparticles. The strong absorption region centered at 695, 834 and 1046 cm^{-1} can be attributed to Ti-O-Ti vibrational modes [29, 32]. A weak band at 995cm^{-1} corresponds to the excitation of the Ti–O antisymmetric stretching of Ti–O–Ti bonds [51]. The bands centered at 1625 and 1666cm^{-1} can be assigned to amide I and amide II bands of protein respectively which are present in biotransformed brookite TiO_2 nanoparticles [52].

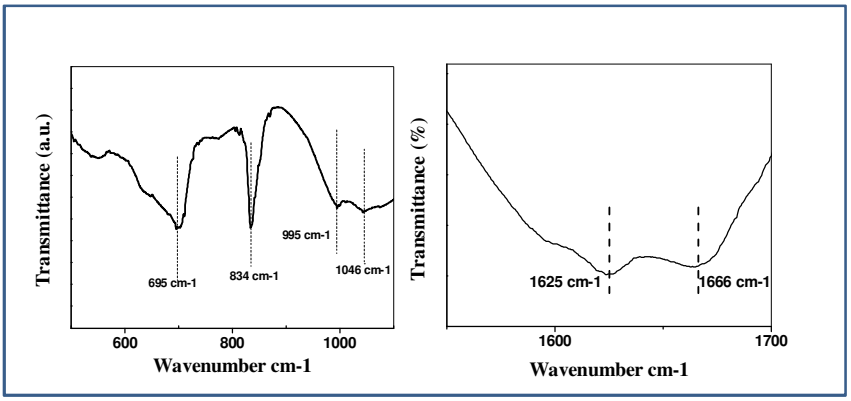

Figure 4.5: FTIR spectra of biotransformed brookite TiO_2 nanoparticles.

Energy Dispersive Analysis of X-rays (EDAX) measurements

Figure 4.7 shows the EDAX analysis (Energy Dispersive Analysis of X-rays) of biotransformed brookite phase of TiO_2 sample indicating the signals from Ti and O in small amounts, since biosynthetic protocols of nanoparticles account for a low yield and confirming the presence of TiO_2 in the sample. Signals are observed from C, O and N. The signals for C, O and N are due to the proteins that are capped onto the surface of the nanoparticles. The highest peak corresponds to silica which is used as a template for analyzing the sample.

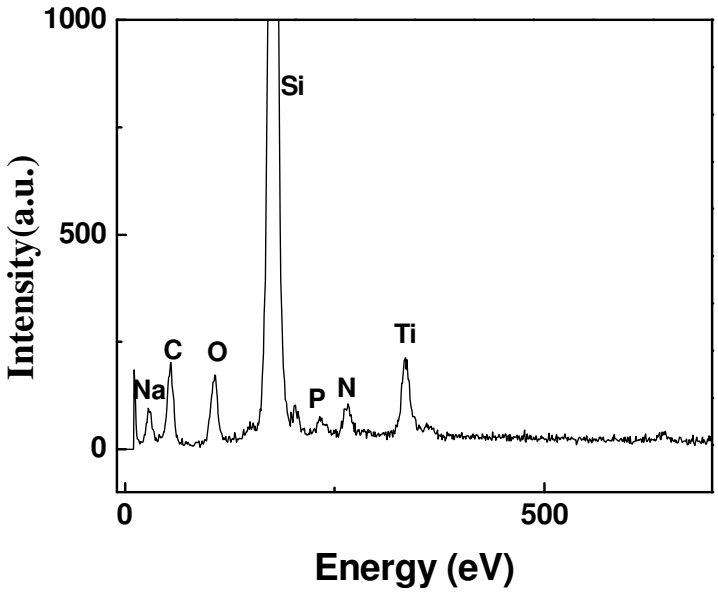

Figure 4.7: EDAX measurements carried out on biotransformed brookite TiO_2 nanoparticles.

X-ray Photo-emission Spectroscopy (XPS) measurements

Figure 4.8 shows the XPS spectra of biotransformed TiO_2 nanoparticles after 96h reaction between anatase type TiO_2 and the fungus *Humicola* sp. at 50^{o}C.The C (1s) XPS spectra is given in Figure 4.8 (A) which has three chemically distinct components centered at 284.8, 286.4 and 290.0 eV. The binding energy peak at 284.8 eV is attributed to the presence of aromatic carbon present in amino acids from proteins bound to the surface of biotransformed brookite TiO_2 nanoparticles [53]. The C (1s) component centered at 286.4 eV is due to electron emission from adventitious carbon present in the sample. The binding energy peak at 290.0 eV is attributed to electron emission from carbons in carbonyl groups (aldehydic or ketonic carbon) present in proteins bound to the nanoparticles surface [54]. The XPS spectra for N (1s) (Figure 4.8 B) could be resolved into three chemically distinct components centering at 398.0 eV, 400. eV and 401.8 eV. These could be assigned respectively to free N_2, neutral amino group NH_2 and the positively charged ammonium group NH^{3+} present in the capping proteins [55]. The O (1s) spectrum (Figure 4.8 C) could be resolved into two chemically distinct components centering at 530.5 eV and 532.8 eV. The O 1s component present at binding energy (530.5 eV) can be assigned to Ti–O–

Ti oxygen while the O(1s) component present at higher binding energy (532.8 eV) is assigned to mixed contributions from surface hydroxide [56] and C=O group present in capping proteins. Hence it is very clear that certain proteins are attached with TiO_2 nanoparticles and some of them may be responsible for the biotransformation of anatase to brookite type TiO_2 nanoparticles. Few of these proteins may also be responsible for capping of biotransformed TiO_2 nanoparticles, preventing their aggregation. From Figure 4.8 (D); one can see that the binding energies of $Ti2p_{3/2}$ and $Ti2p_{1/2}$ are centered at 457.0 and 465.0 eV, respectively. This clearly reveals that the titanium ions are in the oxidation state IV, corresponding to Ti^{4+} (TiO_2) [57].

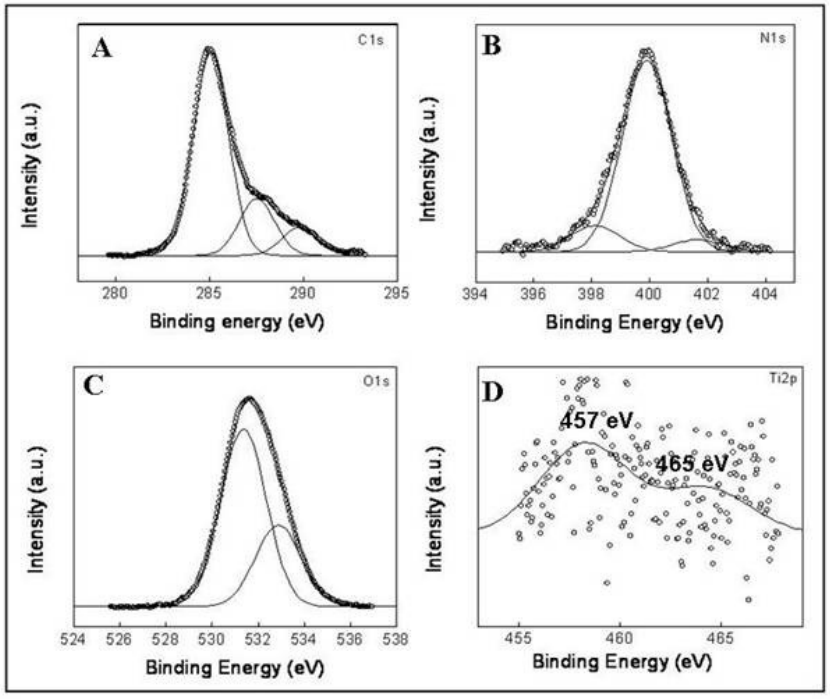

Figure 4.8: XPS spectra of biotransformed brookite TiO_2 nanoparticles recorded after 96 h of reaction between anatase type TiO_2 and fungus Humicola sp. The core level spectra were recorded from (A) C1s, (B) N1s, (C) O1s and (D) Ti2p. The raw data is shown in the form of symbols, while the chemically resolved components are shown as solid lines and details have been discussed in text.

4.6 References

[1] S. J. Kim, S. D. Park,Y. H. Jeong, *J. Am. Ceram. Soc.* **1999**, 82, 927.

[2] L. Gao, Q. Zhang, *Mater. Trans.* **2001**, 42, 1676.

[3] C. C. Wang, J.Y. Ying, *Chem. Mater.* **1999**, 11, 3113.

[4] T. Trung, C. S. Ha, *Materials Science and Engineering C* **2004**, 24,19.

[5] H. D. Nam, B. H. Lee, S. J. Kim, C. H. Jung, J. H. Lee, S. D. Park, *J. Appl. Phys.* **1998,** 37, 4603.

[6] Y. Zheng, E. Shi, Z. Chen, W. Li, X. Hu, *J. Mater. Chem.* **2001**,11,1547.

[7] A. Pottier, C. Chaneac, E. Tronc, L. Mazerolles , J. Jolivet, *J. Mater. Chem.* **2001**, 11, 1116.

[8] S. Watson, D. Beydoun, J. Scott, R. Amal, *J. of Nanoparticle Research* **2004**, 6, 193.

[9] H. Z. Zhang, J. F. Banfield, *J. Mater. Chem.* **1998**, 8, 2073.

[10] A. A. Gribb, J. F. Banfield, *Am. Mineral* **1997**, 82, 717.

[11] L. E. McNeil, R. H. French *Acta Mater.* **2000**, 48, 4571.

[12] Y. Ohko, K. Hashimoto, A. Fujishima, *J. Phys. Chem.* A **1997**, 101, 43, 8057.

[13] G. Wakefield, M. Green, S. Lipscomb, B. Flutter, *Mater. Sci. Technol.* **2004**, 20, 8, 985.

[14] M. Forsyth, D. R. MacFarlane, A. Best, J. Adebahr, P. Jacobsson, A. J. Hill, *Solid State Ionics.* **2002**, 147, 203.

[15] R. Wang, K. Hashimoto, A. Fujishima, M. Chikuni, E. Kojima, A. Kitamura, M. Shimohigoshi, T. Watanabe, *Nature* **1997**, 388, 431.

[16] P. S. Peercy, *Nature* **2000**, 406, 1023.

[17] W.Li, S. I. Shah, Semiconductor nanoparticles for photocatalysis. *In Encyclopedia of Nanoscience and Nanotechnology*; Nalwa, H. S., Ed.; American Scientific Publishers: Stevenson Ranch, CA, 2004; Vol. 9, 669–695.

[18] M. A. Barakat, H. Schaeffer, G. Hayes, S. I. Shah, *Appl. Catal.* B **2004**, 57, 23.

[19] W. Li, Y. Wang, H. Lin, *Appl. Phys. Lett.* **2003**, 83, 4143.

[20] S. I. Shah, W. Li, C. P. Huang, O. Jung, C. Ni, *Proc. Natl Acad. Sci. U.S.A.* **2002**, 99, 6482.

[21] R. Asahi, T. Morikawa, T. Ohwaki, K. Aoki, Y. Taga, *Science* **2001**, 293, 269.

[22] Y. Suda, H. Kawasaki, T. Ueda, T. Ohshima, *Thin Solid Films* **2004**, 162, 453.

[23] Y. Hwu, Y. D. Yao, N. F. Cheng, C.Y. Tung, H. M. Lin, *Nanostruct. Mater.* **1997**, 9, 355.

[24] Y. Zhang, C. K. Chan, J. F. Porter, W. Guo, *J. Mater. Res.* **1998**, 13, 2602.

[25] J. L. Sumerel, W. Yang, D. Kisailus, J. C. Weaver, J. H. Choi, D. E. Morse, *Chem. Mater.* **2003**, 15, 4804.

[26] S. L. Sewell, D. W. Wright, *Chem. Mater.* **2006**, 18, 3108.

[27] H. R. Luckarift, M. B. Dickerson, K. H. Sandhage , J. C. Spain, *Small* **2006**, 2, 640.

[28] K. E. Cole, A. M. Valentine, *Biomacromolecules* **2007**, 8, 1641.

[29] V. Bansal, D. Rautaray, A. Bharde, K. Ahire, A. Sanyal, A.Ahmad, M. Sastry, *J. Mater. Chem.* **2005**, 15, 2583.

[30] K. Prasad, A. K. Jha, A. R. Kulkarni, *Nanoscale Res Lett*. **2007**, 2, 248.

[31] K. Katagiri, H. Inami, T. Ishikawa, K. Koumoto, *J. Am. Ceram. Soc.* **2009**, 92, 181.

[32] Y. Jiang, D. Yang, L. Zhang, L. Li, Q. Sun, Y. Zhang, J. Li, Z. Jiang, *Dalton Trans.* **2008**, 31, 4165.

[33] B. Mazumdar, I. Uddin, S. Khan, V. Ravi, K. Selvraj, P. Poddar, A. Ahmad, *J.Mater.Chem.* **2007**, 17, 3910.

[34] V. Bansal, A. Sanyal, D. Dautaray, A. Ahmad, M.Sastry, *Adv.Mater.***2005**, 17, 7, 4.

[35] V. Bansal, D. Rautary, A. Ahmad, M. Sastry, *J.Mater.Chem.* **2004**, 14, 3303.

[36] J. R. Stephen, S. Maenanghten, *J.Curr.Opin.Biotechnol.* **1999**, 10, 230.

[37] D. E. Rawlings, *J.Ind.Microbiol.Biotechnol.* **1998**, 20, 268.

[38] N. Mulligan, M. Kamali *J.Chem.Technol.Biotechnol.* **2003**, 78, 497.

[39] (a) M. Valix, F. Usai, R. Mahk, *Mater Eng*. **2001**, 14, 197. (b) V. Bansal, P. Poddar, A. Ahmad, M. Sastry, *J.Am.Chem.Soc.* **2006**, 128, 11958.

[40] K. Shimizu, J. Cha, G. D. Slucky, D. E. Morse, *Proc.Natl.Acad.Sci.U.S.A* **1998**, 95, 6234.

[41] M. R. Eftink, C. A. Ghiron, *Anal. Biochem.* **1981**, *114*, 199. (b) Cantor, Schimmel, (Eds.) *Biophysical Chemistry, Part II: Techniques for the Study of Biological Structure and Function*, H. Freeman and Co., San Francisco. **1980**, Ch 7, p 377.

[42] Y. Zhao, C. Li , X. Liu, F. Gu, H. Jiang, W. Shao, L. Zhang, Y. He, *Materials Letters* **2007**, 61, 79.

[43] Y. Wang, N. Herron, *J. Phys. Chem.* **1991**, 95, 525.

[44] Y. H. Tseng, C. S. Kuo, C. H. Huang, Y. Y. Li, P. W. Chou, C. L. Cheng, M. S. Wong, *Nanotechnology* **2006**, 17, 2490.

[45] W. Wunderlich, T. Oekermann, L. Miao, N. T. Hue, S. Tanemura, M. J. Tanemura, *J Ceram Process Res*. **2004**, 5, 343.

[46] The XRD, SAED patterns and *d* vaules were indexed with reference to the crystal structures from the PCPDF files (PCPDF card no.00-029-1360).

[47] Y. Zheng, E. Shi, S. Cui, W. Li, X. Hu, *J. Am. Ceram. Soc.* **2000**, 83, 10, 2634.

[48] H. Kominami, M. Kohno, Y. Kera, *J. Mater. Chem.* **2000**, 10, 1151.

[49] B. Ohtani, J. Handa, S. Nishimoto, T. Kagiya, *Chem. Phys. Lett.* **1985**, 120, 292.

[50] A. Pottier, C. Chaneac, E. Tronc, L. Mazerolles, J. P. Jolivet, *J. Mater. Chem.* **2001**, 11, 1116.

[51] R. Nakamura, A. Imanishi, K. Murakoshi, Y. Nakato, *J. Am.Chem. Soc*. **2003**, 125, 7443.

[52] (a) C. D. Keating, K. K. Kovaleski, M. J. Natan, *J. Phys.Chem. B* **1998**, 102, 9414. (b) A. Gole, C. Dash, V. Ramakrishnan, S. R. Sainkar, A. B. Mandale, M. Rao, M. Sastry, *Langmuir* **2001**, 17, 1674. (c) A. Gole, C. Dash, S. R. Sainkar, A. B. Mandale, M. Rao, M. Sastry, *Anal. Chem.* **2000**, 72, 1401.

[53] S. S. Shankar, A. Rai, A. Ahmad, M. Sastry, *Chem. Mater*. **2005**, 17, 566.

[54] T. Miyama, Y. Yonezawa, *Langmuir* **2004**, 20, 5918. (b) A. Kumar, S. Mandal, P. R. Selvakannan, R. Pasricha, A. B. Mandale, M. Sastry, *Langmuir* **2003**, 19, 6277.

[55] J. F. Moulder, W. F. Stickle, P. E. Sobol, D. Bomben, *Handbook of X-ray Photoelectron Spectroscopy*; Physics Electronics Int.: Eden Prairie, MN, **1995**.

[56] (a) C. D. Wagner, W. M. Riggs, L. E. Davis, J. F. Moulder, G. E. Muilenberg, *Handbook of X-ray photoelectron spectroscopy*, Perkin Elmer Corp. Publishers, Eden Prairie, MN, **1979**, p. 40. (b) A. A. Schiffrin, W. Riemann, Y. Auwarter, A. Pennec, D. Weber-Bargioni, A. Cvetko, A. Cossaro, J. V. B. Morgante, *Proc. Natl. Acad. Sci. U.S.A.* 104, 5279**.** (c) G. Gonella, S. Terreni, D. Cvetko, A. Cossaro, L. Mattera, O. Cavalleri, R. Rolandi, A. Morgante, L. Floreano, M. Canepa, *J. Phys. Chem. B* **2005**, 109, 18003.

[57] L. O. va´ri, J. Kiss, *Appl. Surf. Sci.* **2006**, 252, 8624.

CHAPTER 5

Purification of sulphite reductase and capping protein from *Thermomonospora* sp. and *In Vitro* enzyme mediated synthesis of gold nanoparticles.

Summary

In this particular chapter, sulphite reductase enzyme and low molecular weight protein which we call capping protein, were purified to homogeneity from the extracellular broth of alkalothermophilic actinomycete *Thermomonospora* sp. using Fast Protein Liquid Chromatography (FPLC) system (on anionic column, mono Q), followed by elution of these proteins from preparative SDS-PAGE. The molecular weights of the purified sulphite reductase and capping protein were determined by analytical SDS-PAGE and were found to be 43 kDa and 13 kDa respectively. The approximate pI and Molecular weight of sulphite reductase based on amino acid composition was found to be 4.6 and 40.6 kDa respectively. Optimum pH and temperature of the purified sulphite reductase activity were found to be 8 and 50^{o}C respectively. Purified sulphite reductase and capping protein were then employed for the *in vitro* synthesis of highly monodispersed gold nanoparticles. Prominent role of capping protein was also established in capping and stabilization of gold nanoparticles. Formation of gold nanoparticles was then confirmed by visual inspection, UV-vis spectroscopy, Transmission Electron Microscopy (TEM), X-Ray Diffraction (XRD), Fourier Transform Infrared (FTIR) spectroscopy and X-ray Photoemission Spectroscopy (XPS).

5.1 Introduction

The choice of an environmentally compatible solvent system, an eco-friendly reducing agent and a nonhazardous capping agent for the stabilization of the nanoparticles are the three main criteria for a totally 'green' nanoparticle synthesis. For these reasons, there is a current drive to integrate all the 'green chemistry' approaches to design environmentally benign materials and processes [1, 2]. Use of biological organisms such as microorganisms, plant extracts or plant biomass [3, 4] and biological molecules such as glucose [5, 6], amino acids [7–9], enzymes [10–12] or polypeptides [13, 14] could be an alternative to chemical and physical methods for the production of metal nanoparticles in an eco-friendly manner. Although a very large number of biological systems in general and microbial systems in particular are capable of producing metal nanoparticles, mechanism of nanoparticle biosynthesis still remains a mystery for researchers. One such mechanism of metal nanoparticle biosynthesis by microorganisms is bioreduction [15]. In microbial bioreduction processes, myriads of proteins, carbohydrates and biomembranes are involved [16]. Nanoparticles are formed on cell wall surfaces and the first step in bioreduction is the trapping of the metal ions onto this surface. This probably occurs due to the electrostatic interaction between the metal ions and positively charged groups in enzymes present at the cell wall. This may be followed by enzymatic reduction of the metal ions, leading to the formation of nanoparticles [17]. The microbial cell reduces metal ions by use of specific reducing enzymes like NADPH dependent reductases [18]. The metabolic complexity of viable microorganisms often complicates the analysis and identification of active species in the nucleation and growth of metal nanoparticles. Strategies such as enzymatic oxidation or reduction, absorption on the cell wall and, in some cases, subsequent chelating with extracellular peptides or polysaccharides have been developed and used by microorganisms [19].

Many things about the biochemical and molecular mechanism of enzyme mediated reactions such as reductions and oxidations needs a complete study since most often these processes remain unknown and should be revealed. In fact, the biochemical mechanisms refer to finding materials like enzymes, which may mediate the biosynthesis mechanism. The studies of the enzyme structure and the genes which code these enzymes may help improve our understanding of how metal nanoparticle synthesis is performed. Improvements in chemical composition, size and shape and dispersity of generated nanoparticles could allow the use of nanobiotechnology in a

variety of other applications [20, 21]. *In vitro* biomolecule assisted synthesis could also overcome the problems such as size, shape, stability, etc. Exposure of microorganisms to high concentration of metal ions is known to result in the secretion of enzymes and proteins [22]. These proteins and enzymes in return could reduce/oxidize metal ions to form corresponding nanoparticles [23]. Since nanoparticle formation involves oxidation/reduction reactions, attempts were made to look for oxidoreductases in the extracellular broth of *Thermomonospora* sp., purify and characterize them to evaluate their role in the synthesis of nanoparticles. This chapter is divided into two parts. In the first part we have purified sulphite reductase enzyme and capping molecule (low molecular weight protein). In the second part, *in vitro* synthesis of gold nanoparticles using sulphite reductase and capping protein has been discussed.

5.2 Purification of sulphite reductase and capping protein from *Thermomonospora* sp.

5.2.1 Materials

Malt extract, yeast extract, glucose, bacteriological peptone (Hi Media), Mono Q FPLC column (Biorad), Molecular mass markers (G. E. Healthcare), sodium carbonate, dialysis tubing, acrylamide, TEMED, SDS, 2 (N-Morpholino) ethanesulfonic acid (MES), nicotinamide adenine dinucleotide phosphate (NADP), (NADPH), Coomassie Brilliant Blue G-250, SDS, sodium sulphite, (Sigma Chemicals Co., St Louis, MO, U.S.A) were used. All other chemicals used were of analytical grade.

5.2.2 Microorganism and growth conditions

An alkalothermophilic (extremophilic) actinomycete, *Thermomonospora* sp., having optimum growth at pH 9 and 50°C was isolated from self-heating compost obtained from the Barabanki district of Uttar Pradesh, India. The extremophiles are microorganisms which can grow under extreme conditions, e.g. extremes of temperature, from –14°C (psychrophiles) to 45°C (thermophiles) to 110°C (hyperthermophiles); extremes of pH [from 1 (acidophiles) to 9 (alkalophiles)]; very high barostatic pressure (barophiles); non-aqueous environment containing 100% organic solvents; excess heavy metal concentration; etc. These microorganisms have

developed numerous special adaptations to survive in such extreme habitats, which include new mechanisms of energy transduction, regulating intracellular environment and metabolism, maintaining the structure and functioning of membrane and enzymes, etc. The actinomycete, *Thermomonospora* sp., was maintained on MGYP (malt extract, glucose, yeast extract and peptone) agar slants and was maintained by subculturing at monthly intervals. The actinomycete was grown at pH 9 and 50°C for 96h and the slants were preserved at 15°C. From an actively growing stock culture, subcultures were made on fresh slants and after 96h of incubation at pH 9 and 50°C, were used as the starting material for fermentation experiments.

5.2.3 Methods

For the enzyme and protein purification, the actinomycete, *Thermomonospora* sp., was grown in 250 ml Erlenmeyer flasks containing 100 ml MGYP medium which is composed of malt extract (0.3 %), glucose (1.0 %), yeast extract (0.3 %) and peptone (0.5 %). Sterile 10 % sodium carbonate was used to adjust the pH of the medium to 9. The culture was grown with continuous shaking on a rotary shaker (200 rpm) at 50°C for 72 h. The mycelia (cells) were then separated from the culture broth by centrifugation (5000 rpm) at 10°C for 20 minutes and were washed thrice with sterile distilled water under sterile conditions and then suspended in 100 ml sterile distilled water (Sterile 10 % sodium carbonate was used to adjust the pH to 9) in 250 ml Erlenmeyer flask for 72 h under shaking (200 rpm) conditions. The supernatant was collected by centrifugation, concentrated by lyophilization, dialyzed extensively against Milli Q water followed by dialysis (12kD, cut off membrane) against 20mM MES buffer at pH 6.0 and used as a source of enzyme.

Protein determination

Protein concentration was determined according to Lowry *et al*. [24], using BSA as standard. However, during enzyme purification steps, protein concentrations were determined using the formula 1.55 A_{280} – 0.76 A_{260} = protein (mg/ml) [25].

Detection of gold nanoparticles synthesis

This was carried out by mixing 100 µl of the extracellular broth of *Thermomonospora* sp. with 1 ml each of 1 mM $AuCl_4$ and NADPH following the color development.

Formation of ruby-red color indicates the presence of reductases in the extra cellular broth.

Enzyme assay

Determination of sulphite reductase activity: This was carried out according to Yashimoto *et al*. (1968) [26]. The total reaction mixture of 1.5 ml contained 1.0 mM of freshly prepared sodium sulphite, in 100 mM MES buffer, pH 6.0, containing 1.0 mM EDTA, 0.15 mM NADPH and appropriately diluted enzyme. The reaction was initiated by the addition of NADPH followed by incubation at 50^{o}C. The oxidation of NADPH was monitored spectrophotometrically at 340 nm. Enzyme samples incubated in the absence of sodium sulphite served as blank. One unit of sulphite reductase activity is defined as the amount of enzyme required to oxidize 1 mole of NADPH/min under the assay conditions.

Two-dimensional electrophoresis (2-DE)

Protein samples were precipitated on ice with 100%TCA and the final concentration was adjusted to 10%. Precipitate was recovered by centrifugation at 10,000 rpm at 4°C for 10min and washed twice with chilled acetone and dried in air. Protein precipitate (125 µg) was resuspended in 2D-rehydration buffer (8M urea, 2% CHAPS, 50mM dithiothretiol (DTT) 0.2% (w/v) Bio-Lyte 3/10 ampholytes and trace amount of Bromophenol blue). Protein samples were loaded by in-gel rehydration method onto a 7cm precast immobilized pH gradient IPG strip (pH 3–10) and iso-electrofocusing (IEF) was performed on a PROTEAN IEF Cell from Bio-Rad at 20°C for 10,000V-hr with the end voltage of 4000V. After IEF was achieved, the strip was reduced in equilibration buffer. The strip was then loaded on a 10% Polyacrylamide gel and resolved by SDS-PAGE. Protein spots were visualized by staining with Coomassie brilliant blue R-250.

Purification using Fast Protein Liquid Chromatography (FPLC)

Initial fractionation of concentrated and dialyzed extracellular broth of *Thermomonospora* sp. was performed at ambient temperature using FPLC system (Biorad Biologic Duo flow system) using an anionic exchange resin (source Q packed in 10 ml Triton column, G.E. Healthcare) pre-equilibrated with 20mM MES buffer,

pH 6. The bound fractions were eluted in a linear gradient of 0-0.8M NaCl in the same buffer at a flow rate of 25ml/h.

Preparative SDS-PAGE

One dimensional preparative SDS-PAGE (pH 8.3) was performed in a vertical slab gel unit using 15% separating gels and 5.0% stacking gels [27]. The protein extract (1.0 ml) was separated by preparative SDS-PAGE (180×160×2.5 mm) using Tris-HCl buffer.

Elution of sulphite reductase enzyme and capping protein from preparative SDS-PAGE

After preparative gel electrophoresis, a strip on the right or left of the gel was cut off using a clean scalpel. The molecular weight markers, fraction having sulphite reductase activity and capping proteins used as a reference. The strip was placed in a tray for staining and the rest of the gel was placed on a glass plate (the gel was wrapped in plastic to prevent it from drying while staining the strip). The cut strip of gel was stained using CBB R-250 solution. This strip will function as the "reference" gel strip. The stained strip of gel was then aligned with the unstained gel portion and the portion (band) of gel that aligns with the stained protein of interest in the reference strip was cut out. Bands of gel just above and below the region presumed to contain the protein of interest were also excised and processed. Excised gel pieces were placed in clean microcentrifuge tubes and sufficient volume of elution buffer (50 mM Tris-HCl, 150 mM NaCl, and 0.1 mM EDTA; pH 7.5) was added so that the gel pieces were completely immersed. The gel pieces were crushed using a clean pestle and incubated in a rotary shaker at 30°C for overnight. After incubation period was over, the reaction mixture was centrifuged at 5,000-10,000 rpm for 10 minutes and the supernatant was carefully pipetted out into a new microcentrifuge tube. After extensive dialysis against Milli Q water followed by MES buffer at pH 6, an aliquot of the supernatant was tested for the presence of sulphite reductase activity and further subjected to analytical SDS-PAGE to determine the molecular weight [28-32]. Capping protein was also eluted and purified as described above.

Analytical SDS-PAGE for molecular weight determination

One dimensional analytical SDS-PAGE (pH 8.3) was performed in a vertical slab gel unit using 15% separating gels and 5.0% stacking gels [28] with (1) Phosphorylase b (97 kDa) (2) Bovine Serum Albumin (66 kDa), (3) Ovalbumin (45 kDa), (4) Carbonic anhydrase (30 kDa) (5) Trypsin inhibitor (20.1 kDa) and (6) α- Lactalbumin (14.4 kDa) as reference proteins. After electrophoresis, the gels were stained with Coomassie Brilliant Blue R-250 solution [10% acetic acid, 40% methanol and 0.1% Coomassie Brilliant Blue (CBB)-R250].

Amino acid analysis

The amino acid composition was determined on an AccQ-Fluo (Waters Corporation, USA) equipped with a fluorescent detector. Salt free protein sample (50µg) was hydrolyzed in 6 N HCl at constant boiling, in a vacuum sealed hydrolyzing tube for 24h at 110^{o}C. After hydrolysis, the sample was again lyophilized, dissolved in 100 µl of borate buffer (0.5M, pH9.0) and derivatized with 6-aminoquinolyl-N-hydroxysuccinimidyl carbamate (AQC). 1µl of the hydrolysate was subjected to analysis on an AccQ-Tag Column equipped with a fluorescent detector.

Effect of pH and temperature on sulphite reductase activity

pH optimum: To 1.4 ml reaction mixture with various pH (pH 3.0~5.0: 0.2M citrate buffer; pH 6.0~8.0: 0.2M phosphate buffer; pH 9.0~10.0: 0.2M bicarbonate buffer; pH 11.0~12.0: 0.2M Trimethylamine buffer; all buffers containing 1.0 mM EDTA, 0.15 mM NADPH, 1.0 mM of freshly prepared sodium sulphite), 0.1 ml of sulphite reductase was added and incubated at 50°C for 5 min. The activity was determined from the initial velocity and corrected for the slow oxidation of NADPH in the absence of sulphite (Yoshimoto and Sato, 1968).

Temperature Optimum: To 1.4 ml reaction mixture [0.2M MES buffer (pH 6) containing 1.0 mM EDTA, 0.15 mM NADPH, 1.0 mM of freshly prepared sodium sulphite], 0.1 ml of sulphite reductase was added and incubated at various temperatures (25, 30, 35, 40, 45, 50, 55, 60, 65, 70, 75, 80°C) for 5 min. The activity was determined from initial velocity and corrected for the slow oxidation of NADPH in the absence of sulphite (Yoshimoto and Sato, 1968).

5.2.4 Results and Discussions

Two-dimensional electrophoresis (2-DE)

Two-dimensional electrophoresis of extracellular broth of *Thermomonospora* sp. revealed 15-20 protein spots. From the figure 5.1, it is very clear that majority of the proteins present in the extracellular broth precipitated in the 3-5 pI range suggesting their anionic nature. However, few proteins which migrate further in the IPG strip fall between 7-9 pI range suggesting their cationic nature. There have been reports where sulphite reductases of various sources were found to be of anionic nature [33]. These reports compelled us to assume that our enzyme of interest i.e. sulphite reductase must be of anionic nature having pI between 3-5. Hence in further steps, we would also be dealing with anionic protein fractions of *Thermomonospora* sp.

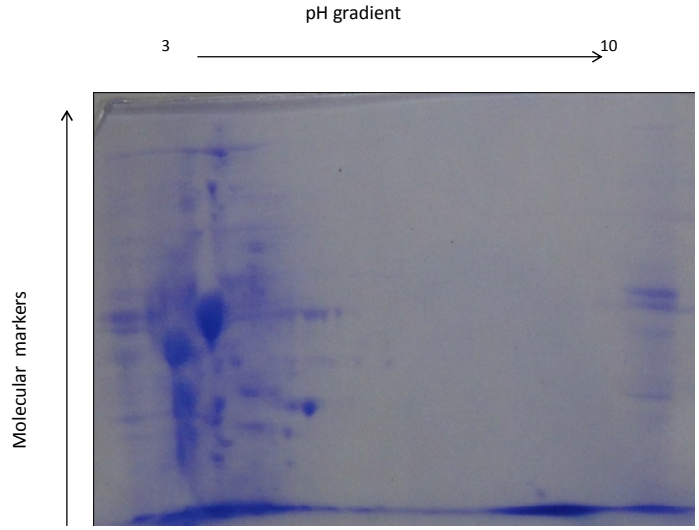

Figure.5.1: Preliminary Two-dimensional electrophoresis of extracellular broth of Thermomonospora sp.*, showing number of spots corresponding to different proteins. A broad range IPG strip (3-10) was used and IEF was carried out horizontally from left to right which was followed by one-dimensional SDS-PAGE (10%) vertically from top to bottom using different molecular weight markers.*

Purification using FPLC

Figure 5.2 shows the FPLC profile of the concentrated and dialyzed extracellular protein sample of *Thermomonospora* sp. The protein sample is bound to Mono Q column and separated into five distinct peaks. These bound peaks were then eluted in a linear gradient of 0-0.8M NaCl at a flow rate of 25ml/h, and 2ml fractions of each peak were collected and checked for the presence of sulphite reductase and capping

protein. The 200 mM eluates containing the sulphite reductase activity were pooled, lyophilized and dissolved in minimum amount of Milli Q water and dialyzed extensively against Milli Q water followed by 20 mM MES buffer, pH 6 containing 150 mM NaCl and used for the next step. 500 mM eluates were also collected to check for the presence of any low molecular weight peptide (capping peptide) which could be responsible for capping of nanoparticles and making them stable [34]. These fractions were also pooled, lyophilized and dissolved in minimum amount of Milli Q water and dialyzed extensively against Milli Q water followed by 20 mM MES buffer, pH 6 containing 150 mM NaCl and used for the next step.

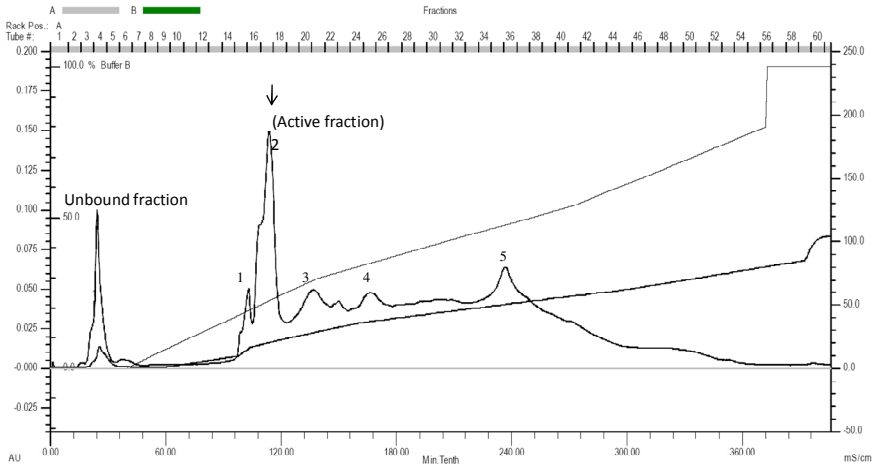

Figure 5.2: FPLC profile of extracellular broth of Thermomonospora sp. unbound fraction collected in isocratic flow and bound proteins were eluted in linear gradient of 0-0.8M NaCl.

Preparative SDS-PAGE Electrophoresis

The fractions (200 mM eluates) containing sulphite reductase activity obtained from the above step were loaded onto preparative SDS-PAGE (15%) at pH 8.3. Preparative SDS-PAGE showed 4-5 sharp protein bands ranging from 14-90 kDa. We assumed that one of these proteins may contain sulphite reductase activity. These bands were separately eluted from the polyacrylamide gel and checked individually for the sulphite reductase activity (elution of the protein bands were carried out as described in references [28-32], SDS removal and renaturation of proteins were performed as described by Hager *et al.* 1980 and Lila *et al.* 1997). The 500 mM eluate was also loaded onto preparative SDS-PAGE to find out the molecular weight of capping protein. This fraction showed two closely spaced bands which were eluted separately and kept for further study to check in combination with the band containing sulphite

reductase activity for the synthesis of gold nanoparticles. (Will be discussed in next part of this chapter).

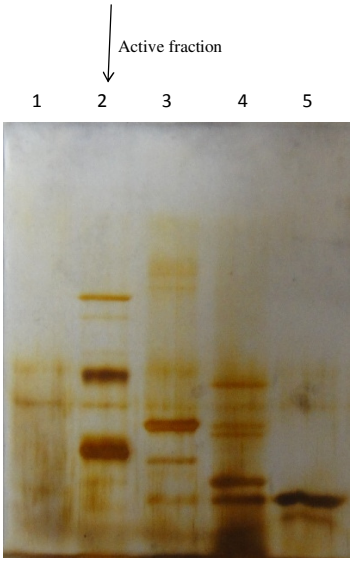

Figure 5.3: Preparative SDS-PAGE (15 %) of different fractions obtained from FPLC. Lane (2) Active fraction for sulphite reductase, Lane (5) Fraction containing capping protein. Lane (1), (3) and (4) Different fractions eluted from FPLC.

Table 5.1: Purification of sulphite reductase

Fraction	**Total Protein (mg)**	**Total Activity (U)**	**Yield (%)**	**Specific activity milliunits / (mg) protein**	**Purification fold**
Crude	315	25.25	100	0.215	1
FPLC (mono Q) Chromatography	23	18.25	73	2.58	12
SDS-PAGE Elution	8	14.2	56	10.1	47

The enzyme was purified 47-fold, with an overall recovery of 56%. The purified enzyme could be stored in Milli Q water at -20^{0}C for a year without any apparent loss of activity.

Analytical SDS-PAGE of sulphite reductase and capping protein

The molecular weights of eluted fractions obtained from preparative SDS-PAGE, which showed sulphite reductase activity and capping protein which could synthesize gold nanoparticles in combination with this fraction (will be discussed in next part of

this chapter) were found to be 43 kDa and 13kDa respectively (figure 5.4 and 5.5). The molecular weight of sulphite reductase of *Thermomonospora* sp. is slightly higher than that of *Fusarium oxysporum* sulphite reductase which was reported equal to 36.5 kDa (Anil *et al.* 2007), but lower than those from *Salmonella typhimurium* (66 kDa) [34] and Spinach (69 kDa) [35]. However, enzymes of *E. coli* [36] *Sacharomyces cerevisiae* [37] and *Thiobacillus denitrificans* [38] are very high molecular weight proteins with molecular weight of 607 kDa, 604 kDa and 160 kDa respectively. The urge for the search of a capping molecule arised from the fact that there have been reports which show the involvement of low molecular weight peptides or molecules for capping of the nanoparticles and hence preventing their aggregation. Phytochelatins, which are low molecular weight peptides made up of repeated *c*-Glu-Cys units are known to act as a capping entity in the *in vivo* synthesis of CdS (cadmium sulphide) nanoparticles by the fission yeast *Schizosaccharomyces pombe*, [39] and in the *in vitro* sulphite reductase mediated synthesis of gold nanoparticles (Anil *et al.* 2007). Amino acids such as lysine, glutamic acid and cysteine have also been reported as capping agents in the synthesis of gold nanoparticles [40-42]. In a radical shift from using commercially available capping molecules, we for the first time have identified and purified a low molecular weight capping molecule (capping protein) from the extracellular broth of *Thermomonospora* sp. This biological capping molecule could render gold nanoparticles water dispersible and stabilizes gold nanoparticles in solution. To the best of our knowledge, this is the first report of its kind where a reducing agent i.e. sulphite reductase and capping agent i.e. capping protein have been identified and purified from the same microorganism.

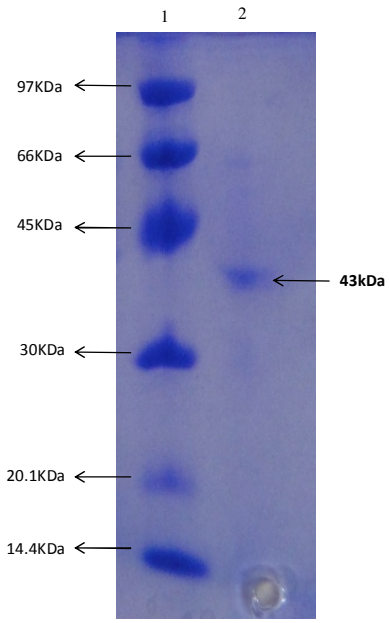

Figure 5.4: Molecular weight determination of the purified sulphite reductase by SDS-PAGE. Lane (1) Molecular mass markers (1) Phosphorylase b (97 kDa) (2) Bovine Serum Albumin (66 kDa), (3) Ovalbumin (45 kDa), (4) Carbonic anhydrase (30 kDa) (5) Trypsin inhibitor (20.1 kDa) and (6) α- Lactalbumin (14.4 kDa). Lane (2) Purified sulphite reductase.

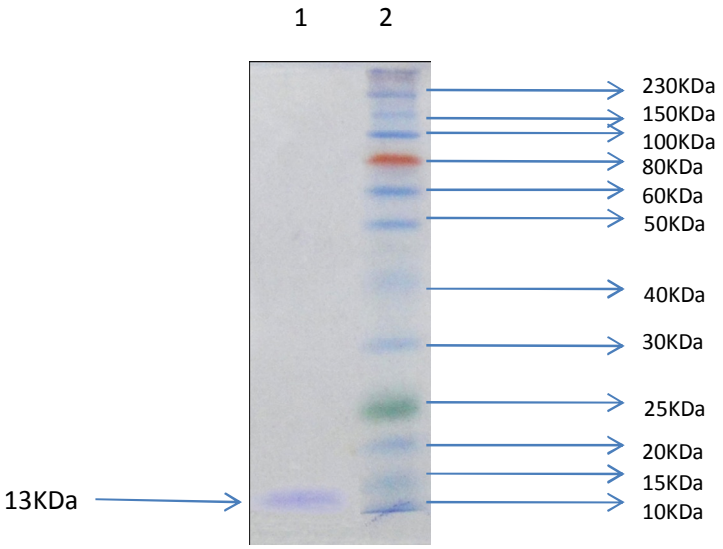

Figure 5.5: Molecular weight determination of the purified capping protein by SDS-PAGE. Lane (1) Purified capping protein. Lane (2) Molecular mass markers.

Amino acid composition of the enzyme sulphite reductase

Molecular weight and pI of purified sulphite reductase based on amino acid composition (shown in Table: 5.2) was found to be 40.6 kDa and 4.6 respectively. (http://isoelectric.ovh.org/)

Table: 5.2 Amino acid composition of sulphite reductase

Amino acid	Number of residues/mol
Ala	27
Met	19
Pro	16
Phe	17
Gly	21
Ile	18
Val	16
Trp[a]	14
Leu	18
Cys[b]	15
Asn	14
Gln	09
Ser	13
Thr	26
Tyr	11
Asp	14
Glu	39
Lys	23
Arg	13
His	07
Total	350

Determined spectrophotometrically according to: a. (Spande and Witkop, 1967) and b. (Cavallini *et al*., 1966) respectively

Effect of pH and Temperature

Sulphite reductase of *Thermomonospora* sp. exhibites an optimum pH and temperature at 8 and 50^{o}C respectively. However, enzymes from *Fusarium oxysporum* (Anil *et al.,* 2007)*, Saccharomyces cerevisiae* (Kobayashi and Yashimoto,

1982), *Salmonella typhimurium* (Ostrowski *et al*., 1989), Spinach (Kruger and Siegel, 1982) and *E. coli* (Siegel *et al*., 1973) showed an optimum pH of 6, 7.3, 7.7, 7.75 and 7.7, respectively. The optimum temperature of the purified enzyme was 50°C. This optimum temperature is more than *Fusarium oxysporum* (Anil *et al.,* 2007) and *E.coli* (Siegel *et al*., 1973) which were reported as 45° and 25°C respectively. The higher optimum temperature and pH may be attributed to the alkalophilic and thermophilic nature of *Thermomonopsora* sp. and since it grows mainly at elevated temperature and pH, its secretional products may also possess the same characteristics.

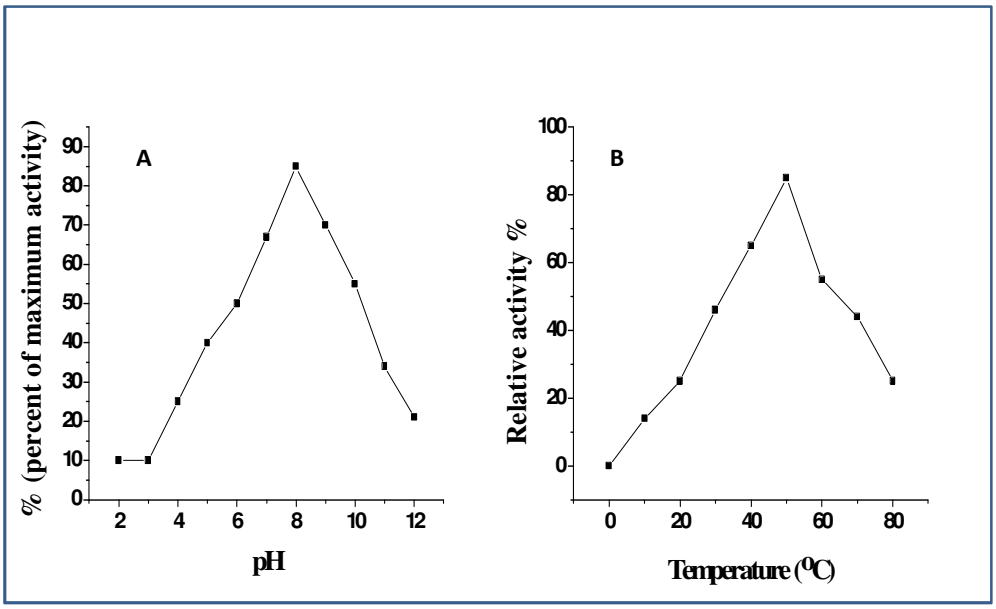

Figure 5.6: Effect of pH and temperature on the activity of sulphite reductase. (A) Optimum pH and (B) Optimum temperature.

5.3 Sulphite reducatse mediated synthesis of gold nanoparticles

5.3.1 Materials and Methods

Chloro auric acid ($HAuCl_4$), Na_2SO_3 and NADPH, (Sigma chemicals Co., St Louis, MO, U.S.A). All other chemicals used were of analytical grade. Sulphite reductase and capping protein were purified as described in previous part.

5.3.2 *In vitro* synthesis of gold nanoparticles

The total reaction mixture of 2 ml containing 1.0 mM each of freshly prepared $HAuCl_4$ and Na_2SO_3, 100 µg of capping protein, 0.15 mM NADPH and 100 µg of sulphite reductase was incubated under aerobic conditions at 50°C for 4h. Reaction

mixture in the absence of capping protein was also incubated at 50^{o}C to confirm its role in the stabilization of gold nanoparticles. Samples were removed at regular intervals and subjected to UV-vis spectroscopy to check for the formation of nanoparticles.

5.3.3 Characterization of *in vitro* synthesized gold nanoparticles

UV-vis spectroscopy

UV-vis spectrophotometric measurements were performed on a Perkin Elmer dual-beam Spectrophotometer (model lambda 750) operated at a resolution of 1 nm.

Transmission Electron Microscopy (TEM)

Samples were prepared by drying a drop of gold nanoparticles solution on carbon coated TEM copper grids followed by measurements on a JEOL Model 1200 EX Transmission electron microscope operated at an accelerating voltage of 80 kV.

X-Ray Diffraction (XRD) measurements

X-Ray Diffraction (XRD) studies of the biosynthesized gold nanoparticles powder casted on glass substrates were carried out on a Philips X'PERT PRO instrument equipped X'celerator. The sample was scanned using X'celerator with a total number of active channels of 121. Iron-filtered Cu Kα radiation (λ=1.5406 Å) was used. XRPD patterns were recorded in the 2 theta range of 20°- 80° with a step size of 0.02° and a time of 5 seconds per step at 40 kV voltage and a current of 30 mA.

Fourier Transform Infrared Spectroscopy (FTIR)

FTIR spectroscopy measurement on as-synthesized gold nanoparticles in KBr pellets was carried out using a Perkin –Elmer Spectrum One instrument. Spectrometer was operated in the diffuse reflectance mode at a resolution of 2 cm^{-1}. To obtain good signal to noise ratio, 128 scans of the film were taken in the range of 450 – 4000 cm^{-1}.

X-ray Photoemission Spectroscopy (XPS)

XPS of the biosynthesized gold nanoparticles was carried-out on a VG MicroTech ESCA 3000 instrument after depositing gold nanoparticles on the Si substrate.

5.3.4 Results and Discussions

Visual inspection

Freshly prepared $HAuCl_4$ when incubated with Na_2SO_3, capping protein, NADPH and sulphite reductase, under aerobic conditions and at 50^oC resulted in the formation of highly monodispersed gold nanoparticles just after 4h, as evidenced by the change in the color of reaction mixture from colorless (0 h) to ruby-red (4 h) (Figure 5.7 A & B respectively).The color change indicates the reduction of gold metal ions from Au^{+3} to Au^0 and arises due to the excitation of SPR (Surface Plasmon Resonance) in the metal nanoparticles [43, 44]. The solution was extremely stable, with no evidence of flocculation of the particles even a month after reaction. From this experiment it is very clear that sulphite reductase plays a very important role in the reduction of gold ions to metallic gold accompanying the reduction of Na_2SO_3 to sulphide. This enzyme sulphite reductase gains electrons from NADPH and oxidizes it to $NADP^+$. The enzyme is then oxidized by the simultaneous reduction of metal ions [23]. Similar enzymatic reduction of gold ions into metallic gold by NADPH-dependent sulphite reductase of molecular weight 35.6 kDa with phytochelatins as capping agent has been shown by Anil *et al.* in 2007. However Yasui and Kimizuka have reported that Glucose oxidase (GOD), an enzyme of oxidoreductases class could reduce Au (III) ions in the presence of β-D-glucose, with FAD as electron donor, forming stable gold nanoparticles with an average diameter of 14.5 nm [45]. Hydrolytic enzyme such as Trypsin has also been shown to reduce gold metal ions, resulting in the formation of three-dimensional (3D) gold nanoflowers with 12 cysteine residues and trypsin as capping agent [46]. A 29-kDa "gold shape-directing protein (GSP)" present in the extract of green algae *Chlorella vulgaris* was used in the bioreduction and in the synthesis of shape-and size-controlled distinctive triangular and hexagonal gold nanoparticles by Kannan *et al.* in 2010.

To ascertain the role of capping protein, the same reaction mixture without the capping protein was incubated at 50^oC for 4h. After the incubation period was over, a less intense color of gold nanoparticles was developed (Figure 5.7 C).This less intense color indicates that reduction of Au (III) to Au (0) might have taken place by sulphite reductase but as there was no capping molecule involved in the synthesis, the size of the gold nanoparticles would not have remained in the nanodimensions. It is to be noted that the color of gold nanoparticles is a direct function of SPR, which in turn depends on the size of the nanoparticles [47]. This experiment clearly suggests a

prominent role of capping protein in stabilizing gold nanoparticles, in absence of which the gold nanoparticles tend to flocculate giving rise to a less intense color.

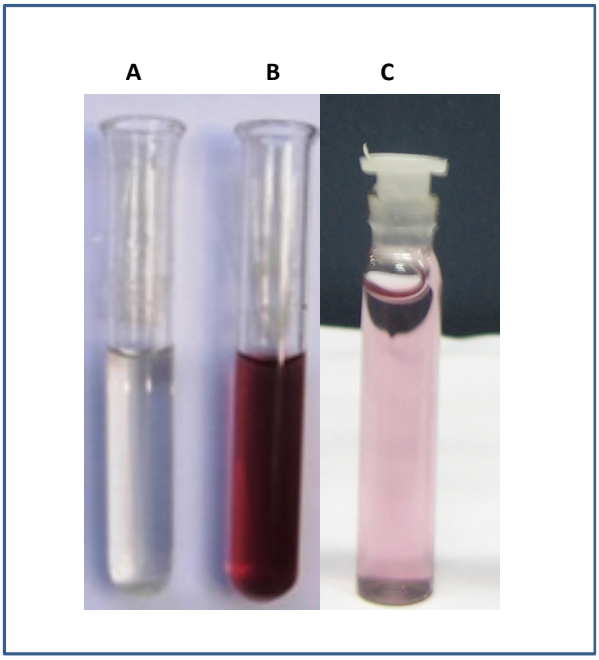

Figure 5.7: Formation of gold nanoparticles in the presence of sulphite reductase and capping protein, (A) at 0 hour, (B) after 4 hour and (C) Formation of gold nanoparticles without capping protein after 4 hour.

UV-vis spectroscopy

The UV-vis spectra for the reaction mixture of gold nanoparticles, as a function of time, (Figure 5.8) showed a well defined Surface Plasmon at 533 nm, which is in very good agreement with the reported SPR band of gold nanoparticles. (A. Henglein 1993, P. Mulvaney 1996 and M. Sastry *et al.* 1998). The intensity of sharp SPR band centered at 533 nm increases with increasing time and gets stabilized after 4h of reaction. Curve 'a' represents the UV-vis spectrum of gold nanoparticles synthesized without capping protein which shows a less sharp SPR band centered at 575 nm. This red shift of UV-vis absorption spectrum may have arised because of agglomeration of gold nanoparticles in the reaction mixture, since the exact position of SPR band depends on the size of the particle also.

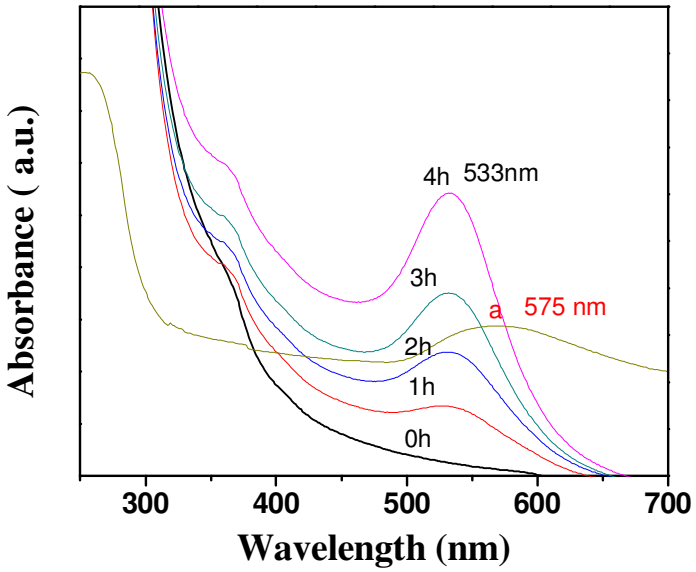

Figure 5.8: UV-vis spectra of enzyme mediated biosynthesized gold nanoparticles (as a function of time) synthesized using sulphite reductase and capping protein from 0 to 4h.Curve 'a' represents UV-vis spectrum of gold nanoparticles without capping protein after 4h.

Transmission electron microscopy (TEM)

Transmission electron microscopy (TEM) analysis of the gold nanoparticles showed that they are monodispersed and are essentially spherical (Figure 5.10A). The particles are well dispersed and show no sign of aggregation; this separation is mainly because of capping protein which is involved in capping of gold nanoparticles and prevents their aggregation. The dispersity shown in TEM image exactly correlates with the color and UV-vis spectroscopy analysis of the gold nanoparticles which showed the nanoparticles to be very stable and monodispersed. The nanoparticles were crystalline in nature as depicted by Selected Area Electron Diffraction (SAED) pattern (Figure 5.10B). Particle size distribution of gold nanoparticles revealed that the particles are having diameter in the range of 2-6 nm with an average of 3nm (Figure 5.10 C). Figure 5.10 (D) shows TEM image of gold nanoparticles synthesized without capping protein, which shows agglomerated gold nanoparticles forming a clump, each of size 40-50 nm. This is the strongest evidence favoring the role of capping protein in stabilizing and capping of the gold nanoparticles and also is in good agreement with UV-vis spectroscopy measurements indicating agglomerated nanoparticles.

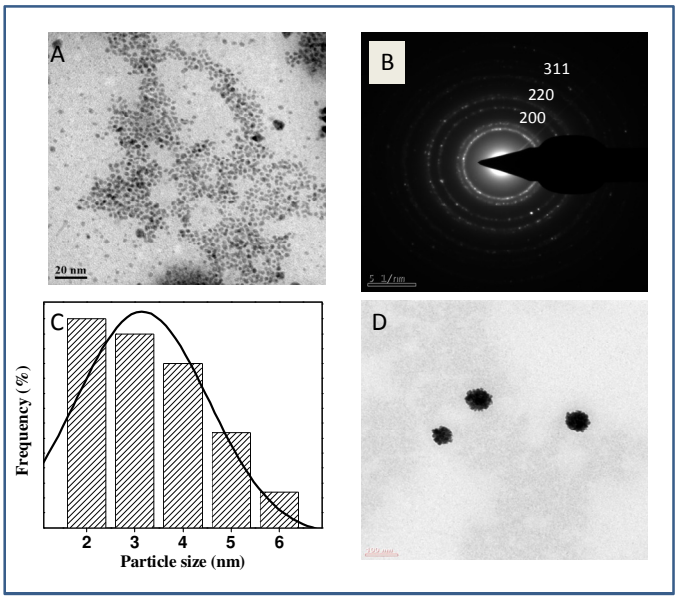

Figure 5.10: (A) TEM micrograph of enzyme mediated biosynthesized gold nanoparticles. (B) Selected Area Electron Diffraction (SAED) pattern recorded from one of the gold nanoparticles shown in Figure (A). (C) Histogram of size distribution of the gold nanoparticles. (D) TEM micrograph of gold nanoparticles synthesized without capping protein.

X-Ray diffraction (XRD) measurements

Figure 5.9 presents an X-Ray diffraction (XRD) pattern of the as-synthesized gold nanoparticles. The X-ray diffraction pattern of gold nanoparticles showed intense peaks at {111}, {200}, {220} and {311} with Braggs reflection at 2θ = 38°.09, 45°, 65° and 78° respectively, and agrees with those reported for the gold nanocrystals. No spurious diffractions due to crystallographic impurities were found. An overwhelmingly strong diffraction peak at 38.09^{o} is assigned to the {111} facets of a face-centered cubic (fcc) metal gold structure [48].

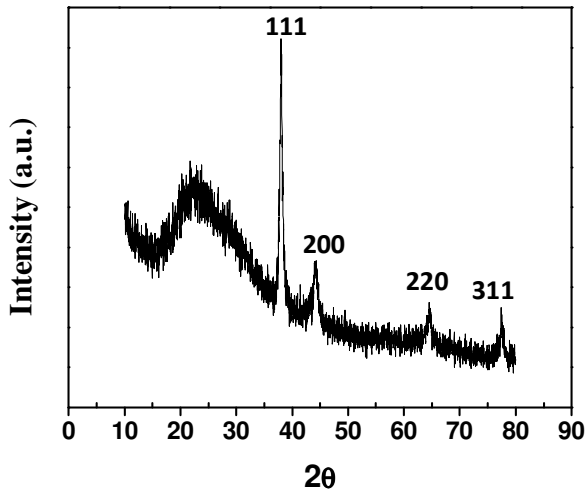

Figure 5.9: XRD pattern of enzyme mediated biosynthesized gold nanoparticles deposited on Si (111) glass plate.

Fourier Transform Infrared Spectroscopy (FTIR)

Figure 5.11 shows Fourier Transform Infrared Spectroscopy (FTIR) spectrum of enzyme mediated synthesized gold nanoparticles after 4h of reaction. The presence of two bands at 1640 and 1584 cm^{-1} are seen in the figure. The 1640 and 1584 cm^{-1} bands may be assigned to the amide I and II bands of proteins and arise due to carbonyl stretch and N-H stretch vibrations in the amide linkages of the sulphite reductase or capping protein respectively.

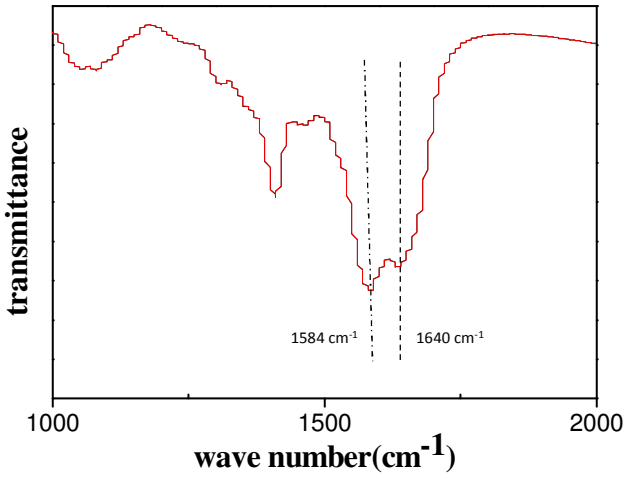

Figure 5.11: FTIR spectrum recorded from drop-cast films of enzyme mediated biosynthesized gold nanoparticles after 4h of reaction. The amide I and II bands are identified in the figure.

X-ray Photoemission spectroscopy (XPS)

Figure 5.12 shows the Au 4f spectrum from the *in vitro* synthesized gold nanoparticles which could be decomposed into two spin-orbit components 1 and 2 (spin-orbit splitting ~ 3.8 eV). The Au 4f (7/2) and 4f (5/2) peaks occurred at a binding energy (BE) of 84.3 eV and 88.2 eV respectively and are characteristic of metallic Au [49]. The absence of higher binding energies for Au 4f component confirms that all the chloroaurate ions are fully reduced by sulphite reductase enzyme and are in metallic form.

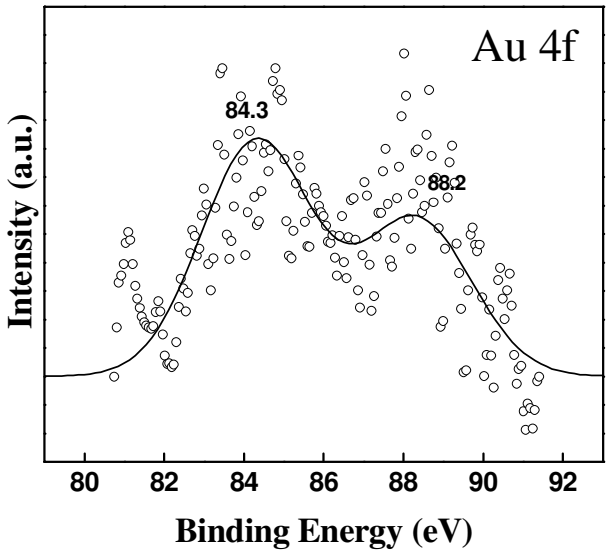

Figure 5.12: X-ray Photoemission spectroscopy of enzyme mediated biosynthesized gold nanoparticles showing Au 4f core level spectra.

5.4 References

[1] P. T. Anastas, J. C. Warner, *Green Chemistry: Theory and Practice* **1998** (New York: Oxford University Press).

[2] A. S. Matlack, *Intrduction to Green Chemistry* **2001** (New York: Dekker).

[3] S. S. Shankar, A. Rai, B. Ankamwar, A. Singh, A. Ahmad, M. Sastry, *Nat. Mater.* **2004**, 3, 482.

[4] A. Ahmad, S. Senapati, M. I. Khan, R. Kumar, M. Sastry, *Langmuir* **2003**, 19, 3550.

[5] P. Raveendran, J. Fu, S. L. Wallen, *Green Chem.* **2006**, 8, 34.

[6] P. Raveendran, J. Fu, S. L. Wallen, *J. Am. Chem. Soc.* **2003**,125, 13940.

[7] Y. Shao, Y. D. Jin, S. J. Dong, *Chem. Commun.* **2004**, 1104.

[8] S. K. Bhargava, J. M. Booth, S. Agrawal, P. Coloe, G. Kar, *Langmuir* **2005**, 21, 5949.

[9] P. Selvakannan, S. Mandal, S. Phadtare , A. Gole, R. Pasricha, S. D. Adyanthaya, M. Sastry, *J. Colloid Interface Sci.* **2004**, 269, 97.

[10] A. S. Kumar, M. K. Abyaneh, S. W. Gosavi, S. K. Kulkarni, R. Pasricha, A. Ahmad, M. I. Khan, *Biotechnol Lett*. **2007**, 29, 439.

[11] A. Ahmad, P. Mukherjee, D. Mandal, S. Senapati, M. I. Khan, R. Kumar, M. Sastry, *J. Am. Chem. Soc*. **2002**, 124, 12108.

[12] T. Yang, Z. Li, L. Wang, C. Guo, Y. Sun, *Langmuir* **2007***,* 23, 10533.

[13] Z. Wang, J. Chen, P. Yang, W. Yang, *Appl. Organometal.Chem.* **2007***,* 21, 645.

[14] R. Djalali, Y. F. Chen, H. Matsui, *J. Am. Chem. Soc.* **2003***,* 125, 5873.

[15] K. M. Moghaddam, *The journal of young investigations* **2010**, 19, 19.

[16] Kannan, B. Narayanan, N. Sakthivel, *Advances in Colloid and Interface Science* **2010**, 156, 1.

[17] V. Bansal, D. Rautray, A. Ahamd, M. Sastry, *J Mater Chem.* **2004**, 14, 3303.

[18] D. Mandal, M. Bolander, D. Mukhopadhay, G. Sarkar, P. Mukherjee, *Applied Microbial Biotechnology* **2006**, 69, 485.

[19] N. Krumov, *Chem. Eng. Technol*. **2009**, 32, 1026.

[20] A. Bharde, D. Rautaray, V. Bansal, A. Ahmad, I. Sarkar, S. M. Yusuf, M. Sanyal, M. Sastry, *Small* **2006**, 2, 135.

[21] A. Bharde, A. Kulkarni, M. Rao, A. Prabhune, M. Sastray, *Journal of Nanoscience and Nanotechnology* **2007**, 7, 1.

[22] E. Martino, B. Franco, G. Piccoli, V. Stoccli, S. Perotto, *Mol. And Cell.Biochem.* **2002**, 231, 179.

[23] S. Senapati, A. Ahmad, M. I. Khan, M. Sastry, R. Kumar, *Small* **2005**, 1, 517.

[24] O. H. Lowry, N. H. Rosenbrough, A. Farr, R. J. Randall, *J. Biol. Chem***. 1951**, 193, 265.

[25] C. M. Stoscheck, *Methods Enzymol*. **1990**, 182, 50.

[26] A. Yoshimoto, R. Sato, *Biochim. Biophys. Acta*. **1968**, 153, 555.

[27] U. K. Laemmli, *Nature* **1970**, 227, 680.

[28] (a) R. Lila, Castellanos-Serra, C. Fernandez-Patron, E. Hardy, H. Santana, V. Huerta, *Journal of Protein Chemistry*, 1**997**, 16, 415. (b) M. P. Deutscher, (ed.). *Guide to Protein Purification* **1990**, Vol. 182. Academic Press, San Diego, CA.

[29] P. Jeno, M. Horst. **1996**. *Electroelution of proteins from polyacrylamide gels*, p. 207-214. In J. M. Walker (ed.),The Protein Protocols Handbook. Humana Press, Totowa, NJ.

[30] J. H. Waterborg, H. R. Matthews. **1994**. *The electrophoretic elution of proteins from polyacrylamide gels*, p. 169-175. In J. M. Walker (ed.), *Basic Protein and Peptide Protocols*, Vol. 32. Humana Press, Totowa, New Jersey.

[31] D. A. Hager, R.R. Burgess, *Anal Biochem.* **1980**, 109, 76.

[32] E. Jacobs, A. Clad, *Anal Biochem.* **1986**, 154, 583.

[33] S. Anil Kumar, M.K. Abyaneh, S.W. Gosavi, S. K. Kulkarni, A. Ahmad, M. I. Khan *Biotechnol. Appl. Biochem*. **2007**, 47, 191.

[34] J. Ostrowski, M. J. Barber, D. C. Rueger, B. E. Miller, L. E. Siegel, N. M. Kredich, *J. Biol. Chem* .**1989**, 264, 15796.

[35] R. J. Krueger, L. M. Siegel, *J. Biol. Chem*. **1982**, 21, 2892.

[36] L. M. Siegel, M. J. Murphy, H. Kamin, *J. Biol. Chem.* **1973**, 248, 251.

[37] K. Kobayashi, A. Yashimoto, *Biochemica. Biophysica. Acta***. 1982**, 705, 348.

[38] M. Schedel, H. G. Truper, *Biochemica. Biophysica. Acta*. **1979**, 568, 454.

[39] J. D. Holmes, P. R. Smith, R. Evans-Gowing, D. J. Richardson, D. A. Russell, J. R. Sodeau, *Arch. Microbiol.* **1995**, 163, 143. (b) P. R. Smith, J. D. Holmes, D. J. Richardson, D. A. Russell, J. R. Sodeau, *J. Chem. Soc.*, *Faraday Trans.* **1998**, 94, 1235.

[40] P. R. Selvakannan, S. Mandal, S. Phadtare, R. Pasricha, M. Sastry, *Langmuir* **2003**, 19, 3545.

[41] N. Wangoo, K. K. Bhasin, S. K. Mehta, C. Raman Sur, *Journal of Colloid and Interface Science* **2008**, 323, 247.

[42] (a) S. N. Sarangi, A. M. P. Hussain, S. N. Sahu, *Appl. Phys. Lett.* **2009**, 95, 073109-1. (b) T.F. Spande, B. Witkop, *Methods Enzymol.* **1967**, 11, 498. (c) D. Cavallini, M. T. Graziani, S. Dupre, *Nature* **1966**, 212, 294.

[43] (a) A. Henglein, *J. Phys. Chem.* **1993**, 97, 5457. (b) M. Sastry, K. Bandyopadhyay, K. S. Mayya, *Colloid. Surf. A* **1997**, 127, 221. (c) M. Sastry, V. Patil, S. R. Sainkar, *J. Phys. Chem. B* **1998**, 102, 1404.

[44] P. Mulvaney, *Langmuir* **1996**, 12, 788.

[45] K. Yasui, N. Kimizuka, *Chemistry Letters* **2005**, 34, 416.

[46] L. Li, J. Weng, *Nanotechnology* **2010**, 21, 1.

[47] M. B. Mohamed, V. Volkov, S. Link, M. A. El-Sayed, *Chem. Phys. Lett.***2000**, 317, 517.

[48] D. V. Leff, L. Brandt, J. R. Heath, *Langmuir* **1996**, 12, 4723.

[49] C. S. Fadley, D. A. Shirley, *J. Res. Natl. Bur. Stand.* **1970**, 74A, 543.

CHAPTER 6

General Discussion and Conclusions.

Summary

This chapter presents the major outcome of the thesis and gives the general conclusions of the extracted results from the work done in this particular thesis. It also emphasizes on the potential scope for future work required to be done in this field.

6.1 Summary of the work

The work done in this thesis mainly focuses on the biological synthesis of oxide nanoparticles using microorganisms. The details of the work have been described in different chapters and the summary for each chapter with their conclusions has been described here. This thesis mainly revolves around three microorganisms: i) thermophilic fungus *Humicola* sp. ii) mesophilic fungus *Fusarium oxysporum* and iii) alkalothermophilic actinomycete *Thermomonospora* sp. The reasons why each of the above mentioned microorganisms are used for the synthesis of specific inorganic nanomaterials are as follows:

i) We have screened a number of mesophilic, thermophilic, alkalophilic and alkalothermophilic microorganisms in order to synthesize oxide nanoparticles of medical importance such as gadolinium oxide and cerium oxide nanoparticles at different pH and temperatures. Out of the several microorganisms screened, only thermophilic fungus *Humicola* sp. produces protein capped water dispersible extracellular gadolinium and cerium oxide nanoparticles at just 50^{o}C.

ii) Our group has already shown *Fusarium oxysporum*–based bioleaching approach towards the room temperature synthesis of oxide nanoparticles using cheap naturally available raw materials (white sand and zircon sand) as well as agro-industrial by-products (rice husk). This led us into thinking towards the possibility of extraction of protein capped nanoparticles such as SiO_2 from fly-ash.

iii) We had already reported the extracellular biosynthesis of monodispersed gold nanoparticles from the whole cells of a novel extremophilic actinomycete, *Thermomonospora* sp. In order to know the exact mechanism of synthesis of monodispersed gold nanoparticles, we decided on further investigating this extremophilic actinomycete.

In this thesis, we have shown that the fungus *Humicola* sp. can be used for the extracellular biosynthesis of lanthanide nanoparticles such as gadolinium and cerium. The choice for these metals may be justified by the fact that these metals started gaining their importance in biomedical applications but their biosynthetic routes have not been explored yet. We have shown that when the aqueous solutions of oxide precursors such as Gadolinium chloride ($GdCl_3$) and Cerium (III) nitrate hexahydrate ($CeN_3O_9.6H_2O$) were exposed to fungus *Humicola* sp., the fungus was able to synthesize oxide nanoparticles of gadolinium and cerium respectively. Transmission

electron microscopic analysis confirmed that Gd_2O_3 nanoparticles are in the range of 3-8 nm with an average size of 6 nm, whereas CeO_2 nanoparticles are in the range of 12-20nm with 16nm as average diameter. Surface characterization techniques such as X-ray diffraction and X-ray photoemission spectroscopy also confirm the synthesis of Gd_2O_3 and CeO_2 nanoparticles with the aforementioned sizes. The highly fluorescent protein capped Gd_2O_3 nanoparticles were radiolabelled with Technicium-99m and injected into rats in order to see biodistribution. These nanoparticles reach out to the liver and kidneys and pass through urine very fast. Since these nanoparticles reach out to the liver, they can be used for targeted drug delivery for liver cancer. In order to avoid any side effects of taxol, we conjugated taxol with protein capped Gd_2O_3 nanoparticles with the help of EDC coupling protocol. To achieve proper conjugation, taxol was first derivatized and modified to 1, 6 hexane diamine taxol and electrostatically conjugated to free carboxyl groups of capping peptide involved in the capping of the Gd_2O_3 nanoparticles using EDAC coupling reaction. The conjugation was then confirmed with the help of UV-vis spectroscopy and flourimetric analyses. Unbound drug molecules were removed by HPLC which finally gave the purified Gd_2O_3-taxol conjugate. Cytotoxicity of Gd-taxol conjugate was checked on THP-1 cell lines (cancer cell lines) to access its potential in the treatment of cancer. IC_{50} values of taxol and Gd-taxol conjugate showed that Gd-taxol conjugate is more effective in killing cancer cells than taxol alone. It can be concluded that the conjugation of taxol to Gd_2O_3 nanoparticles enhances its hydrophilicity so that the drug can easily penetrate deep inside the cells with the help of endocytosis, phagocytosis or other receptor mediated internalization processes. We believe this work could open new doors for nanosized drug delivery applications in cheap treatment of cancers.

In an attempt to obtain oxide nanoparticles purely through eco-friendly routes and negate the requirement of chemical precursors, we have extended the concept of fungal bioleaching from agro - based by-products to waste material such as fly-ash. We have shown that the fungus *Fusarium oxysporum* when exposed to fly-ash was able to leach crystalline silica nanoparticles extracellulary in solution. Hence, a cheap and environment friendly approach has been derived to obtain commercially important oxide (silica) nanoparticles out of waste materials using the fungus.

In a very novel discovery of its kind, we have shown that the fungus *Humicola* sp. can be used for the biotransformation of shape, size and phase of bulk anatase type TiO_2 particles. When we treated the fungus *Humicola* sp. with disc shaped micron size anatase type TiO_2 particles, to our pleasant surprise we found that the fungus could successfully transform the disc shaped micron size anatase type TiO_2 particles into circular brookite type TiO_2 nanoparticles. It is to be noted here that the phase transformation of TiO_2 is an extremely difficult process and requires very high temperature to occur successfully. However, we were able to achieve this task at just 50^oC.

Mechanistic aspect of formation of nanomaterials through biological route which is still seldom encountered in literature has been discussed in details in this thesis. We have purified an NADPH dependent sulphite reductase enzyme and capping protein from *Thermomonospora* sp. to synthesize gold nanoparticles. We chose gold because one can easily track the formation of gold nanoparticles synthesis through visual inspection and could further confirm it by UV-vis spectroscopy which is rather difficult in case of oxide nanoparticles. When we incubated the purified sulphite reductase enzyme along with NADPH, capping protein, $HAuCl_4$ and sodium sulphite, the enzyme could synthesize gold nanoparticles within just 4h of reaction. The electrons required for the reaction were provided by NADPH. Transmission electron microscopic (TEM) analysis showed that the particles were almost monodispersed and were in the range of 2-4nm. Capping protein which was also added in the reaction mixture provided the required stability and prevented aggregation of nanoparticles in solution. The role of capping protein in providing stability was further confirmed when the same reaction mixture was incubated without capping protein and when observed under TEM, the gold nanoparticles were found to be agglomerated and tend to cluster. Here, we have shown that by purifying the biomolecules and capping entities associated with the synthesis and capping of nanomaterials, one can synthesize nanoparticles *in vitro* with desired size.

6.2 Scope for future work

Biological synthesis of oxide nanomaterials using microorganisms is still a new field and the oxide nanoparticles synthesized in this thesis were chosen according to the growing applications of these materials especially in biology. For example,

gadolinium finds its application in magnetic resonance imaging technique and cerium oxide nanoparticles are being used in various biomedical applications such as wound healing, inhibition of cellular ageing, treatment of neurodegenerative diseases, etc. However, there is still a long way to go when these biosynthesized oxide materials start replacing conventional chemically synthesized materials. The foremost question which needs to be answered is the scale-up method of biosynthesized products. The underlying mechanism involving the formation of oxide nanoparticles needs to be completely worked out in order to synthesize tailor made nanomaterials and gain access to control over shape and size. Complete biosynthetic pathways needs to be elucidated and a series of enzymes and proteins responsible for the synthesis need to be purified and can be genetically engineered in some other sources to maximize the production of desired valuable products. Time dependent kinetics need to be carried out for maximum production of nanomaterials. Selection of the type of microorganisms for obtaining desired nanomaterials needs to be done. One can broaden the vision on fungal bioleaching and look for waste materials to obtain valuable products by employing microorganisms. However, certain protocols need to be standardized in order to get maximum output in lesser time. Pharmacokinetic and pharmacodynamic studies in case of conjugation of nanoparticles to drug need to be performed. Quantitative studies of drug release kinetics inside the cancer cells will help us in designing better strategies for conjugation of nanomaterials to different anticancer drugs.

We have already made significant progress towards biological synthesis of inorganic nanoparticles of different sizes, shapes and chemical compositions along with complete characterization of nanomaterials and synthesis of nanoparticle-drug conjugates. Since nanomaterials which we are making from microbial routes are capped with natural proteins and are water dispersible, they may bind to cell adhesion molecules (CAMs) like integrins or VEGFs (vascular endothelial growth factors). Therefore, targeting CAMs such as integrins and VEGFs is a novel anti–angiogenesis strategy for targeting of solid tumor. The nanomaterials which we are synthesizing using fungal routes may also bind to various receptors such as LHRH (Leutinizing hormone releasing hormone), EGFR (Epidermal growth factor receptor) and EpCAM (Epithelial cell adhesion molecule) without a targeting agent. Hence, these nanoparticles which are until now considered only as delivery agents in targeted drug

delivery treatment, can also be taken into consideration to be used directly as a drug in future ; with no side–effects and much cheaper than the ones currently being used.